Development of quantitative ^{1}H-NMR method for serum iron with application to infectious diseases

E Mathuthu

orcid.org/0000-0001-7889-5455

Dissertation accepted in partial fulfilment of the requirements for the degree *Master of Science in Biochemistry* at the North-West University

Supervisor: Dr S Mason

Graduation November 2021

27113787

PREFACE (TOC_HEADING)

And acknowledgements

Before you lies a dissertation “Development of a quantitative ^{1}H-NMR method for serum iron with application to infectious diseases" whose basis generated from my passion for developing new diagnostic and treatment methods for infectious diseases that have pillaged the world as we know it. How will we manage to win this war? It is my passion to fight the good fight. Our campaign against Covid 19 now seems fruitful. However, it is equally important not to lose focus on other diseases on the side lines. Despite the challenges thrown at us by 2020, I managed to submit my thesis in March 2021. Completing this dissertation, a product of years’ work. I feel deeply indebted to many people for their support during my MSc study at North-West University and the writing of this dissertation.

First and I am grateful to my supervisor Dr Shayne Mason for his invaluable advice, continuous support, and patience during my MSc study. His immense knowledge, guidance, encouragement and generous help have encouraged me through-out my academic research and daily life. I would also like to thank the Centre for Human Metabolomics (CHM) for making this project a reality. His advice that; if you are losing weight, getting stressed all the time, know that you are doing something right is what propelled me to finish this study in time. From Dr Shayne Mason, I learnt not only the knowledge of Analytical Biochemistry but also the rigorous scientific approach and the dedicating spirit for work. Also, he has infused me with enthusiasms for researching and developing new treatments for infectious diseases. Without his supervision, I would not have completed this challenging project. I would also like to thank Angelique Janse van Rensburg and Dean Du Plessis for their great contribution to our first publication. Not forgetting my good friends Sbonelo, Tumelo, Tian and Katlego.

I owe a huge debt of gratitude to Ms Retha Potgieter for her generous support during the difficult times I faced during my Masters. They say it takes a village to raise a kid, I'm grateful and humbled by her kindness. She played the role of a parent when she didn’t have to. For her I am thankful, and I will make sure that I, in turn, inspire someone as she has done.

To my family, I thank them for their patience and belief in me. They have provided me with the necessary resources and made sure that I am on the right path to making a name for myself in the academic world. Ayanda, for the advice she gave me during the darkest hours of my life. I

wish to thank my cousin Anthony Ndiripo for inspiring me from my high school days till now. I remember attending his classes in Bulawayo and how proud I was of him. From back then, I knew that I had no choice but to walk in his footsteps. Isaac and family, I am very thankful for the financial support, hoping that I will be there for you someday.

ABSTRACT (TOC_HEADING)

Accurate quantification methods for biologically important elements are crucial for the diagnosis, treatment and monitoring of infectious diseases. Current methods are chemistry based, expensive, time consuming and are not designed for bio-fluid analysis. This study aims to add an array of information obtained from ^{1}H-NMR serum metabolomics by developing a quantitative ^{1}H-NMR method for serum iron quantification. ^{1}H-NMR is a robust, information rich technology that is capable of synchronously quantifying and identifying biomolecules. Unfortunately, ^{1}H-NMR can only analyse compounds with C-H bonds hence it cannot analyse iron. Chelating agents like EDTA and DFO chelate iron and make iron analysis possible. Excess EDTA was used to develop an ^{1}H-NMR method to quantify Fe, Zn, K, Mg and Ca. Mg, Ca and Zn were quantified whilst K and Fe could not be quantified at physiological pH range. Further, DFO a ferric ion (Fe^{3+}) chelating agent was used in excess and in the presence of a catalyst to develop a method for serum iron quantification, but the final prepared serum sample was unstable over time. Additional research on higher field strength catalyst(s) that can transfer more iron from iron binding proteins, as well as methods of stabilizing the final prepared serum sample to quench chemical reactions must be done.

Key terms

Proton nuclear magnetic resonance (^{1}H-NMR) spectroscopy; iron; chelation; deferoxamine (DFO) method development, Ethylenediamine tetra acetic acid (EDTA), chelation, biological ions.

TABLE OF CONTENTS (HEADING 0)

PREFACE (TOC_HEADING) ..... **II**

ABSTRACT (TOC_HEADING) ..... **IV**

CHAPTER 1 INTRODUCTION **13**

1.1 Introduction **13**

1.2 Dissertation Layout **14**

1.3 Declarations **15**

1.4 References **16**

CHAPTER 2 LITERATURE REVIEW **18**

2.1 Introduction **18**

2.2 Iron **18**

2.2.1 Homeostasis 19

2.2.2 Absorption and transport 20

2.2.3 Serum iron 21

2.2.3.1 Transferrin bound 21

2.2.3.2 Non-transferrin-bound iron (NTBI) 21

2.2.3.3 Serum ferritin 22

2.3 Infectious diseases **22**

2.3.1 The past, present and future 22

2.3.2 Epidemiology 23

2.3.3 Iron content in infectious diseases 23

2.4 Current methods to measure body iron content **24**

2.4.1 Serum transferrin as a quantitative iron measure 25

2.4.2 Serum non-transferrin-bound iron assessments....25

2.4.3 Serum ferritin....25

2.4.4 Laboratory gold standard....26

2.5 ^{1}H-NMR spectroscopy....26

2.5.1 Chelation NMR....29

2.5.1.1 Ethylenediaminetetraacetic acid (EDTA)....29

2.5.1.2 Deferoxamine (DFO)....30

2.6 Problem statement....32

2.7 Aim....32

2.8 Objectives....32

2.9 References....34

CHAPTER 3 EVALUATING EDTA AS A CHELATING AGENT USING ^{1}H-NMR SPECTROSCOPY....43

3.1 Introduction....43

3.2 Biologically important ions....43

3.2.1 Calcium (Ca)....44

3.2.2 Magnesium (Mg)....45

3.2.3 Potassium (K)....46

3.2.4 Zinc....47

3.3 Motivation for paper 1....49

3.4 Paper 1: EDTA as a chelating agent in quantitative ^{1}H-NMR of biologically important ions....50

3.5 Abstract....52

3.6 Introduction....53

3.7 Materials and methods....56

3.7.1.1 Reagents....56

3.7.1.2 Preparation of solutions....56

3.7.1.3 Method development....58

3.7.1.3.1 Experiment 1....58

3.7.1.3.2 Experiment 2....59

3.7.1.3.3 Experiment 3....59

3.7.1.4 ^{1}H-NMR analysis....59

3.8 Results....60

3.8.1.1 Experiment 1....60

3.8.1.2 Experiment 2....64

3.8.1.3 Experiment 3....66

3.8.1.3.1 Accuracy....68

3.8.1.3.2 Precision and linearity....70

3.8.1.3.3 Repeatability....70

3.9 Discussion....73

3.10 Conclusion....76

3.11 Declarations....78

3.12 References....79

CHAPTER 4 EVALUATING DFO AS A CHELATING AGENT USING ^{1}H-NMR SPECTROSCOPY....88

4.1 Introduction....88

4.2 Paper 2: Chelation ^{1}H-NMR method development for quantifying iron in serum using deferoxamine....88

4.3 Abstract....91

4.4 Introduction....92

4.5 Materials and methods....96

4.5.1 Chemicals 96
4.5.2 Precautions to avoid iron contamination 96
4.5.3 Stock solutions 96
4.5.4 Method development 97
4.5.4.1 Determining $FeCl_3$ levels 98
4.5.4.2 Deferoxamine determination 98
4.5.4.3 Ferrioxamine determination 98
4.5.4.4 Determining possible catalyst(s) 98
4.5.4.5 Vortex duration 99
4.5.4.6 Repeatability 99
4.5.4.7 Linearity and precision 99
4.5.4.8 Miniaturization: from 600µL to 60µL 99
4.5.4.9 Application to human serum 100
4.5.4.10 ^{1}H-NMR parameters 101
4.5.4.11 Statistical analysis 101
4.6 Results 102
4.6.1 Method development 102
4.6.1.1 UV spectrophotometry 102
4.6.1.2 ^{1}H-NMR spectroscopy 104
4.6.2 Application of method to human serum 111
4.6.2.1 Unfiltered serum 111
4.6.2.2 Filtered serum 112
4.6.3 Linearity of DFO 115
4.7 Discussion 117
4.8 Conclusion 120

4.9 Declarations....121

4.9.1 Declaration of interest....121

4.9.1.1 Funding....121

4.9.2 CRediT authorship contribution statement....121

CHAPTER 5 DISCUSSION....129

5.1 Introduction....129

5.2 Proof-of-concept of chelation NMR as a quantitative ^{1}H-NMR method for biologically important ions using EDTA as a chelating agent. 129

5.3 Iron quantification using EDTA as a chelating agent in ^{1}H-NMR 130

5.4 Developing a quantitative DFO chelation NMR for iron using as a pure compound....130

5.5 Applying developed quantitative NMR method to spiked serum samples....130

5.6 Filtered serum sample ^{1}H-NMR analysis....131

5.7 Conclusions....131

5.8 References....132

ANNEXURES (TOC HEADING)....134

LAST UPDATED: 30 MARCH 2021....ERROR! BOOKMARK NOT DEFINED.

LIST OF TABLES (HEADING 0)

Table 1: Reference ranges of concentrations of Ca, Mg, K, Fe and Zn in blood and CSF, under normal and pathological conditions, based upon literature. 57

Table 2: Fourteen serial stock dilutions of Mg, Ca, K, Fe, Zn as 25%, 50%, 75%, 100%, 125%, 150% & 175% of both the upper and lower values of their normal reference ranges from Table 1. 58

Table 3: Chemical shifts and peak splitting of EDTA-chelated Zn, Mg and Ca.....64

Table 4: Quantitative output of experiment 3 for the 4-proton and 8-proton EDTA chelated complexes across 14 concentration levels of Ca, Mg and Zn, including the true values. 67

Table 5: Accuracy measured via % recovery for both the 4-proton and 8-proton EDTA complex of Ca, Mg and Zn.....69

Table 6: Calculated CVs (%) across Ca, Mg and Zn chelated complexes. 72

Table 7: EDTA-metal complex stability constants 75

Table 8: Spiked serum iron concentrations based upon 14 serial dilutions of FeCl3 used in method development.....100

Table 9: Actual FeCl3 values (µM) at 14 concentration levels, as determined by UV spectrophotometry at 340nm. 102

Table 10: Quantitative results of method assessment across 14 levels of FeCl3 concentrations, measured in triplicate. Values were calculated as percentages relative to TSP. 110

Table 11: Average R2 values for DFO peaks for the initial experiment (Hr_0), and after 24 hours (Hr_24) and 72 hours (Hr_72) in the auto-sampler. 116

LIST OF FIGURES (HEADING 0)

Figure 1: The normal global distribution of iron in a human body (Michels *et al*., 2015). 20

Figure 2: 3D Conformational change in the EDTA structure during chelation (Hafer *et al*., 2020) 30

Figure 3: ^{1}H NMR spectra of free DFO (Tian *et al*., 2016). 31

Figure 4: Published manuscript in Biochemistry and Cell Biology on 15 January 2021 (Mathuthu *et al*., 2020). 51

Figure 5: Qualitative assessment of ^{1}H-NMR spectra (relative to IS) to determine sufficient EDTA concentration for complete chelation of the highest concentration investigated for Zn (top), Mg (middle) and Ca (bottom). All measurements done at pH 7.00 ± 0.05. 62

Figure 6: Qualitative assessment of representative 1H-NMR spectra across pH range 6.50, 6.80, 7.00, 7.20 and 7.50 for Zn (left), Mg (middle) and Ca (right). Red boxes indicate regions where free EDTA peak infringes upon chelated EDTA peak. 66

Figure 7: Linearity plots (with STD error bars) for Zn (top), Mg (middle) and Ca (bottom). 71

Figure 8: Comparison of conditional stability constants for various metal–EDTA complexes as a function of pH (Kim & Ong, 1999). 75

Figure 9: Proof of submission.....90

Figure 10: Change in 3D conformation of DFO during chelation with ferric iron (reprinted with permission from Codd *et al*., 2018). 94

Figure 11: Schematic of method development. 97

Figure 12: UV spectrophotometric determination of DFO between 200-240nm for A: 10mM DFO, and B: 1mM DFO 103

Figure 13: UV spectrophotometric determination at absorbance of 430nm of FOB alone (pure) and effects of ligands. NTA = nitrilotriacetic acid; CdCl3 = cadmium chloride 104

Figure 14: ^{1}H-NMR spectra of DFO (bottom; black) and FOB (top; blue), relative to IS. 105

Figure 15: The effect of the ligands CdCl3 and NTA on the concentrations of DFO and high (500µM), medium (250µM) and low (125µM) levels of $FeCl_3$. 106

Figure 16: The effect of vortex duration on method repeatability. 107

Figure 17: Assessment of repeatability (CV) of method at 600µL and comparison to miniaturization of method at 60µL, which shows slightly, improved repeatability. 108

Figure 18: Overlay of ^{1}H-NMR spectra at 14 levels of $FeCl_3$ concentrations, relative to TSP, with the box zoomed in at the spectral region of 2.775 ppm to illustrate that a singlet was observed to increase with $FeCl_3$ concentration.....109

Figure 19: Quantitative results of the singlet at 2.775ppm for all 42 samples, analysed in triplicate across 14 concentration levels of $FeCl_3$. The measured values are relative to the TSP(%). A trend line was added to show that a linearity of R^2=0.95 was obtained. 110

Figure 20: ANOVA of binned, unfiltered serum samples spiked across 5 levels of $FeCl_3$ concentrations. Red dots in the ANOVA indicate regions in the 1H-NMR spectra that showed statistically significant variance. The box plots of these 15 spectral regions are also given. A general downward trend is observable across all 15 significant bins (i.e. chemical compounds in the serum samples are decreasing as the $FeCl_3$ concentrations increase).....111

Figure 21: PLS-DA scores plot showing a drift in the data sets over time, indicating that the prepared serum samples are not stable at room temperature. Hr_0 (red Δ) is the initial experiment, Hr_24 (green +) is the experiment repeated after sitting for 24 hours in the auto-sampler, and Hr_72 (blue X) is the experiment repeated after sitting for 72 hours in the auto-sampler. 113

Figure 22: VIP scores of the PLS-DA plot showing four bins with VIP scores greater than 2.0.....114

Figure 23: Plot showing linearity of DFO at 2.06 ppm measured (averages of triplicates) as spectral intensity relative to TSP across 5 concentration levels of FeCl3, for the initial experiment (Hr_0) and after sitting for 24 hours (Hr_24) and 72 hours (Hr_72) in the auto-sampler. 115

Figure 24: Newly proposed method. 5ml of blood is collected in Vacutainer SST tubes and allowed to coagulate at room temperature for an hour. The blood is centrifuged at 1300 *g* for 10 minutes to collect serum. 255Mm NTA is added to the serum samples to bind any NTBI if present in serum. Proteins including apo-transferrin may interfere with the iron measurements hence serum is filtered through a 10kDa membrane at 3000 *g* for 10 minutes. 50µL of the filtrate is collected using an e*Vol* analytical syringe and 6µL of the 20mM internal standard is added to the sample before 4µL of 10mM DFO. The sample is transferred into 2mm NMR tubes then analysed using ^{1}H-NMR. 119

CHAPTER 1 INTRODUCTION

Introduction

Trace elements play fundamental roles in a human body for cell functions at biological, chemical and molecular levels (Prashanth et al., 2015). They are called trace elements due to their scarcity and essentiality in human bodies (Fraga, 2005). Prashanth et al. (2015) expresses their role as dual – in normal levels they are crucial for stabilization of the cellular structures, but in deficiency states may stimulate alternate pathways and cause diseases. Deficiencies can be prevented by adequate supplementation; however, overabundant amounts lead to toxicity (Fraga, 2005; Fulgenzi &Ferrero, 2019).

Iron (Fe) is an essential trace element to almost all life (Fraga, 2005), and the focus element of this MSc study. Human body iron is found in four classes of proteins: 1) heme proteins containing more than 2/3 of the total body iron content, 2) iron storage proteins, 3) Fe-Sulphur enzymes, and 4) iron-activating or iron-containing enzymes. Each class is crucial for the proper functioning of the human body.

Despite fine-tuned iron homeostasis, dysregulation is a common phenomenon (Gozzelino & Arosio, 2016). Iron deficiency refers to the decrease in iron levels which affect a quarter of the world's population (Dev & Babitt, 2017). Lower total body iron content (TBIC) causes mild or severe anaemia and compromised organ function (Gozzelino & Arosio, 2016). A healthy diet can prevent iron deficiency whilst adequate supplementation can reverse the effects (Puntarulo, 2005). Serum iron exists in two forms – transferrin bound, or non-transferrin bound; the latter signalling excess. Excess iron must be excreted as it is toxic because it generates oxidative stress, and it is usually associated with hereditary disorders (Anderson & Frazer, 2017). From the above, it can be concluded that iron has a high clinical significance. Nearly all infectious disease-causing agents are dependent on host iron for survival (Weinberg, 2009). Microbial agents have developed sophisticated uptake systems to acquire iron from hosts that can be divided into three main categories: siderophore-based systems, heme acquisition systems, and transferrin/lactoferrin receptors (Skaar, 2010). Iron quantification methods evolved and improved with technology (Cramer *et al.,* 1984). Current methods use biological indicators (Infusino *et al.,* 2012*)*. Each indicator has both advantages and disadvantages, as a result the search for a more efficient non-invasive method is still on (Infusino *et al.,* 2012*)*. ^{1}H-NMR is the best analytical technique as it is

having been shown to be highly reproducible and repeatable across many fields of analytical biochemistry (Emwas *et al*., 2019). It is an ideal tool to analyze bio-fluids like serum since it requires simple sample preparation and does not alter the original state of samples. Developing a new quantitative method requires a highly selective instrument, ^{1}H-NMR identifies fewer compounds as compared to its competitors (Emwas et al., 2019). More importantly, ^{1}H-NMR has lower running costs and can analyze compounds that are difficult to analyze by LC or GCMS.

Dissertation Layout

Chapter 1 – an introduction, which gives an overview of the whole dissertation followed by problem statement. The aims and objectives are listed in this chapter.
Chapter 2 – the literature. Biological information on the properties of iron that makes it so important in biological organisms and its regulation and consequences of dysregulation are explained here. This is followed by epidemiology of iron-related conditions. Current methods to quantify iron are compared. The worth of ^{1}H-NMR as the analytical tool chosen for this method is compared with other worthy competitors.
Chapter 3 – proof-of-concept of NMR chelation in the form of a peer-reviewed paper published in the journal *Biochemistry and Cell Biology*, entitled: 'EDTA as a chelating agent in quantitative ^{1}H-NMR of biologically important ions' (doi.org/10.1139/bcb-2020-0543).
Chapter 4 – focus upon iron and the development of a quantitative ^{1}H-NMR assay in the form of a manuscript submitted to *Biochemistry and Cell Biology* (under review), entitled: 'Chelation ^{1}H-NMR method development for quantifying iron in serum using deferoxamine'.
Chapter 5 – discussion of results and objectives of this MSc study, followed by conclusions and future recommendations.

Declarations

I, Emmanuel Mathuthu (27113787), hereby declare that this dissertation is a record of my own work, unless stated, and that this research has not been submitted anywhere else.

X

Emmanuel Mathuthu
student

References

Anderson, G.J. & Frazer, D.M. 2017. Current understanding of iron homeostasis. *The American Journal of Clinical Nutrition*,106(suppl_6):1559S-66S.

Cramer, S.M., Nathanael, B. & Horváth, C. 1984. High-performance liquid chromatography of deferoxamine and ferrioxamine: interference by iron present in the chromatographic system. *Journal of Chromatography A*, 295(1):405-411.

Dev, S. & Babitt, J.L. 2017. Overview of iron metabolism in health and disease. *Hemodialysis International*, *21*:S6-S20.

Fraga, C.G. 2005. Relevance, essentiality and toxicity of trace elements in human health. *Molecular Aspects of Medicine*, *26*(4-5):235-244.

Fulgenzi, A. & Ferrero, M.E. 2019. EDTA chelation therapy for the treatment of neurotoxicity. *International Journal of Molecular Sciences*, *20*(5):1019.

Gozzelino, R. & Arosio, P. 2016. Iron homeostasis in health and disease. *International Journal of Molecular Sciences*, *17*(1):130.

Infusino, I., Braga, F., Dolci, A. & Panteghini, M. 2012. Soluble Transferrin Receptor (sTfR) and sTfR/log FerritinIndex for the Diagnosis of Iron-Deficiency Anemia. *American Society for Clinical Pathology,* 138:642-649.

Mast, A.E., Blinder, M.A., Gronowski, A.M., Chumley, C. & Scott, M.G. 1998. Clinical utility of the soluble transferrin receptor and comparison with serum ferritin in several populations. *Clinical Chemistry*, *44*(1):45-51.

Prashanth, L., Kattapagari, K.K., Chitturi, R.T., Baddam, V.R.R. & Prasad, L.K. 2015. A review on role of essential trace elements in health and disease. *Journal of Dr. NTR University of Health Sciences*, *4*(2):75.

Puntarulo, S. 2005. Iron, oxidative stress and human health. *Molecular Aspects of Medicine*, 26(4-5):299-312.

Skaar, E.P. 2010. The battle for iron between bacterial pathogens and their vertebrate hosts. *PLoS Pathog*, *6*(8):1000949.

CHAPTER 2 LITERATURE REVIEW

2.1 Introduction

Iron is an essential element that plays critical both in human lives and bodies; as a result, it must be carefully modulated within a human body. In some infectious diseases, hereditary and degenerative diseases body iron content can be altered, and this phenomenon is used to diagnose diseases. To properly diagnose these diseases methods are still being optimized and developed.

2.2 Iron

Empires have been forged, and have fallen, at the tip of spears made of iron. Iron has not only sharpened the course of human history, but evolution itself. Within the human body, iron exists both intra and extracellular (Milto *et al.,* 2016). Iron is a crucial trace element in biological life that naturally exists in ferrous (Fe^{2+}) and ferric (Fe^{3+}) forms. The electron transfer between these oxidation states is facilitated by a reducing or oxidizing agent. Under physiological conditions ferric iron is the most stable. The reduction of oxygen by ferrous iron results in the formation of free radicals — potent oxidants that attack proteins, carbohydrates, and nucleic acids, and trigger lipid peroxidation and apoptosis (Sousa *et al.,* 2019). Organisms have not yet developed mechanisms to prevent toxicity of free iron.

Iron has three major compartments that describe iron status: iron stores, transport iron, and functional iron (Pfeiffer & Looker, 2017). Excess iron saturates iron stores and exists in the form of ferritin and haemosiderin (Yiannikourides & Latunde-Dada, 2019). The depletion of total body iron is termed iron deficiency (Camaschella, 2015). Crucial metabolic processes such as DNA replication and energy production are sustained by iron (Farthing, 1989; Gonçalves *et al*., 2019). Altered body iron content and/or disorders related to iron deficiency lead to a broad spectrum of diseases (Sousa *et al.,* 2019). Hence, cellular iron concentrations require strict regulation (Puntarulo, 2005). An average adult with a normal diet, will have a total iron body content of 3–4 g, distributed among functional compounds, transporter chelates, and storage complexes (Puntarulo, 2005).

2.2.1 Homeostasis

Iron balance must be cautiously regulated to avoid deleterious effects of iron overload or iron deficiency (Provan & Gribben, 2010). The human body has no effective way of excreting iron. Thus, regulation of iron absorption plays a critical role in iron homeostasis (Muñoz *et al*., 2009). Regulation involves cellular import, export and partitioning (Provan & Gribben, 2010). Under steady-state conditions, iron absorption balances the daily loss of iron by exfoliation of epithelial surfaces and microscopic bleeding (Ganz, 2019). Iron stores regulate internal absorption of iron. There are four known regulators of iron absorption. The iron store regulator increases absorption when there is iron deficiency and decreases when there is iron overload. The erythroid regulator can increase iron absorption many-fold when there is deficient iron for erythropoiesis – production of red blood cells. The hypoxia regulator elevates iron absorption in response to hypoxia. The inflammation regulator decreases iron absorption in response to inflammation (Provan & Gribben, 2010). The internal turnover of iron is essential to meet requirements for erythropoiesis (Muñoz *et al.*, 2009).

As everyone knows the human body cannot excrete excess iron, regulation of iron homeostasis relies on the translation/post-translation control of ferritin and transferrin receptor mRNA. In cells, iron responsive elements (IREs) – phylogenetically conserved hairpin structures, were originally identified in the 5'UTR of the mRNA encoding ferritin (Hentze *et al*., 1987). The IRE has two binding sites activated by elevated affinity for iron during starvation. Cytoplasmic proteins – iron regulatory proteins (IRP1 and IRP2), interact with IREs (Weiss, 2002). IRPs modulate translation and stability of the RNA. Ferroportin expression on the basolateral membrane of enterocytes controls the rate of iron influx through this transport system (Andrews & Ganz, 2019). Increased ferritin expression means that there is an increase in iron uptake, and the opposite is also true (Andrews & Ganz, 2019). Enterocytes have a relatively short life span and are transported the gut lumen once used (Andrews & Ganz, 2019).

Hepcidin partitions iron through post-translational degradation of the ferroportin (Andrews & Ganz, 2019). Hepcidin, a peptide consisting of 25 amino acids, is likely to be the main effector of iron stores, erythroid, hypoxia and inflammation (Provan & Gribben, 2010). The hepcidin-ferroportin interactions play an important role in the determination of the overall efficiency of iron (Andrews & Ganz, 2019). Hepcidin binds to ferroportin eliciting its endocytosis and degradation (Ganz, 2019). Factors affecting internal absorption (erythroid, inflammation, hypoxia and iron stores) affect hepcidin production. Internal absorption is inversely proportional to liver expression (Fleming & Bacon, 2005). In the enterocytes, internalisation of ferroportin results in the down regulation of iron absorption whilst in

hepatocytes it elevates iron storage (Fleming & Bacon, 2005). The global distribution of iron is depicted in the figure below (Michels *et al.,* 2015).

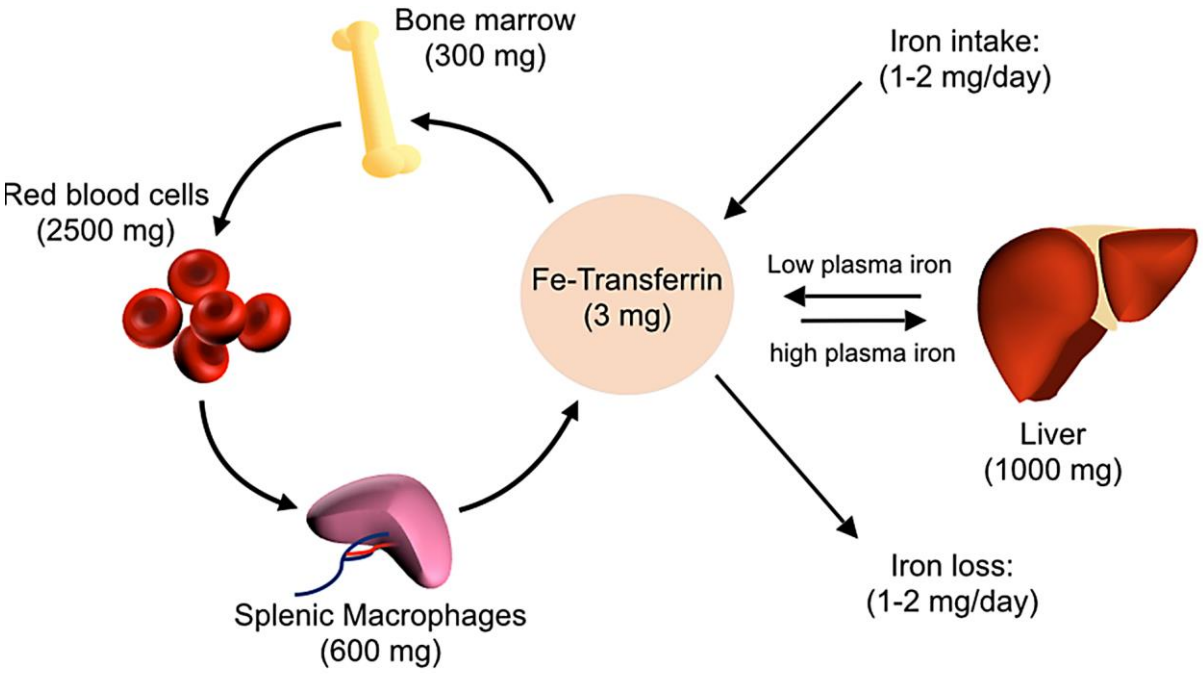

Figure 1: The normal global distribution of iron in a human body (Michels *et al*., 2015).

2.2.2 Absorption and transport

A healthy diet can provide adequate dietary iron. Cereals, nuts, shellfish, red meat and animal offal, especially liver, are the most important dietary sources of iron (Gonçalves *et al*., 2019). Almost all of iron absorption occurs in the duodenum. There are two chemical forms of dietary iron: heme (10%) and non-heme (90%) iron. Heme iron is found bound to porphyrin in meat (i.e. some enzymes, haemoglobin, myoglobin), and is bioavailable. Heme iron is transported from the small intestine lumen into the enterocytes by HCP1/PCFT, a protein localised in the apical part of the enterocyte plasmalemma (Milto *et al.,* 2016). Heme iron binds to this protein and induces receptor-mediated endocytosis. When inside the cell then heme iron is degraded. The transporter of heme iron is a (not yet totally identified) carrier protein that is in the proximal intestine, a site for elevated heme iron absorption (Muñoz *et al*., 2009). Non-heme iron is predominantly of vegetable origin (Lopez *et al*., 2016). Non-heme iron is in the oxidized state and is not bio-available, and therefore needs reduction to the Fe^{2+} state before it enters the intestinal epithelium (Milto *et al.,* 2016; Muñoz *et al*., 2009). The enzyme ferric reductase reduces Fe^{3+} to Fe^{2+} thus making it soluble. Once

it reaches the duodenum, the divalent metal transporter (DMT1) cotransports Fe^{2+} and H^{+} (Phelan *et al.,* 2018) from the lumen to the cytosol.

The iron exporter ferroportin-1 facilitates the movement of iron out of cells when required (Phelan *et al*., 2018). In the blood, Fe^{3+} binds to transferrin, which plays a pivotal role in iron dissemination by accepting the iron from parenchymal cells, mucosal cells from the intestines and reticuloendothelial cells and delivers it to the marrow (Harrison & Arosio, 1996). If ferrous iron is available, it is oxidised and transported (Kontoghiorghes, 2005). Under physiological conditions, the trivalent iron has high stability and complexes with transferrin (Milto *et al.,* 2016). Upon reaching the cell surface, the iron-laden transferrin binds to the transferrin receptor-1 on the cell surface (Abbaspour *et al.,* 2014). The transferrin bound iron and the iron transferrin receptor-1 enters the target cell by endocytosis. Fe^{3+} is released whilst transferrin and the receptor are recycled (Phelan *et al.,* 2018).

2.2.3 Serum iron

Iron in the blood is mostly found in two forms: transferrin-bound iron or non-transferrin-bound iron (NTBI) (Kohgo *et al.,* 2008).

2.2.3.1 Transferrin bound

In 1946, both serotransferrin and transferrin were isolated and purified simultaneously by independent groups (Crichton & Charloteaux-Wauters, 1987). Serum transferrin is true to iron transport and maintenance of iron homeostasis (WHO, 2014). Transferrin co-binds tightly but reversibly to ferric iron and two carbonate ions (Crichton, 2016). Iron overload is a condition whereby all transferrin is saturated, and this leads to organ damage through radical formation (Ito *et al.,* 2016). At neutral pH, serum has a high affinity for iron, and iron release is dependent on a specific membrane receptor (Worwood, 2002). Circulating serum transferrin receptor (sTfR) is a soluble form of the membrane receptor produced by proteolytic cleavage (Malope *et al*., 2001). Since the discovery of sTfR in human serum by Kohgo *et al.* (1986), it has been used as an indicator of functional iron deficiency and enhanced red cell production (Cook *et al.*, 1994).

2.2.3.2 Non-transferrin-bound iron (NTBI)

Transferrin molecules in the body are finite. Evidently, excess iron leads to complete saturation. From the name, NTBI can be defined as every form of iron in the blood bound to ligands other than transferrin (Breuer *et al.,* 2000a). NTBI has a trifold clinical significance: it is a potential target of iron chelators; it could serve as an indicator of the iron status of an

individual who is already iron overloaded or at risk; and it may participate as one of the causative factors of tissue loading with iron, which can lead to organ dysfunction (Breuer *et al.,* 2000b; Gosriwatana *et al.,* 1999).

2.2.3.3 Serum ferritin

Ferritin has been the cornerstone of iron storage measurements in clinical practice (Wang *et al.,* 2010). Infection, acute and chronic inflammation influence serum ferritin (Kohgo *et al.,* 2008). Serum ferritin is one of many important tests routinely ordered to diagnose and manage iron related conditions (Wang *et al.,* 2010). The normal ranges of serum ferritin are 10–220 µg/L in males and 10–85 µg/L in females (Kohgo *et al.,* 2008). Lower serum concentration can be due to iron deficiency (Kohgo *et al.,* 2008) and/or hyperferritinemia in rare cases, hereditary disorders that do not cause iron overload (Wang *et al*, 2010). On the other hand, high serum ferritin may be indicative of iron overload, inflammation, collagen disease, malignancy, and hepatic diseases (Kohgo *et al.,* 2008). Ferritin and hemosiderin concentrations together reflect the total body iron stores. Fe^{2+} is stored within ferritin light and heavy chains. Ferritin, a highly stable and symmetric protein, is adapted for iron storage since:

- It has a large cavity that can accommodate up to 4000 iron ions.
- It can attract iron and induce its mineralization.
- Iron is protected by a protein coat.

The main iron storage organ is the liver. Iron is released when serum iron concentration is lowered. The liver has an extremely large capacity to store iron, but it can be overloaded. Hence, the liver is the first organ to be damaged during iron overload.

2.3 Infectious diseases

2.3.1 The past, present and future

Despite the ground-breaking developments in technology and living conditions from the beginning of the last century, there has been an emergence of more than 300 infectious diseases (Jones *et al.,* 2008). The public health burden has increased despite the progress made in their prevention and control (Chowell & Rothenberg, 2018). Infectious diseases pose a profound impact on human life (Fauci & Morens, 2012). Throughout history,

infectious diseases have been the greatest threat to mankind (Oli *et al.,* 2006). The unpredictability and potential for an explosive global effect set them apart from other diseases (Fauci & Morens, 2012). Several infectious diseases are still a threat to date; the most recent being the COVID-19 pandemic.

2.3.2 Epidemiology

When and where is the next epidemic going to start? A question that can save millions of lives if answered correctly. As epidemiological approaches to infectious diseases are now diverse, high-throughput and near-real time genome sequencing is transforming infectious disease epidemiology. With all the technology in the world, there are unexplored territories within infectious disease epidemiology. Several types of infectious diseases, such as seasonal (e.g. childhood measles), faecal–oral infections (e.g. cholera), vector-borne diseases (e.g. malaria), and even sexually transmitted diseases e.g. gonorrhoea (Grassly & Fraser, 2006). According to Altizer *et al*. (2006), annual changes in host and parasite biology can bring about seasonal infectious diseases. The onset of infectious diseases can be adamant in the absences of therapy (Fauci & Morens, 2012). Seasonal changes evoke biological changes in hosts, pathogens and pathogens that determine the production rate of infected hosts (Altizer *et al.,* 2006). According to Altizer et al. (2006) there are multiple drivers that generate periodical variation in the host and pathogen biology that were discovered last century such as school terms, crop and livestock management.

There has been a devastating trend of infectious diseases emerging and re-emerging almost every year due to increased global population, aging, travel, urbanization, and climate change (Bloom *et al.,* 2017). Evidently, travel has accelerated exportation of epidemic SARS (a newly emerging disease) from Guangdong Province in China to Hong Kong, and from there to Beijing, Hanoi, Singapore, Toronto and elsewhere (Morens *et al*, 2004).

The incidence of infectious diseases is difficult to predict. In that regard, the next best thing is to investigate the common trends and their properties to reduce their impact. In the human body they each have unique destructive ramifications. In order to survive and reproduce, pathogens acquire raw materials (nutrients) from the hosts. Upon infection, the availability of the acquired raw materials within the host decreases resulting in their deficiency. Minerals, such as iron, are a good example of raw materials acquired by pathogens.

2.3.3 Iron content in infectious diseases

Iron is a crucial nutritional element for both humans and microbes (Cassat & Skaar, 2013). Most microbial agents are known to acquire iron from hosts (Weinberg, 2009). Hosts

withhold iron which is essential for invading microbial growth (Weinberg, 2009). Iron overload patients are not only affected by oxidative cell damage but also have high risk to infection (Cassat & Skaar, 2013). From a mammalian, biological point of view what matters the most is the total amount of iron and its speciation (Kell & Pretorius, 2014).

2.4 Current methods to measure body iron content

Why is body iron content so important? Accurate serum iron measurements are of paramount importance to provide comparability in diagnosis, treatment and monitoring of the condition at hand (Xu *et al.,* 2017). In Clinical practise, iron status plays an important role in the diagnosis of many diseases. Mostly it is done by looking at the symptoms that patients exhibit when there is iron overload or iron deficiency. Iron deficiency can be simply determined by . (a) Koilonychia: typical 'spoon' nails. (b) Angular cheilosis: fissuring and ulceration of the corner of the mouth (Hoffbrand & Moss, 2016). Severity and causes are usually confirmed by analysing blood smears under a microscope. Early stages of iron overload on the other hand are easily confirmed by melanin pigmentation of the skin (Hoffbrand & Moss, 2016).

The nature of NTBI in iron overload is largely unknown (Jacobs *et al*., 2005). To date there is still no universal method to assess it evidenced by Jacobs et al. (2005). NTBI is measured differently throughout the whole world using different approaches and practical application (Jacobs *et al*., 2005). Methods may differ but there are only 2 test principles. The first mobilises NTBI by a shuttle molecule, such as EDTA or nitrilotriacetic acid (NTA), followed by separation of the chelated iron from serum proteins (Loreal *et al.,* 2000). The products are ultra-filtered and then analysed using various technologies. Highly reliable results are obtained but are labour intensive to obtain (Jacobs *et al*., 2005).

The second principle involves assays that mobilizes and detects NTBI without separation of the serum proteins from chelated iron. The bleomycin method where Fe^{3+} is reduced to Fe^{2+} by adding bleomycin whilst quantifying the redox-active iron (Von Bonsdor *et al*., 2002). The complexes and degrades DNA. The degraded products are measured by colorimetric assays to quantify iron since they are proportional to iron present. Jacobs et al. (2005) states that this assay can be influenced by other serum substances and there is no guarantee that all the iron will be reduced.

Total body iron burden assessment is a critical part in the evaluation of hemochromatosis patients (Beutler *et al.,* 2001). Total body iron can be assessed by the total iron binding capacity (TIBC), which is a measure of the total amount of iron saturated in serum transferrin (Yamanishi *et al.,* 1997). Several serum-based indicators (such as: serum ferritin, transferrin saturation, and soluble serum transferrin receptor (sTfR), as well as erythrocyte protoporphyrin) can be used to assess iron status (Pfeiffer & Looker, 2017).

2.4.1 Serum transferrin as a quantitative iron measure

Normally, serum transferrin is the only non-heme form of iron. Only 20–35% serum transferrin is saturated (Gosriwatana *et al.,* 1999). Soluble serum transferrin receptor (sTfR) plays a major role in iron delivery to all tissues. Tissue iron requirements are reflected by the receptor (Looker *et al*., 1999; Speeckaert *et al.,* 2011). sTfR is neither an acute-phase reactant nor a sensitive iron deficiency indicator (Punnonen *et al.,* 1994). Punnonen et al. (1994) suggests that sTfR can be used to distinguish between iron deficiency anaemia (IDA) and anaemia of chronic disease (ACD). STfR is affected by IDA. IDA increases sTfR concentration whilst ACD does not (Infusino *et al., 2012)*. The first immunological sTfR assays were immunoradiometric assays (IRMA), enzyme-linked immunosorbent assays (ELISA), immunonephelometry and immunoturbidimetry (Speeckaert *et al.,* 2011). As of late, many sTfR assays have been developed. Unlike transferrin and ferritin, the major limitation of sTfR is that it is affected by inflammation (Infusino *et al.,* 2012*)*.

2.4.2 Serum non-transferrin-bound iron assessments

Non-transferrin-bound iron (NTBI) can be quantified by many assays. According to Jacobs et al. (2005) there are two approaches towards quantifying serum NTBI. 1) Mobilize NTBI by a shuttle molecule, such as NTA or EDTA, followed by isolation of the iron molecule from the serum proteins. 2) Mobilize and detect NTBI in the reaction mixture without isolating serum proteins from chelated iron. Both principles have their disadvantages with the first being labor intensive and the second being influence by other iron-like substances (Jacobs *et al.,* 2005). Inaccuracy due to partial mobilization of transferrin bound iron and lack of specificity and insensitivity also affect NTBI assays (Gosriwatana *et al.,* 1999).

2.4.3 Serum ferritin

Human serum ferritin concentration is usually associated with iron stores (Kell & Pretorius, 2014). In clinical practice human serum ferritin and iron stores are measured alongside to indicate iron status of a patient (Knovich *et al.,* 2009). Lower serum ferritin has been found in hypothyroidism and ascorbate deficiency (Knovich *et al.,* 2009). Serum ferritin, however, has

several pitfalls as an iron quantification method. 1.) It is an acute phase reactant meaning it is affected by inflammation. 2) A high quantity of sample is required, which can be troublesome, especially if the patient is an infant. According to Burns *et al.* (1990) serum ferritin lack sensitivity and specificity to diagnose iron deficiency. Hence a battery of tests has been long sought. Most of the tests have significant limitations since neither mean corpuscular volume nor expert evaluation of a peripheral blood smear has enough sensitivity; and the TIBC and transferrin saturation lack specificity (Burns *et al.,* 1990).

2.4.4 Laboratory gold standard

In chemistry, inductively coupled plasma-mass spectrometry (ICP-MS) one of the most efficient tools primarily, due to its high sensitivity. ICP-MS can quantify analytes as low as ng/mL or low µg/mL concentration range in samples (Harrington *et al*., 2014). According to D'Ilio et al. (2011), one major disadvantage of ICP-MS is the occurrence of mass interferences, caused by atomic or polyatomic species having the same mass/charge ratio of the analyte. Consequently, it can only report Fe instead of Fe^{2+} and Fe^{3+}. Despite the maturity of ICP-MS, the procedure depends on the elements being determined, concentration levels and desired sample throughput. The matrix composition of serum with high salt and protein (6–8%) concentrations is too complex to be analysed directly by ICP-MS. Hence, for ICP-MS analysis, the sample must be treated by either sample dilution or digestion (Abduljabbar *et al.,* 2019).

2.5 ^{1}H-NMR spectroscopy

Nuclear magnetic resonance (NMR) spectroscopy is one of the information-rich technologies that give atomic-specific information and has earned its place thereof (Keun *et al.,* 2002). It is a powerful technique capable of concurrently quantifying and identifying biofluid metabolites (Sinclair *et al.,* 2010). The basic principle behind ^{1}H-NMR is that a proton has a charge and a spin. Its spin results in the generation of a nuclear magnetic dipole therefore protons can be described as elementary magnets (Holzgrabe, 2017). In the absence of an applied magnetic field the spin direction of protons is random; however, when placed within an applied magnetic field they snap into place along the field lines. Some snap into a parallel (energetically favourable) state and others into an antiparallel state.

When protons are pulsed with precisely tuned radio frequency, they all go into an antiparallel (energised) state: this stage it is said the nuclei is in resonance with the radiation. Turning off the radio frequency returns the nuclei to their energetically favourable (parallel) state, a

process known as precession. The NMR probe contains a coil surrounding the sample that can detect, amplify and process energy released by the protons, known as of Free Induction Decay (FID). The frequency at which a given nucleus resonates is dependent on its chemical environment. Thus, spectroscopists can deduct from a spectrum which atoms are bound to which, and what atoms are located nearby. Fourier transformation converts the FID from time domain to frequency domain to produce the NMR spectra.

Its value for structural and quantification analysis is attributed to its element selective detection, sensitivity to nuclear spin properties to the intra and inter-molecular environment and to the quantitative and robust nature of NMR measurement (Fan *& Lane,* 2016). NMR was chosen as the analytical platform for my project due to its repeatability and reproducibility. NMR contributes immensely to metabolomics-based projects as it has many advantages over MS (Markley *et al*., 2017).

Advantages of NMR over MS:

- Simple sample preparation: can analyse biofluids, cell extracts and tissues without the need for elaborate sample preparation or fractionation. After analysis the samples can be analysed in other technologies without altering the original state.
- Robust and global look at the metabolome: it is nonbiased and can analyse compounds that are difficult to ionize (LC-MS) or derivatize (GC-MS).
- Lower running costs: the initial costs of setup are expensive but NMR analysis per sample is cheap.
- Highly selective: fewer metabolites are identified via NMR but with higher confidence than MS. NMR can identify compounds with identical masses but with different isotopomer (isomers that have different distributions of isotope) distributions.
- NMR has an unparalleled level of high reproducibility and repeatability.

The major limitation of NMR is its spectral resolution (i.e. lower sensitivity than MS counterpart), but this can be improved upon by experimenting at higher magnetic field strengths, and using more sensitive cryo-probes (Reo, 2002).

NMR based metabolic profiling as infectious disease diagnostic tool

Metabolomics studies have proved useful in the diagnosis of various infectious diseases. According to Silva et al (2020) NMR-based metabolomics was used to diagnose various

infectious diseases including individuals with sepsis and septic shock. Before and during the development of clinical symptoms most human diseases have characteristic modifications in the metabolite profiles (Lussu *et al*., 2017).). The most used detection samples for biomarkers are urine, blood, saliva and diseased tissue (Song *et al*., 2018). Metabolomics monitors changes in the concentration of small metabolites in tissues and biofluids (Nicholson *et al*., 1999). These changes in turn provide useful information in response to diseases as biomarkers (Blakebrough-Hall *et al*. 2020). With the aid of multivariate multivariable prediction model NMR has been able to diagnose diseases using biomarkers to an accuracy of 99.5% (Lussu *et al*., 2017).

Alternatively, Identification of microbial species is pivotal for infectious disease diagnoses . Palama et al. (2016) showed that ^{1}H-NMR-based can rapidly discriminate and identify several bacterial species that relies on untargeted metabolic profiling of supernatants from bacterial culture media. They proposed diagnosing infectious diseases by identifying microbial species. Combined with the fact that NMR provides faster and more comprehensive assessment of the biological samples in human models(Silva *et al,* 2020) this is no longer an impossible task.

Why use NMR?

NMR has proved capable across pharmaceutical and biomedical fields (Lodge *et al*., 2021). Over the years there has been exponential improvement in NMR due to higher field strengths and its applications have followed suit (Webster & Kumar, 2014). According to Webster and Kumar (2014) there is a paradigm shift in the pharmaceutical industry from chromatography to NMR especially in the early drug development stages. NMR provides more accurate and precise than standard HPLC methods (Holzgrabe *et al*., 2005). Moreover, iron analysis using chromatography requires complicated sample preparation to avoid contamination in the column that may contain iron. Obviously, in the NMR there is no column hence no contamination of results. As stated in literature iron exists bound to other molecules in biofluids. Iron can be quantified directly or indirectly in biofluids. There is no need to remove impurities in NMR as they can provide extra information regarding the sample being analysed (Holzgrabe *et al*., 2005). NMR produces qualitative and quantitative data, to detect a great variety of metabolites even at low concentrations in a non-destructive manner (Silva *et al*, 2020). It is a quick, economic technology that can determine potency without having a standard (Webster & Kumar, 2014) and easy to perform leading to high

reproducibility (Holzgrabe et al., 2005). Most importantly NMR is a green analytical technique meaning there is no CO_2 produced (Webster & Kumar, 2014)

To better understand the strengths of NMR one must know its limitations. Low sensitivity has been well documented in literature. Fortunately, low sensitivity can be overcome by:

- Using high field strength (≥ 600)
- increasing the number of scans
- precise (gradient) shimming techniques
- using inverse and cryo probes which increase the signal to-noise ratio (by a factor of about 10)
- maximizing of concentration and optimizing solvent volume

2.5.1 Chelation NMR

Only specific metabolites containing a hydrogen linked to carbon can be analysed with ^{1}H-NMR. Iron on its own is invisible on the ^{1}H-NMR but when in complex with a visible molecule, such as an iron chelator, then iron becomes visible on the ^{1}H-NMR spectrum. Iron chelators produce an unique ^{1}H-NMR spectral pattern. When in chelation with iron there is a change in 3D conformation. The 3D conformation change also changes the resulting ^{1}H-NMR spectral pattern.

2.5.1.1 Ethylenediaminetetraacetic acid (EDTA)

EDTA is one of the most studied chelating agents. Owing to its ability to chelate both transition metals and main group elements at different pH values (Panda & Chaudhuri, 2007), it has a wide range of applications. Ubale (2010) describes EDTA as an amino derived organic compound that is a strong hexadentate chelating agent. EDTA chelates metals ions to form highly stable complexes which dissociate gradually (Ubale, 2010). Structurally, EDTA is a linear molecule that folds around a metal cation during chelation. An example of how chelation of EDTA with a metal ion results in the formation of a complex with a unique 3D conformation is shown in Figure 2. It's four carboxylic and two amine groups, with an unshared pair of electrons, gives EDTA a coordination number of 6 (Mohammadi *et al*., 2013). The chelated metal ion remains in solution, but its reactivity is diminished (Mohammadi *et al*., 2013). As a result of diminished reactivity, the amount of metal ions in solution decreases consequently.

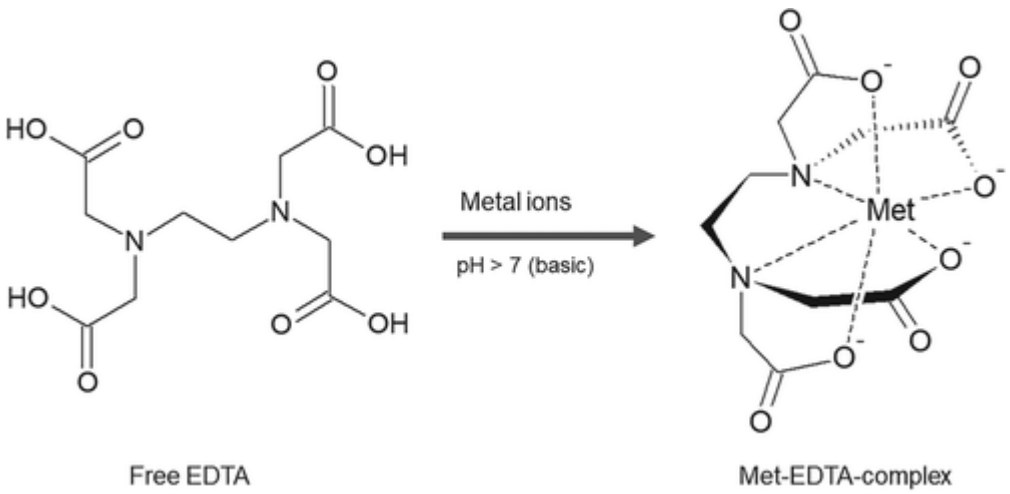

Figure 2: 3D Conformational change in the EDTA structure during chelation (Hafer *et al*., 2020)

Low EDTA concentration in solution elevates availability and solubility of many metals (Ubale, 2010). The ability of EDTA to sequester trivalent and divalent ions enables it to play various crucial roles in our everyday lives (Mohammadi *et al*., 2013). EDTA is used in both environmental and biomedical fields to remove/eliminate heavy metals. In haematological studies, EDTA is attached to the blood collection tubes and prevents clotting. Free EDTA is expected to produce 2 clear single peaks in the ^{1}H-NMR spectrum – a singlet at 3.65ppm (represented by 4 protons) and another singlet at 3.88ppm (represented by 8 protons), at pH 7.0.

Deferoxamine (DFO)

More than half a century ago, a compound, which will later save countless lives, was characterized (Codd *et al*., 2018). It was discovered that the compound belonged to a group of compounds with high affinity for iron known as siderophores – low molecular weight compounds with high affinity for iron (III) (Hider & Kong, 2010). From all the siderophores that were isolated and identified from 1949 – 1972, ferrioxamine was the most stable (Hider & Kong, 2010), with a stability constant of about 10^{31} (Tian *et al*., 2016). Taking the high stability constant, DFO can mobilize iron at low concentrations. Since the ground-breaking discovery of DFO, its effects have been studied both *in vitro* and *in vivo*. Studies, such as Yu *et al*. (2017), agree that DFO is a free radical scavenger.

DFO chelation of iron in iron overload has been well documented in literature (Breuer *et al*., 2000a). DFO has been used in clinical practice for more than four decades in iron overload conditions (Selim, 2008). Thalassemia is an autosomal inherited disease resulting in failure

to synthesize hemoglobin; hence, iron overload. Failure to administer DFO injections in such cases can lead to mortality (Marmion *et al*., 2004). Unfortunately, DFO is large and hydrophilic in nature hence it cannot cross membranes easily (Dayani *et al*., 2004), and it has a short plasma half-life.

As shown in Figure 3, DFO is a linear molecule that contains C-H bonds; hence, it can be analyzed by ^{1}H-NMR spectroscopy. At pH 7.0, free DFO is expected to produce 2 triplet peaks in the ^{1}H-NMR spectrum at 2.00ppm and 2.80ppm, assigned to protons of -CH_3 and CH_3-SO_3H, respectively. Figure 3 shows the ^{1}H-NMR spectra produced by pure DFO. Ferrioxamine, like EDTA, changes its 3D conformation into one that is circular, around a ferric iron. Ferrioxamine is not present in any online ^{1}H-NMR pure compound database, nor is FOB's ^{1}H-NMR spectral pattern described in literature; but this molecule is expected to produce a different spectral pattern than DFO, of which I intend to identify and quantify in my study.

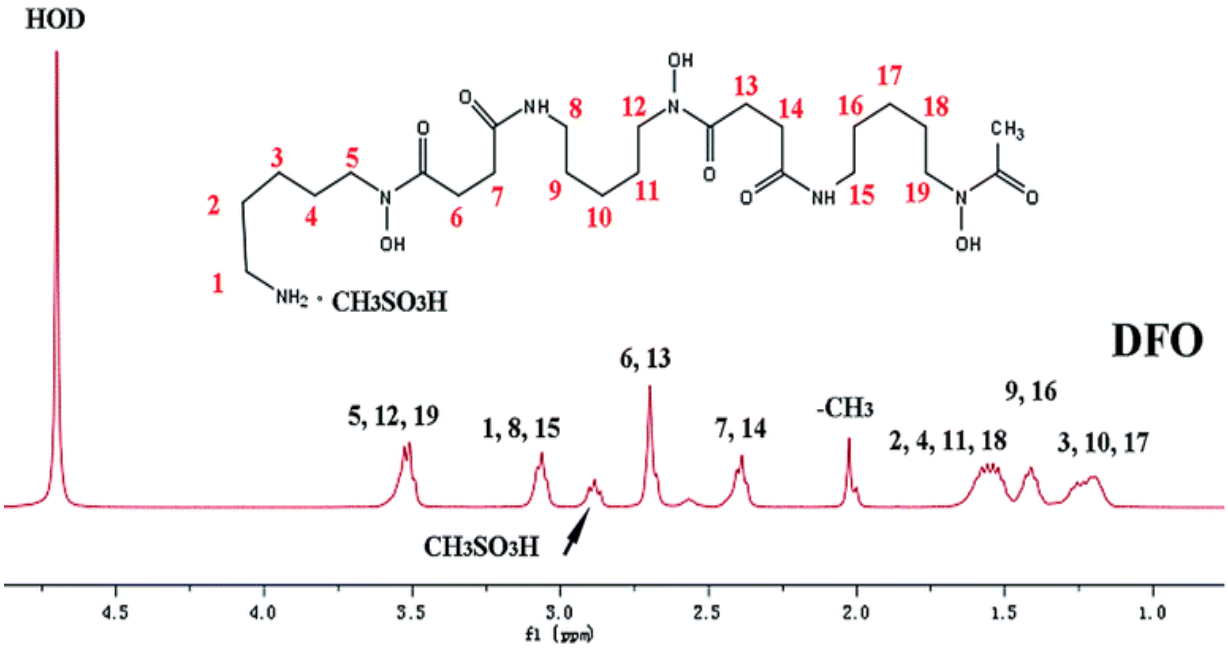

Figure 3: ^{1}H NMR spectra of free DFO (Tian *et al*., 2016).

Problem statement

Serum is the primary carrier of molecules in the body and its usefulness in the diagnosis of infectious diseases is paramount (Zhang *et al*., 2012). No other bio-fluid has been more intensively studied and more advantageous than serum (Psychogios *et al.,* 2011). It is easily accessible in large volumes and is information rich. It has the means to identify the changes in metabolites that take part in biochemical processes hence illuminating the biological processes (MacIntyre *et al.,* 2010). Accurate serum iron measurements are crucial for global comparability in diagnosis, treatment and monitoring of infectious diseases (Xu *et al*., 2017). Currently, there exists various chemistry-based methods to quantify levels of iron, including atomic absorption spectrometry, flow injection, gold nanoclusters sensing and the gold standard of ICP-MS (Hourani *et al*., 2018). However, these existing analytical methods are expensive and time-consuming, involve complex sample preparation, and are not designed to specifically analyse iron in biological samples (such as serum) – often requiring at least 1 mL sample, which is not practical within serum metabolomics research projects as volume is limited (Xu *et al*., 2017). ^{1}H-NMR is a quick and highly repeatable method that is good at absolute quantification, does not require expensive isotopic standards and can analyse lower volumes (100 µL) of serum. Hence, there is a need to develop and apply a ^{1}H-NMR method to quantify levels of iron in serum that is quick, cheap and requires minimal sample volume.

Aim

Developing a quantitative ^{1}H-NMR method that will potentially add to the existing array of information obtained from ^{1}H-NMR serum metabolomics studies by including serum iron concentrations.

Objectives

1. Assess the concept of chelation NMR as a quantitative ^{1}H-NMR method for biologically important ions using EDTA as a chelating agent.

    - Use B.Sc. Hons work (2019) “Method development of ^{1}H-NMR analysis of biologically important ions (Fe, K and Ca) - theoretical application to biofluids

- , perform additional experiments and publish results under the title: “EDTA as a chelating agent in quantitative ^{1}H-NMR of biologically important ions”.

1. Draw conclusions of the use of EDTA as a chelating agent for iron.
2. Further develop the concept of chelation NMR as a quantitative ^{1}H-NMR method for iron using DFO as a chelating agent using pure compounds.
    - Determine what, if any, catalyst(s) are required for chelation.
    - Optimize chelation by stress testing pH, incubation temperature and time.
    - Determine linearity, accuracy, precision and repeatability by performing 3 repeat analyses at various concentration levels determined as ±25%, 50%, 75% of the lower and upper normal physiological ranges of iron in the blood.
3. Apply developed quantitative ^{1}H-NMR method to spiked serum samples
    - Acquire NWU-HREC approval, collect blood samples from volunteers and create a pooled serum sample (~100 mL).
    - Create serial spiked serum samples, each with a known iron concentration.
    - Assess repeatability, linearity, accuracy and precision of newly developed quantitative ^{1}H-NMR method.
    - Use other spectrophotometric methods (e.g. UV spectrophotometry) as alternative method of iron quantification and compare results.
4. Report results of quantitative ^{1}H-NMR method of iron in serum using DFO as a chelating agent in the form of a submitted manuscript.
5. Discuss overall results of MSc study and provide insight on the experimental challenges.

References

Abbaspour, N., Hurrell, R. & Kelishadi, R. 2014. Review on iron and its importance for human health. *Journal of Research in Medical Sciences*, *19*(2):164–174.

Abduljabbar, T.N., Sharpb, B.L., Reidb, H.J., Barzegar-Befroeidc, N., Petod, T. & Lengyelc, I. 2019. Determination of Zn, Cu and Fe in human patients' serum using micro-sampling ICP-MS and sample dilution. *Talanta*, *204*:663–669.

Altizer, S., Dobson, A., Hosseini, P., Hudson, P., Pascual, M. & Rohani, P. 2006. Seasonality and the dynamics of infectious diseases. *Ecology Letters*, *9*:467–484.

Andrews, N.C. & Ganz, T., 2019. The molecular basis of iron metabolism. *Molecular Hematology*, pp.161-172.

Beutler, E., Felitti, V., Ho, N.J. & Gelbart, T. 2002. Relationship of body iron stores to levels of serum ferritin, serum iron, unsaturated iron binding capacity and transferrin saturation in patients with iron storage disease. *Acta Haematologica*, *107*(3):145–149.

Blakebrough-Hall, C., Dona, A., D'occhio, M.J., McMeniman, J. & González, L.A. 2020. Diagnosis of Bovine Respiratory Disease in feedlot cattle using blood ^{1}H NMR metabolomics. *Nature Scientific Reports*.10:115-127.

Bloom, D.E., Black, S. & Rappuoli, R. 2017. Emerging infectious diseases: a proactive approach. *Proceedings of the National Academy of Sciences*, *114*(16):4055–4059.

Breuer, W., Hershko, C. & Cabantchik, Z.I. 2000a. The importance of non-transferrin bound iron in disorders of iron metabolism. *Transfusion Science*, *23*(3):185–192.

Breuer, W., Ronson, A., Slotki, I.N., Abramov, A., Hershko, C. & Cabantchik, Z.I. 2000b. The assessment of serum nontransferrin-bound iron in chelation therapy and iron supplementation. *Blood, 95*(9):2975–2982.

Burns, E.R., Goldberg, S.N., Lawrence, C. & Wenz, B. 1990. Clinical utility of serum tests for iron deficiency in hospitalized patients. *American Journal of Clinical Pathology*, *93*(2):239–245.

Camaschella, C. 2015. Iron-deficiency anaemia. *New England Journal of Medicine*, *372*(19):1832-1843.

Cassat, J.E. & Skaar, E.P. 2013. Iron in infection and immunity. *Cell host & microbe*, *13*(5): 509-519.

Chin, C.D., Laksanasopin, T., Cheung, Y.K., Steinmiller, D., Linder, V., Parsa, H., ... & Karita, E. 2011. Microfluidics-based diagnostics of infectious diseases in the developing world. *Nature Medicine*, *17*(8):1015.

Chowell, G. & Rothenberg, R. 2018. Spatial infectious disease epidemiology: on the cusp, 1-5.

Codd, R., Richardson-Sanchez, T., Telfer, T.J. & Gotsbacher, M.P. 2018. Advances in the chemical biology of desferrioxamine B. *ACS Chemical Biology*, *13*(1):11-25.

Cook, J.D., Baynes, R.D. and Skikne, B.S. 1994. The physiological significance of circulating transferrin receptors. *Nutrient regulation during pregnancy, lactation, and infant growth*, 119-126.

Crichton, R. 2016. *Iron metabolism: from molecular mechanisms to clinical consequences*. John Wiley & Sons.

Crichton, R.R. and Charloteaux-Wauters, M. 1987. Iron transport and storage. *European Journal of Biochemistry*, *164*:485-506.

D'Ilio, S., Violante, N., Majorani, C. and Petrucci, F. 2011. Dynamic reaction cell ICP-MS for determination of total As, Cr, Se and V in complex matrices: Still a challenge? A review. *Analytica Chimica Acta*, *698*(1-2):6-13.

Dayani, P.N., Bishop, M.C., Black, K. & Zelter, P.M. 2004. Desferoxamine (DFO)–mediated iron chelation: rationale for a novel approach to therapy for brain cancer. *Journal of Neuro-Oncology*, 67(3):367-377.

Eybpoosh, S., Haghdoost, A.A., Mostafavi, E., Bahrampour, A., Azadmanesh, K. & Zolala, F. 2017. Molecular epidemiology of infectious diseases. *Electronic Physician*, 9(8):5149-5158.

Fan, T.W.M. & Lane A.N. 2016. Applications of NMR spectroscopy to systems biochemistry. *Progress in Nuclear Magnetic Resonance Spectroscopy*, 92:18-53.

Farthing, M.J. 1989. Iron and immunity. *Acta Paediatrica*, 78: 44-52.

Fauci, A.S. & Morens, D.M. 2012. The perpetual challenge of Infectious diseases. *The New England and Journal of Medicine*, 66:454-61.

Fernández-Carballo, B.L., Broger, T., Wyss, R., Banaei, N. & Denkinger, C.M. 2019. Toward the development of a circulating free DNA-based in vitro diagnostic test for infectious diseases: a review of evidence for tuberculosis. *Journal of Clinical Microbiology*, *57*(4).

Flaschka, H.A. 2013. *EDTA* titrations: an introduction to theory and practice. *Elsevier*.

Fleming, R.E. & Bacon, B.R. 2005. Orchestration of iron homeostasis. *The new England Journal of Medicine*, 352(17):1741-1744.

Gonçalves, J.L., Silva, M.C.A., Roma, E.H., Grinsztejn, B., dos Santos de Lemos, A., Moreira, N.G. & de Brito, P.D. 2019. Iron intake is positively associated with viral load in antiretroviral naïve Brazilian men living with HIV. *Memórias do Instituto Oswaldo Cruz*, 114.

Gosriwatana, I., Loreal, O., Lu, S., Brissot, P., Porter, J. & Hider, R.C. 1999. Quantification of Non-Transferrin-Bound Iron in the presence of unsaturated transferrin. *Analytical Biochemistry,* 273: 212-220.

Grassly, N.C. & Fraser, C. 2006. Seasonal infectious disease epidemiology. *Proceedings of the royal society* B, 273: 2541–2550.

Grauslys, A., Phelan, M.M., Broughton, C., Baines, P.B., Jennings, R., Siner, S., … Carrol, E.D. 2020. NMR-based metabolic profling provides diagnostic and prognostic information in critically ill children with suspected infection. *Nature*, 10(20198):1-12.

Harrison, P.M., & Arosio, P. 1996. The ferritins: molecular properties, iron storage function and cellular regulation. *Biochimica et Biophysica Acta (BBA)-Bioenergetics*, 1275(3):161–203.

Hentze, M.W., Caughman, S.W., Rouault, T.A., Barriocanal, J.G. DancIs, A. Hauof J.B. & Klausner, R.D. 1987. Identification of the iron-responsive element for the translational regulation of human ferritin mRNA. *Science*, 238(4833):1570-1573.

Hider, R.C. & Kong, X. 2010. Chemistry and biology of siderophores. *Natural Product Reports*, *27*(5):637-657.

Hoffbrand, A.V. & Moss, P.A.H. 2016. Hoffbrand's Essential Haematology. John Wiley & Sons Ltd. 7th ed.

Holzgrabe, U. 2017. NMR spectroscopy in pharmaceutical analysis, *Elsevier*.

Holzgrabe, U., Deubner, R., Schollmayer, C. & Waibel, B. 2005. Quantitative NMR spectroscopy—Applications in drug analysis*. Journal of Pharmaceutical and Biomedical Analysis,* 38:806–812.

Infusino, I., Braga, F., Dolci, A. & Panteghini, M. 2012. Soluble Transferrin Receptor (sTfR) and sTfR/log FerritinIndex for the Diagnosis of Iron-Deficiency Anemia. *American Society for Clinical Pathology.* 138:642-649.

Ito, S., Ikuta, K., Kato, D., Lynda, A., Shibusa, K., Niizeki, N., ... Iizuka, N. 2016. In vivo behavior of NTBI revealed by automated quantification system. *International Journal of Hematology*, *104*(2):175-181.

Jacobs, A., Beamish, M.R. & Allison, M. 1972. The measurement of circulating ferritin. *Journal of Clinical Pathology*, *25*(11):1003.

Jacobs, E.M., Hendriks, J.C., van Tits, B.L., Evans, P.J., Breuer, W., Liu, D.Y., ... Scheiber-Mojdehkar, B. 2005. Results of an international round robin for the quantification of serum non-transferrin-bound iron: need for defining standardization and a clinically relevant isoform. *Analytical Biochemistry*, *341*(2):241-250.

Jones, K.E., Patel, N.K., Levy, M.A., Storeygard, A., Balk, D., Gittleman, J.L. & Daszak, P. 2008. Global trends in emerging infectious diseases. *Nature*, 541:990-994.

Kell, D.B. & Pretorius, E. 2014. Serum ferritin is an important inflammatory disease marker, as it is mainly a leakage product from damaged cells. *Metallomics*, *6*(4):748-773.

Keun, H.C., Ebbels, T.M., Antti, H., Bollard, M.E., Beckonert, O., Schlotterbeck, G., … Nicholson, J.K. 2002. Analytical reproducibility in ^{1}H NMR-based metabonomic urinalysis. *Chemical Research in Toxicology*, *15*(11):1380-1386.

Knovich, M.A., Storey, J.A., Coffman, L.G., Torti, S.V. & Torti, F.M. 2009. Ferritin for the clinician. *Blood Reviews*,*23*(3):95-104.

Kohgo, Y., Ikuta, K., Ohtake, T., Torimoto, Y. & Kato, J. 2008. Body iron metabolism and pathophysiology of iron overload. *The Japanese Society of Hematology*. 88:7–15.

Kohgo, Y., Nishisato, T., Kondo, H., Tsushimay, N., Iitsu O. & Rushizak. I. 1986. Circulating transferrin receptor in human serum. *British Journal* of *Haematology*, 64: 277-281.

Lodge, S., Nitschke, P., Loo, R.L., Kimhofer, T., Bong, S., Richards, T., … Nicholson, J.K. 2021. Low Volume in Vitro Diagnostic Proton NMR Spectroscopy of Human Blood Plasma for Lipoprotein and Metabolite Analysis: Application to SARS-CoV-2 Biomarkers. *Journal of Proteome Research, 20: 1415-1423.*

Looker, A.C., Loyevsky, M. & Gordeuk, V.R. 1999. Increased serum transferrin saturation is associated with lower serum transferrin receptor concentration. *Clinical Chemistry* 45(12):2191–2199.

Lopez, A., Cacoub, P., Macdougall, I.C. & Peyrin-Biroulet, L. 2016. Iron deficiency anaemia. *Lancet*, 387:907–16.

Loreal, O., Gosriwatana, I., Guyader, D., Porter, J., Brissot, P. & Hider, R.C. 2000. Determination of non-transferrin-bound iron in genetic hemochromatosis using a new HPLC-based method. *Journal of Hepatology*, 32:727–733

Lussu, M., Camboni, T., Piras, C., Serra, C., Del Carratore, F., Griffin, J., … Manzin, A. 2017. H NMR spectroscopy-based metabolomics analysis for the diagnosis of symptomatic E. coli-associated urinary tract infection (UTI). *Bio Med Central Microbiology*, 17:201-208.

MacIntyre, D., Jimenez, B., Lewintre, E.J., Martín, C.R., Schäfer, H., Ballesteros, C.G.... Pineda-Lucena, A. 2010. Serum metabolome analysis by ^{1}H-NMR reveals differences between chronic lymphocytic leukaemia molecular subgroups. *Leukemia*, 24(4):788-797.

Malope, B.I., MacPhail, A.P., Alberts, M. and Hiss, D.C. 2001. The ratio of serum transferrin receptor and serum ferritin in the diagnosis of iron status. *British Journal of Haematology*, *115*(1):84-89.

Markley, J.L., Bru¨ schweiler, S., Edison, R.A., Eghbalnia, H.R., Powers, R., Raftery, D. & Wishart, D.S. 2017. The future of NMR-based metabolomics. *Current Opinion in Biotechnology*, 43:34-40.

Marmion, C.J., Griffith, D. & Nolan, K.B. 2004. Hydroxamic acids− an intriguing family of enzyme inhibitors and biomedical ligands. *European Journal of Inorganic Chemistry*, *2004*(15):3003-3016.

Michels, K., Nemeth, E., Ganz, T. & Mehrad, B. 2015. Hepcidin and host defense against infectious diseases. *PLOS Pathogens*, 11(8):1004998.

Miller, J.M., Binnicker, M.J., Campbell, S., Carroll, K.C., Chapin, K.C., Gilligan, P.H., … Yao, J.D. 2018. A Guide to Utilization of the Microbiology Laboratory for Diagnosis of Infectious Diseases: 2018 Update by the Infectious Diseases Society of America and the American Society for Microbiology. *Clinical Infectious Diseases*, 67(6):1–94.

Milto, I.V., Suhodolo, I.V., Prokopieva, V.D. & Klimenteva, T.K. 2016. Molecular and cellular bases of iron metabolism in humans. *Biochemistry (Moscow)*, 81(6):549-564.

Mohammadi, Z., Shalavi, S. and Jafarzadeh, H. 2013. Ethylenediaminetetraacetic acid in endodontics. *European Journal of Dentistry*, *7*(1):S135.

Morens, D.M., Folkers, G.K. & Fauci, A.S. 2004. The challenge of emerging and re-emerging infectious diseases. *Nature*, 430:243-249.

Muñoz, M., Villar, I. & García-Erce, J.O. 2009. An update on iron physiology. *World Journal of Gastroenterology*. *WJG*, 15(37):4617.

National Toxicology Program, 1977. Bioassay of trisodium ethylenediaminetetraacetate trihydrate (EDTA) for possible carcinogenicity (CAS No. 150-38-9). *National Cancer Institute Carcinogenesis Technical Report Series*, *11*:1.

Nicholson, J. K., Lindon, J. C. & Holmes, E. 1999.'Metabonomics': understanding the metabolic responses of living systems to pathophysiological stimuli via multivariate statistical analysis of biological NMR spectroscopic data. *Xenobiotica*, 29:1181–1189.

Palama, T.L., Canard, I., Rautureau, G.J.P., Mirande, C., Chatellier, S. & Elena-Herrmann, B. 2016. Identification of bacterial species by untargeted NMR spectroscopy of the exo-metabolome. : *Analyst*, 141, 4558-4561.

Panda, S.K., & Chaudhuri, S. 2007. Chelating ligand-mediated synthesis of hollow ZnS microspheres and its optical properties. *Journal of Colloid and Interface Science*, 313(1):338–344.

Pang, T. & Peeling, R.W. 2007. Diagnostic tests for infectious diseases in the developing world: two sides of the coin. *Transactions of the Royal Society of Tropical Medicine and Hygiene*, *101*(9):856-857.

Pfeiffer, C.M. & Looker, A.C. 2017. Laboratory methodologies for indicators of iron status: strengths, limitations, and analytical challenges. *The American Journal of Clinical Nutrition*, 106(6):1606S-1614S.

Phelan, J.J., Basdeo, S.A., Tazoll, S.C., McGivern, S., Saborido, J.R. & Keane, J. 2018. Modulating iron for metabolic support of TB host defence. *Frontiers in Immunology*, 9:2296.

Přibil, R. 2013. Analytical applications of EDTA and related compounds: *International Series of Monographs in Analytical Chemistry* (52). Elsevier.

Provan, D. & Gribben, J. eds. 2010. *Molecular Hematology*. John Wiley & Sons.

Psychogios, N., Hau, D.D., Peng, J., Guo, A.C., Mandal, R., Bouatra, S., ... & Young, N. 2011. The human serum metabolome. *PloS One*, *6*(2):16957.

Punnonen, K., Irjala, K. & Rajamäki, A. 1994. Iron deficiency anaemia is associated with high concentrations of transferrin receptor in serum. *Clinical Chemistry*, *40*(5):774-776.

Puntarulo, S. 2005. Iron, oxidative stress and human health. *Molecular Aspects of Medicine*, 26(4-5):299-312.

Reo, N.V. 2002. NMR-based metabolomics. *Drug and Chemical Toxicology*, 25(4):375–382.

Rybkowska, N., Strzelak, K. & Koncki, R. 2018. A comparison of photometric methods for serum iron determination under flow analysis conditions. *Sensors and Actuators B: Chemical*, 254:307-313.

Seely, D.M., Wu, P. and Mills, E.J. 2005. EDTA chelation therapy for cardiovascular disease: a systematic review. *BMC Cardiovascular Disorders*, *5*(1):1-6.

Selim, M. 2009. Deferoxamine mesylate Anew hope for intracerebral haemorrhage: From bench to clinical trials. *Stroke*, 40(1):90-91.

Shalev, O., Repka, T., Goldfarb, A., Grinberg, L., Abrahamov, A., Olivieri, N.F., Rachmilewitz, E.A. and Hebbel, R.P. 1995. Deferiprone (L1) chelates pathologic iron deposits from membranes of intact thalassaemic and sickle red blood cells both in vitro and in vivo. *Blood*, 88(5):2008-2013.

Shortanov, R.A. 2020. Research on the Multisectoral Impact of Infectious Diseases on the Economy. *Journal of Pharmaceutical Research International,* 32(27):47-57.

Silva, R.A., Pereira, T.C.S., Souza, A.R. & Ribeiro, P.R. 2020. ^{1}H NMR-based metabolite profiling for biomarker identification. *Clinica Chimica Acta*, 502:269–279.

Sinclair, A.J., Viant, M.R., Ball, A.K., Burdon, M.A., Walker, E.A., Stewart, P.M., Rauz, S. & Young, S.P. 2010. NMR-based metabolomic analysis of cerebrospinal fluid and serum in neurological diseases – a diagnostic tool? *NMR Biomed*, 23:123–132.

Smith, K.F., Goldberg, M., Rosenthal, S., Carlson, L., Chen, J., Chen, C. & Ramachandran, S. 2014. Global rise in human infectious disease outbreaks. *Journal of the Royal Society Interface*, *11*(101):20140950.

Song, Z., Wang, H., Yin, X., Deng, P. & Jiang, W. 2019. Application of NMR metabolomics to search for human disease biomarkers in blood. *Clinical Chemistry Laboratory Medicine*, 57(4): 417–441.

Sousa, C., Moutinho, C., Vinha, A.F. & Matos, C. 2019. Trace Minerals in Human Health: Iron, Zinc, Copper, Manganese and Fluorine. *International Journal of Science and Research Methodology*, 13:57-80.

Speeckaert, M.M., Speeckaert, R. & Delanghe, J.R. 2011. Biological and clinical aspects of soluble transferrin receptor. *Critical Reviews in Clinical Laboratory Sciences*, 47(5–6):213–228.

Tian, M., Chen, X., Li, H., Ma, L., Gu, Z., Qi, X.... You, C. 2016. Long-term and oxidative-responsive alginate–deferoxamine conjugates with a low toxicity for iron overload. *RSC Advances*, 6(39):32471-32479.

Tomlins, A.M., Foxall, P.J., Lynch, M.J., Parkinson, J., Everett, J.R. and Nicholson, J.K. 1998. High resolution ^{1}H NMR spectroscopic studies on dynamic biochemical processes in incubated human seminal fluid samples. *Biochimica et Biophysica Acta (BBA)-General Subjects*, *1379*(3):367-380.

Ubale, A.U. 2010. Effect of complexing agent on growth process and properties of nanostructured Bi2S3 thin films deposited by chemical bath deposition method. *Materials Chemistry and Physics*, *121*(3):555-560.

Von Bonsdor, L., Lindeberg, V.E., Sahlstedt, L., Lehto, J. & Parkkinen, J. 2002. Bleomycin-detectable iron assay for non-transferrin-bound iron in hematologic malignancies. *Clinical Chemistry*, 48:307–314.

Wang, W., Knovich, M.A., Coffman, L.G., Torti, F.M. & Torti, S.V. 2010. Serum ferritin: Past, present and future. *Biochimica et Biophysica Acta*,1800:760–769.

Webster, K. & and Kumar, S. 2014. Expanding the Analytical Toolbox: Pharmaceutical Application of Quantitative NMR. *American Chemical Society*, 86, 11474−11480.

Weinberg, E.D. 2009. Iron availability and infection. *Biochimica et Biophysica Acta (BBA)-General Subjects*, *1790*(7):600-605.

Weiss, G. 2002. Iron and immunity: a double-edged sword. *European Journal of Clinical Investigation*, 32:70-78.

World Health Organization, 2014. *Serum transferrin receptor levels for the assessment of iron status and iron deficiency in populations* (No. WHO/NMH/NHD/EPG/14.6). World Health Organization.

Worwood, M. 2002. Serum transferrin receptor assays and their application. The *Association of Clinical Biochemists*, 39:221-230.

Xu, C., Ding, Y., Leung, H.W., Tong, B.M.K., Shin, R.Y.C. & Lee, T.K. 2017. Development of high accuracy methods for the certification of calcium, iron, magnesium and potassium in human serum. *Journal of Trace Elements in Medicine and Biology*, 40: 61-66.

Yamanishi, H., Kimura, S., Iyama, S., Yamaguchi, Y. & Yanagihara, T. 1997. Fully automated measurement of total iron-binding capacity in serum. *Clinical Chemistry*, 43(12):2413-2417.

Yiannikourides, A. & Latunde-Dada, G.O. 2019. A Short Review of Iron Metabolism and Pathophysiology of Iron Disorders. *Medicines*, 6:85-100.

Yu, J., Yuan, Q., Sun, Y.R., Wu, X., Du, Z.Y., Li, Z.Q., & Hu, J. 2017. Effects of deferoxamine mesylate on hematoma and perihematomal edema after traumatic intracerebral hemorrhage. *Journal of Neurotrauma*, 34(19):2753–2759.

Zhang, A., Sun, H. and Wang, X. 2012. Serum metabolomics as a novel diagnostic approach for disease: a systematic review. *Analytical and Bioanalytical Chemistry*, *404*(4):1239-1245.

CHAPTER 3 EVALUATING EDTA AS A CHELATING AGENT USING ^{1}H-NMR SPECTROSCOPY

3.1 Introduction

Crucial metabolic processes in the human body are dependent on a steady supply of important trace metals (Tian *et al*., 2016). 11 elements are classified as trace elements because their biological essentiality and scarcity in humans (Fraga, 2005). According to Mehri (2020) trace elements are double faced. In this regard trace elements are beneficial and/or toxic. At optimum levels, trace elements are required for various metabolic and physiological functions whilst their deficiencies cause various metabolic disorders (Rajan *et al*., 1997). Rajan *et al*. (1997) goes on to say higher levels of trace elements are toxic and adversely affect metabolic processes. Trace element analysis in biological samples has been the focus of many scholars (Prashanth *et al*., 2015). Colometric and spectrographic methods are mostly used to analyse trace elements whilst single elemental analysis, atomic spectroscopy and electrochemical methods are frequently applied (Prashanth *et al*., 2015).

According to MalzH & Jancke, (2005) NMR is a quantitative tool because the intensity of a resonance line is directly proportional to the number nuclei (spins). With that in mind NMR can be used to quantify biological substances. ^{1}H-NMR can only utilise the C-H bond therefore it cannot analyse trace elements. For this study it is wise to use EDTA, a chelating agent that can be recognised by ^{1}H-NMR.

Here, a protocol to quantify biologically important ions is developed. In Chapter 3.2, the biologically important ions analysed are stated and their biological roles are described. Motivation for a paper on the development of a new method to quantify biologically important ions using ^{1}H-NMR is explained in chapter 3.3. Chapter 3.4 is the first published paper for the thesis.

3.2 Biologically important ions

Trace elements, as per definition, occur in low amounts in the human body. Insufficient amounts of essential trace elements and/or presence of lethal trace elements have both

been linked to adverse consequences to human health (Avino *et al.,* 2011). Homeostatic balance of these trace elements must be mantained because their imbalance may affect organ function (Razzaque, 2018). An elaborate system for the management and regulation of trace elements occurs in the circulatory system and in cells (Osredkar & Sustar, 2011). Currently there are ways to estimate the amounts of these trace elements in the body but there is also a great need for more accurate and reliable measurement (Avino *et al.,* 2011). More cutting-edge research must be done to boost our understanding of the effects of metals on the human body. Apart from the obvious organic chemical combinations between C, H, N, O, P, and S which give both physical cellular constructs and take part in chemical activities, all cells have essential quantitative demands for Na, K, Mg, Ca, Fe and/or (some of) Mn, Co, Zn, Mo, Se, Cl (Da Silva & Williams, 2001). For the purpose of this investigation, Ca, Mg, K, Fe and Zn were identified as being biologically important ions. The biological importance of iron in the human body was discussed in Chapter 2. Here, a brief background of the biological importance of Ca, Mg, K and Zn will be given.

3.2.1 Calcium (Ca)

Approximately 98% of calcium in adults is stored in the form of a hydroxyapatite reservoir in bones while the other 2% of calcium is in the ionic form (Ca^{2+}) in the extracellular fluid and various tissues, predominantly in skeletal muscle. Ca^{2+}, also called free calcium, is not attached to proteins (Goldstein, 1990). Ca^{2+} is crucial in multiple functions within the body, including muscle contraction and relaxation, blood clotting, oocyte activation, neuronal activity, building strong bones and teeth, as well as regulation of blood pressure and osmotic balance within cells (Bouillon, 2019; Pravina *et al*., 2013).

Calcium, through dietary intake, can be intestinally absorbed from food such as dairy products, seafood, green leafy vegetables and legumes. The daily body requirement of calcium is 450 mg, and for adults the recommended daily intake can be up to 1300 mg. Calcium deficiency signs include muscle cramping, dry skin and brittle nails; but, over long periods, loss in bone mass, osteoporosis, cardiac arrhythmias and seizures may arise (Pravina *et al*., 2013). A patient may suffer from convulsive seizures due to hypocalcaemia causing an increase in central and peripheral neural excitability (Goldstein, 1990). High calcium doses may lead to symptoms like nausea and vomiting; while heart problems, kidney damage and hypercalcemia may follow later. Hypercalcemia of a mild to moderate degree causes symptoms such as memory impairment, chronic recurrent headache,

depression and acute brain syndrome (Goldstein, 1990). A range of symptoms, from mental confusion or delirium, stupor and even comas, occur due to more distinct calcium elevations.

A 2018 study by Dave and Jha (2018) considers calcium signalling by the brain as one of the most important physiological functions, as Ca^{2+} serves as a second messenger in various information transformations. Intracellular communication and transmission are made possible through calcium. LaFerla (2002) mentions how neural processes, including apoptosis and synaptic plasticity, are modulated by calcium in the brain. Ca^{2+} helps to maintain extracellular fluid pH at 7.4, while buffering intracellular fluid at an optimum pH of 6.6–6.9. These pH ranges are important to generate electrical potentials of -70 and -90 mV between the cell membrane's outer and inner surface to allow cell excitation for neuron impulses. LaFerla (2002) further states that neurons control Ca^{2+} signals by regulating the Ca^{2+} influx into the cell from the extracellular environment or through the endoplasmic reticulum, which serves as an internal source that releases Ca^{2+}. The dysregulation of intracellular calcium signalling has also been associated with the pathogenesis of the disease termed Alzheimer's (LaFerla, 2002).

It is therefore important to have adequate amounts of calcium available for physiological functions and cellular processes, as well as having regulation mechanisms to ensure homeostasis hereof in humans. According to Bouillon (2019) Ca^{2+} in serum is feed-back regulated by calcitonin, 1,25-dihydroxy vitamin D and parathyroid hormone. Interactions of the endocrine, skeletal, digestive and urinary systems also control calcium homeostasis, for example, renal excretion of calcium.

3.2.2 Magnesium (Mg)

The significance of magnesium (Mg) can be traced back to the origin of life in the composition of the earth crust, to chlorophyll in plants and finally to animal cells where it is bound to ATP (Fawcett *et al*., 1999). Mg is one of the main, essential intracellular trace elements in the human body (Lvova *et al*., 2018). and is necessary for growth and development (De Baaij *et al.,* 2015). More than 300 enzymes involved in many crucial body reactions require Mg as a cofactor and stabilizer (Jahnen-Dechent & Ketteler, 2012). Particularly, all reactions that require or form ATP also require Mg for substrate formation (Rude, 1998). Mg-ATP or Mg-ADP active substrates of enzyme activity and in some cases as allosteric activators (Laires *et al*., 2004). The rate of catalysis of chemical reactions is

influenced by Mg through binding with ATP, binding to active sites and facilitation of aggregation of multi-enzyme complexes (Swaminathan, 2003).

Mg stabilizes membranes by forming complexes with membrane phospholipids, resulting in lowered fluidity and permeability (Laires *et al*., 2004). Mg often acts as a calcium antagonist. Membrane receptor sites and transport of ions such as calcium and potassium can be altered by Mg (Laires *et al*., 2004). Therefore, Mg competes with calcium for membrane binding sites and maintains a low resting intracellular ion concentration which is paramount for various cellular reactions (Swaminathan, 2003). Mg maintains the 3D conformation of nucleic acids (Jahnen-Dechent & Ketteler, 2012). Protein synthesis is indirectly affected by Mg through the facilitation of nucleic acid polymerization, enhancing the binding of mRNA to ribosomes, acceleration of synthesis and degradation of DNA and regulation of protein (Noronha & Matuschak, 2002). Mg also helps in the regulation of heart rhythm, vascular tone, bone formation, and platelet-activated thrombosis, and modulates insulin signal transduction and cell proliferation by influencing intracellular calcium concentration and electrical activity (Jahnen-Dechent & Ketteler, 2012).

Altered Mg balance is associated with conditions such as diabetes mellitus, chronic renal failure, nephrolithiasis, osteoporosis, aplastic osteopathy, and heart and vascular disease (Arnaud, 2008). To maintain Mg homeostasis an individual must have adequate dietary intake and normal absorption of Mg (Elin, 2010). Mg deficiency in the body can be treated by Mg supplements, whereas excess Mg is treated by hydration or dialysis, depending on the circumstances (Musso, 2009). No known hormone directly regulates Mg concentration (Barbagallo *et al*.,2009). Some hormones affect Mg transport and balance (e.g., parathyroid hormone, calcitonin, vitamin D and insulin (Barbagallo *et al*., 2009). Hence, the distribution of Mg must be continuously regulated in all cells (Vormann, 2003, 2016).

3.2.3 Potassium (K)

Potassium (K^+), plays an important bio-functional role in the brain with regards to signal transduction in neurons, activation and mobilization of immunological cells (T-lymphocytes, B-cells etc.), maintenance of membrane potentials in cells and regulation of pH (Bittner & Meut, 2013). K^+ channels are also one of the most abundantly found ion-channels in the brain. Voltage-gated K^+ channels KV1.3 (KCNA3) are critically involved in the activation and effector function of T lymphocytes (Bittner & Meuth, 2013). K^+ channels maintain a negative membrane potential needed for longer-lasting Ca^{2+} influx (needed for further activation) which, when blocked, reduces functions such as cytokine production and proliferation rates which indirectly causes an increase in neuroinflammation due to its dysfunctionality (Bittner

& Meuth, 2013). In B lymphocytes, KV1.3 are involved in the process of differentiation of naïve and early memory immunoglobulin D cells into class-switched memory B cells. Respective blocking results in a reduction of B-cell proliferation. Apart from KV1.3, Dendritic cells also express KV1.5 & KV1.3/KV1.5 heteromeric channels to different degrees. Dendritic cells, after stimulation, differentiation and migration into the CNS, has anti-inflammatory properties, and when the K^+-channels are blocked, dendritic cells cannot perform their anti-inflammatory functions. In neurons, K^+ is responsible for action potential conduction and the ability for axons to discharge repetitively. Demyelination induces increased exposure of fast K^+-channels which leads to membrane hyperpolarization. According to Vigil *et al*. (2020). KCNQ2-5 voltage-gated K^+-channels could play a vital role in the therapeutic intervention against post-traumatic brain injury (TBI) brain damage and dysfunction. Vigil *et al*. (2020) state “that systemic administration of the prototype M-channel "opener", retigabine, 30 min after TBI, reduces the post-TBI cascade of events, including spontaneous seizures, enhanced susceptibility to chemo-convulsants, metabolic stress, inflammatory responses, blood-brain barrier breakdown, and cell death”. Hence, research on K^+ in the regulation of inflammatory responses in the brain is topical and emerging as important.

At rest, neuronal membranes maintain a membrane potential of -70mV. When an action potential is being relayed along these cells, the membranes are depolarized to approximately +30mV due to the influx of sodium (Na^+) and K^+. However, the cell is then repolarized when the Na^+- K^+ pump is activated, as well as when the fast K^+-channels are activated, allowing K+ to flow out of the cell to repolarize the cell from +30mV to -70mV. If these K^+-channels are exposed due to demyelination, there is a larger efflux of K^+ from the cell which leads to hyperpolarization which surpasses the resting threshold of -70mV. Demyelination, therefore, leads to abnormal K^+ outward currents associated with slow action potential conduction, conduction failure or changes in the axons capacity to repetitively discharge. The demyelination also leads to loss of structural proteins that anchor KV-channels to membranes Bittner & Meuth, (2013). Thus, K^+ plays an important role in neuroinflammation, and the immunity thereof, as well as other neuronal activities of the brain.

3.2.4 Zinc

Zinc (Zn), one of the most used essential trace elements in all life forms (Mewara *et al*., 2018). Zn is in almost all body cell mostly as the structure of more than 2 700 proteins (Baltaci, *et al*., 2018). Zn is paramount for basic yet crucial metabolic processes hence it is crucial for optimal growth, immunocompetence and visual acuity (Wieringa *et al*., 2015). Zn

homeostasis is regulated by the balance of intestinal absorption and endogenous loses through faeces (Kondaiah *et al*., 2019). Zn homeostasis is solely orchestrated through elevated rates of absorption when deficient, and excretion during repletion (Kondaiah *et al*., 2019). The human body has not evolved a mechanism to store Zn for use when deficient, therefore it solely depends on dietary supply (Lowe *et al*., 2009). Brain, bones, muscles, liver, kidneys and the liver are the major organs where Zn accumulates in the human body (Osredkar & Sustar, 2011). Metallothionine serves as a reservoir and a transporter of cellular zinc and can bind up to seven zinc ions (Maret, 2009). Total body Zn concentration, however, cannot be reliably represented by serum Zn concentration, which responds sharply to dietary restrictions and consistently elevates during supplementation regardless of the initial value (Hess *et al*.,2007). Intracellular zinc concentration is tightly regulated by zinc transporters, zinc sensors and zinc-binding molecules (Murakami & Hirano, 2008). Zinc transporters are responsible for zinc influx and efflux in cells and regulate intracellular and extracellular zinc concentrations (Osredkar & Sustar, 2011).

The Lewis acids traits of the zinc divalent ion (Zn^{2+}) (i.e. its single redox state flexible coordination sphere and kinetic liability of coordinated ligands) are responsible for its broad functions in the human body (Lim *et al*., 2005); categorized into catalytic, regulatory and structural roles (Osredkar & Sustar, 2011). According to Lim *et al*. (2005), zinc is a catalytic component of more than 200 enzymes. In some proteins, like the enzyme protein kinase C, zinc has a structural function (Lim *et al*., 2005). It is believed that zinc also has antioxidant properties, meaning it reduces the rate of ageing (Osredkar & Sustar, 2011). According to Murakami & Hirano (2008) zinc maintains the structural integrity of more than 2 000 transcriptional factors that work to regulate gene expression. Zinc fingers, forming part of the transcriptional factors, are small protein structural motifs characterized by the coordination of one or more zinc ions in order to stabilize the fold. The zinc finger domain is one of the most frequently used DNA-binding motifs (Cassandri *et al*., 2017). Zinc plays a pivotal role in DNA synthesis and cell division (Osredkar & Sustar, 2011), a structural role in zinc fingers. Many reports in the literature have identified abnormal zinc levels in malignant cells hence zinc may be involved by regulating gene expression profiles which are partly mediated by tumor-induced changes in zinc transporters (Gibson *et al*., 2008).

Zn deficiency is one of the world's most ubiquitous micronutrient deficiencies (Wieringa *et al*., 2015). This ubiquitous nature of zinc in the human body indicates that zinc deficiency is catastrophic as it leads to a broad range of pathologies (Lim *et al*., 2005). Lowering of Zn concentration can be used to fight pathogens, where it is a signal for danger within cells (Dierichs *et al*., 2018). Zn is redistributed to different compartments, increasing the

susceptibility of the pathogen (s) to ROS (Dierichs *et al*., 2018). Zn deficiency is associated with a range of pathological conditions, including impaired immunity, retarded growth, brain development disorders and delayed wound healing (Osredkar & Sustar, 2011).

3.3 Motivation for paper 1

For my BSc Hons (2019), we tested the proof-of-concept of chelation NMR using EDTA. My focus was on iron, while two of my fellow BSc Hons students tested Ca and K. It is already well-known that EDTA produces two clear single peaks within a ^{1}H-NMR spectrum and that chelated EDTA complexes produce unique ^{1}H-NMR spectral patterns, depending upon the chelated ion (Jimenez-Jimenez *et al*., 1998; Sampson *et al*., 1997). Hence, ^{1}H NMR spectroscopy has already been proposed as an alternative and simple method for the determination of several diamagnetic metal ions (Sampson *et al*., 1997, Abd El-Hafeez *et al*., 2003). Of note, the group of Hafer *et al*. (2020) recently reported a similar concept for the quantitative determination of various ions by ^{1}H-NMR; however, the utility of the method shown by Hafer *et al.* (2020) for the analysis of divalent cations was intended for food and pharmaceutical products. My BSc Hons project (2019) tested the method of chelation NMR as a proof-of-concept specifically for application in the field of ^{1}H-NMR metabolomics. The following paper, titled: “EDTA as a chelating agent in quantitative ^{1}H-NMR of biologically important ions”, published in Biochemistry and Cell Biology, is a report of the outcomes of our BSc Hons work using EDTA, with the inclusion of experiments for Mg and Zn, which I performed. In this paper, factors like the ratio of the chelating agent (EDTA), the quantity of ion being chelated, and pH had to be principally considered for the development of the method. The method development described in this paper was taken into consideration in the development of the method using DFO in my MSc – described in Chapter 4.

3.4 Paper 1: EDTA as a chelating agent in quantitative ^{1}H-NMR of biologically important ions

Emmanuel Mathuthu[a], Angelique Janse van Rensburg[a], Dean Du Plessis[a], Shayne Mason[a,*]

[a] Human Metabolomics, Faculty of Natural and Agricultural Sciences, North-West University, Potchefstroom, South Africa.

[*] Corresponding author: Shayne Mason (https://orcid.org/0000-0002-2945-5768)
North-West University
Private Bag X6001
Potchefstroom
South Africa
2531

Email: nmr.nwu@gmail.com

Email addresses:
Emmanuel Mathuthu: emmanuelmathuthu@gmail.com
Angelique Janse van Rensburg: nwulica@gmail.com
Dean Du Plessis: dupled11@gmail.com

Keywords: metabolomics methodology, proton nuclear magnetic resonance (^{1}H-NMR) spectroscopy, Ethylenediamine tetraacetic acid (EDTA), chelation, biological ions.

Published in *Biochemistry and Cell Biology* on 15 January 2021
Mathuthu, E., Janse van Rensburg, A., Du Plessis, D. and Mason, S., 2021. EDTA as a chelating agent in quantitative ^{1}H-NMR of biologically important ions. *Biochemistry and Cell Biology*, (online, ahead of print). doi.org/10.1139/bcb-2020-0543

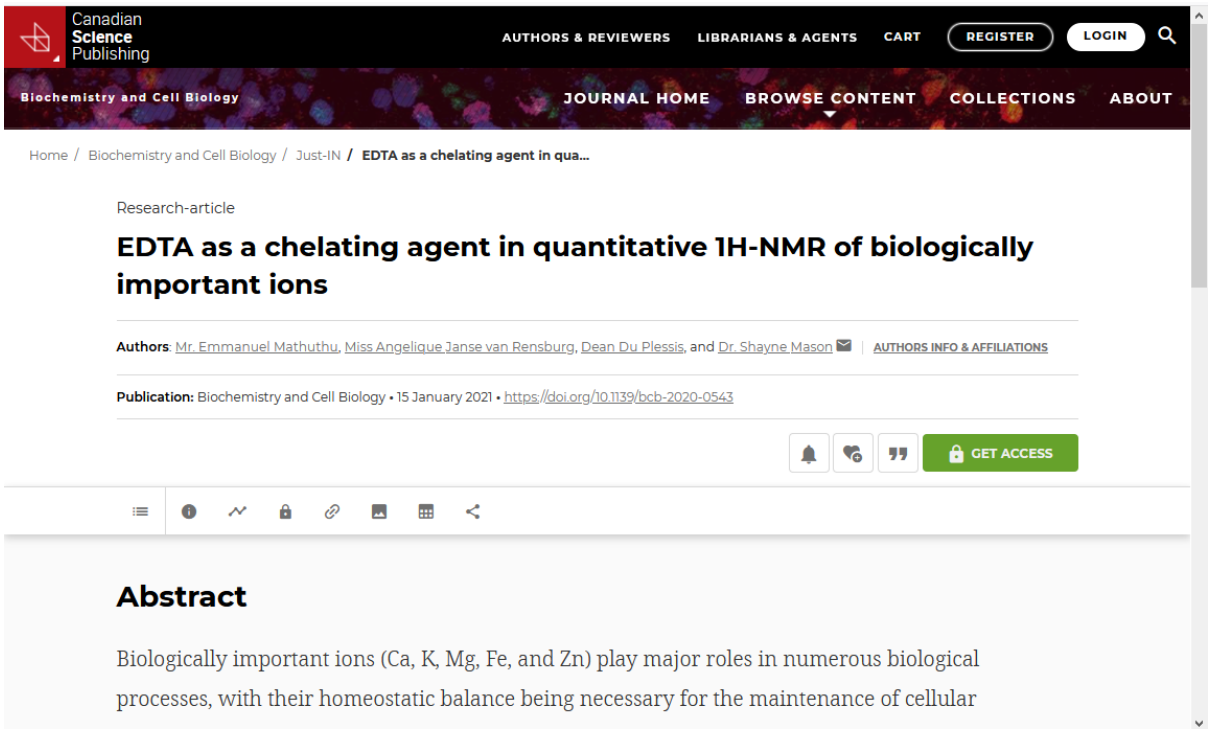

Figure 4: Published manuscript in Biochemistry and Cell Biology on 15 January 2021 (Mathuthu *et al*., 2020).

3.5 Abstract

Biologically important ions (Ca, K, Mg, Fe, and Zn) play major roles in numerous biological processes, with their homeostatic balance being necessary for the maintenance of cellular mechanisms. Sudden and severe loss in homeostasis of just one biologically important ion can cause cascading negative effects. Being able to quickly, accurately and reliably quantify biologically important ions in human bio-fluid samples is something that has been sorely lacking within the field of metabolomics. ^{1}H-NMR is a well-known analytical platform in metabolomics, but ions are invisible on ^{1}H-NMR spectra. The foundation of our investigation was based upon *a priori* knowledge that free EDTA produce two clear single peaks on ^{1}H-NMR spectra, and that EDTA chelated to different ions produce unique ^{1}H-NMR spectral patterns due to 3D conformational changes in the chemical structure of chelated-EDTA and varying degrees of electronegativity. The aim of this study was to develop and test a ^{1}H-NMR-based method, with application specifically to the field of metabolomics, to quantify biologically important ions within the physiological pH range of 6.50-7.50 using EDTA as a chelating agent. Our method produced linear, accurate, precise and repeatable results for Ca, Mg and Zn; however, K and Fe did not chelate with EDTA.

3.6 Introduction

Apart from the obvious organic chemical combinations between C, H, N, O, P, and S which give both physical cellular constructs and take part in chemical activities, all cells have essential quantitative demands for Na, K, Mg, Ca, Fe and/or (some of) Mn, Co, Zn, Mo, Se, Cl (Da Silva & Williams, 2001) For the purpose of our investigation, we identified Ca, Mg, K, Fe and Zn as being biologically important ions. A brief background of their biological importance in the human body will firstly be described, before articulating the aims of this study.

Calcium (Ca) – approximately 98% is stored in the form of a hydroxyapatite reservoir in bones while the other 2% of calcium is in the ionic form (Ca^{2+}) (Goldstein, 1990). Ca^{2+} is crucial as a second messenger in various information transformations, in muscle contraction and relaxation, blood clotting, oocyte activation, neuronal activity, synaptic plasticity and regulation of blood pressure and osmotic balance (Goldstein, 1990; LaFerla, 2002). Hypocalcemia can lead to loss in bone mass, osteoporosis, cardiac arrhythmias and seizures (Pravina *et al*., 2013) while hypercalcemia can lead to heart problems, kidney damage, memory impairment, chronic recurrent headache, depression and acute brain syndrome (Goldstein, 1990).

Magnesium (Mg) – an essential intracellular trace element (De Baaij *et al*., 2015, Swaminathan, 2003), acts as a calcium antagonist and stabilizes membranes (Laires *et al*., 2004) maintains 3D conformation of nucleic acids (Jahnen-Dechent & Ketteler, 2012), and regulates protein synthesis. An imbalance in Mg has been associated with diabetes mellitus, chronic renal failure, nephrolithiasis, osteoporosis, aplastic osteopathy, and heart and vascular disease (Arnaud, 2008). Hence, the distribution of Mg must be continuously regulated in all cells (Vormann, 2016).

Potassium (K^+) – plays an important bio-functional role in the brain with regards to signal transduction in neurons, activation and mobilization of immunological cells (T-lymphocytes, B-cells etc.), maintenance of membrane potentials and regulation of pH; particularly via voltage-gated ion channels (Bittner & Meuth, 2013; Vigil, 2020). At rest, neuronal membranes maintain a membrane potential of -70 mV, which depolarizes to approximately +30 mV upon action due to the influx of sodium (Na^+) and K^+. Demyelination of neurons leads to a large efflux of K^+ associated with conduction failure, repetitive discharge of axons

and loss of neuronal membrane structural proteins (Bittner & Meuth, 2013, Watari *et al*., 2012), all hallmarks of the disease multiple sclerosis.

Iron (Fe) – most stable in its ferric form (Fe^{3+}), is stored as ferritin and hemosiderin when in excess (Yiannikourides & Latunde-Dada, 2019). Iron is an important component of enzymes (Puntarulo, 2005, Weiss, 2002) and cofactors (Weiss, 2002; Farthing, 1989), redox reactions (Milto *et al*., 2016; Harrison & Arosio, 1996), stabilization of proteins (Milto *et al*., 2016). Iron homeostasis is crucial (Provan & Gribben, 2010; Muñoz *et al*., 2009), as iron overload expedites reactive oxygen species (ROS) formation (Ozment & Turi, 2009, Nasrallah *et al*., 2019) and iron deficits (anemia) reduce oxygen availability for cells (Ifeanyi, 2018)

Zinc (Zn) – one of the most used trace elements (Mewara *et al*., 2018), particularly in proteins (Baltaci *et al*., 2018; Auld, 2009), responsible for catalytic, regulatory and structural functions (Osredkar & Sustar, 2011) in its divalent form (Zn^{2+}) (Lim *et al*., 2005). The human body, unable to store Zn, solely relies upon dietary Zn (Lowe *et al*., 2009). Metallothioneins serve as a reservoir and transporter of cellular Zn (Maret, 2009), modulating flux of cellular Zn (Osredkar & Sustar, 2011; Murakami & Hirano, 2008). Zn fingers – small protein structural motifs – are pivotal in DNA synthesis (Cassandri *et al*., 2017). Abnormal Zn levels have been associated with malignant cells (Gibson *et al*., 2008), and Zn deficiencies linked to impaired immunity, retarded growth, brain development disorders and delayed wound healing (Osredkar & Sustar, 2011; Dierichs *et al*., 2018).

Quantitative nuclear magnetic resonance (qNMR) spectroscopy, a well-known analytical chemistry technique, has had increasingly greater use within the field of biochemistry (Giraudeau, 2017). Since the emergence of the field of metabolomics in biochemistry at the turn of the millennium (Nicholson *et al*., 2005) the two most common analytical platforms have been mass spectrometry (MS), typically coupled to chromatography (gas or liquid), and ^{1}H-NMR spectroscopy — used to analyze biological samples/systems in order to assess patterns and profiles of low molecular weight compounds (metabolites). The significant role of NMR within metabolomics research over the past two decades is undeniable (comprehensively reviewed by Emwas *et al*. (2019). However, within metabolomics both NMR and MS-based protocols are not designed to detect/quantify biologically important ions. In fact, all ions are invisible on a ^{1}H-NMR spectrum as only hydrogens (protons) are visible. Biologically important ions play a significant role in biochemistry, yet there are no metabolomics-based standard operating procedures (SOPs) set up for the quantification of these ions. Currently, the most common techniques used to quantify ions are used in chemistry, which includes ion chromatography, flame atomic absorption spectrometry and inductively coupled plasma mass spectrometry. These chemistry-based methods often have

complex sample preparation and require sample volumes of at least 1 mL – a problem with biological samples in metabolomics as volumes are typically limited (~100 µL). Hence, there is a need within the field of metabolomics to incorporate SOPs of qNMR of biologically important ions into existing high-throughput protocols.

Ethylenediaminetetraacetic acid (EDTA), an excellent chelating agent, forms stable transition metal complexes and metal group ions chelate in solutions of various pH levels (Panda & Chaudhuri, 2007). EDTA consists of four carboxylic acid groups and two amine groups with an unshared pair of valence electrons (Mohammadi *et al*., 2013). The structure of EDTA allows it to interact with a single ion at a total of six positions (Keowmaneechai & McClements, 2002; Hafer *et al*., 2020). Within biochemistry, one of the most commonly used applications of EDTA is in blood collection tubes, where EDTA is attached to the blood collection tubes and binds to Ca^{2+}, resulting in the interruption, and prevention, of the blood clotting cascade (i.e. EDTA acts as an anticoagulant). In the current study, factors like the ratio of the chelating agent (EDTA), the quantity of ion being chelated, and pH were taken into consideration during method development (Tandy *et al*., 2004).

It is already well-known that EDTA produces two clear single peaks within a ^{1}H-NMR spectrum and that chelated EDTA complexes produce unique ^{1}H-NMR spectral patterns, depending upon the chelated ion (McEwen, 2010; Somashekar *et al.,* 2006). The use of EDTA complexation for measuring Ca and other metal ions in body fluids such as plasma has been known for decades, going back to a paper in 1983 (Nicholson *et al.,* 1983). Hence, ^{1}H NMR spectroscopy has already been proposed as an alternative and simple method for the determination of several diamagnetic metal ions (Han & Ba 2004; Somashekar *et al.,* 2006). Of note, the group of Hafer *et al.* (2020) recently reported a similar concept for the quantitative determination of various ions by ^{1}H-NMR; however, the utility of the method shown by Hafer *et al.* for the analysis of divalent cations was intended for food and pharmaceutical products. It is important to state that the intended application for the method described in this paper is specifically for metabolomics purposes in the field of biochemistry. Hence, our aim was to provide proof-of-concept for the further development of this method into a SOP for metabolomics laboratories with access to ^{1}H NMR spectroscopy.

3.7 Materials and methods

3.7.1.1 Reagents

Trimethylsilyl-2,2,3,3-tetradeuteropropionic acid (TSP; Merck; CAS#: 24493-21-8) as the NMR internal standard. Deuterium oxide (D_2O; Merck; CAS#: 7789-20-0). Ethylenediamine tetraacetic acid (EDTA; Sigma-Aldrich; CAS#: 60-00-4) as the chelation agent. Double-distilled water (ddH_20; Sigma-Aldrich; CAS#: 7732-18-5). Potassium chloride (KCl; Sigma-Aldrich; CAS#: 7447-40-7). Calcium chloride ($CaCl_2$; Saarchem, CAS#: 152-49-00). Ferric chloride ($FeCl_3$; Sigma-Aldrich; CAS#: 10025-77-1). Zinc chloride ($ZnCl_2$; Sigma-Aldrich; CAS#: 7646-85-7). Magnesium chloride ($MgCl_2$; Merck; CAS#: 7786-30-3). Solutions of sodium hydroxide (NaOH; Sigma-Aldrich; CAS#: 1310-73-2) and hydrogen chloride (HCl; Sigma-Aldrich; CAS#: 7647-01-0) were used to adjust the pH of the samples.

3.7.1.2 Preparation of solutions

A 100 mL volume of 10 mM stock solution was prepared of each ion under investigation in ddH_20, as well as a 100 mL stock solution (10 mM) of EDTA in ddH_2O. An internal standard (IS) solution of 100 mL volume of 20 mM TSP in D_2O was prepared and aliquoted into 5 mL tubes and frozen, until needed, to maintain stability of TSP. Normal and pathological reference ranges of ions in serum and cerebrospinal fluid (CSF) in humans were determined based upon literature, including medical detection limits (Table 1). Fourteen serial stock dilutions of each individual ion stock solution were created as 25%, 50%, 75%, 100%, 125%, 150% & 175% of both the upper and the lower range values (Table 2) of the normal reference ranges highlighted in bold in Table 1, so as to include all the pathological values.

Table 1: Reference ranges of concentrations of Ca, Mg, K, Fe and Zn in blood and CSF, under normal and pathological conditions, based upon literature.

	Normal range[1,2]		Pathological range		Medical detection limit
	Blood	CSF	Blood	CSF	
Ca	2250–2590	**1020–1340**	AD: 1582–1846[3] PD: 1800–3000[13]	PD: 600–764[14]	CSF: 4750[4]
Mg	**570–830**	550–1230	AD: 663–863[3] PD: 659–927[5] MS: 1292–1776[16]	AD: 12,7–14,0 PD: 864–946[14]	
K	4200–4400[11]	**2500–3300**	PD: 2800–5400[13]	TBM: 2380–3760[10]	CSF: 4500[1]
Fe	**9,0–31,3**	3,89–7,25	AD: 22,7–24,43[12] PD: 4–28[13]	AD: 39,7–44,3 PD: 3,04–3,76[8]	Blood < 1
Zn	**13,6–19,8**	0,37–0,60	AD: 8,71–14,53[7] PD: 9,02–16,06[8]	AD: 0,45–3,21[7] PD: 0,61–2,45[8]	Blood: 200[9]

Concentrations in micromolar (µM). AD = Alzheimer's disease; PD = Parkinson's disease; MS = Multiple sclerosis; TBM = tuberculous meningitis. Bolded normal reference ranges indicate the ranges selected for our investigation. References: [1]Lentner,1992; [2]Wu, 2006; [3]Bocca *et al.,* 2005; [4]Smith, 2005; [5]Forte *et al.,* 2005a; [6]Forte *et al.,* 2005b; [7]Molina *et al.,* 1998; [8]Jimenez-Jimenez *et al.,* 1998; [9]Sampson *et al.,* 1997; [10]Abd El-Hafeez *et al.,* 2003; [11]Aldahl *et al.,* 2017; [12]Ozcankaya & Delibas, 2002; [13]Hegde *et al.,* 2004; [14]Alimonti *et al.,* 2007.

Table 2: Fourteen serial stock dilutions of Mg, Ca, K, Fe, Zn as 25%, 50%, 75%, 100%, 125%, 150% & 175% of both the upper and lower values of their normal reference ranges from Table 1.

	Mg		Ca		K		Fe		Zn	
	570^{L}	830^{U}	1020^{L}	1340^{U}	2500^{L}	3300^{U}	$9{,}0^{L}$	$31{,}3^{U}$	$13{,}6^{L}$	$19{,}8^{U}$
25%	142,5	207,5	255	335	625	825	2,25	7,8	3,4	5,0
50%	285	415	510	670	1250	1650	4,5	15,7	6,8	9,9
75%	427,5	622,5	765	1005	1875	2475	6,75	23,5	10,2	14,9
100%	570	830	1020	1340	2500	3300	9	31,3	13,6	19,8
125%	712,5	1037,5	1275	1675	3125	4125	11,25	39,1	17	24,8
150%	855	1245	1530	2010	3750	4950	13,5	47,0	20,4	29,7
175%	997,5	1452,5	1785	2345	4375	5775	15,75	54,8	23,8	34,7

Volumes given as microliter (µL). ^{L} = lower reference range. ^{U} = upper reference range.

3.7.1.3 Method development

3.7.1.3.1 Experiment 1

The aim of experiment 1 was to determine a enough concentration of EDTA required for complete chelation with the highest concentration of each ion in Table 2. Firstly, a 50ml stock solution of the highest upper reference value of each ion was prepared and labelled level 14. Then, from each level 14 solution, four 510µL solutions were transferred into Eppendorf tubes. A volume of 60µL IS (2M TSP in D_2O) and 30µL EDTA solution were added to each Eppendorf tube, according to the 90:10 ratio of sample:D_2O as per typical NMR metabolomics protocol (Beckonert *et al*., 2007). EDTA concentration varied depending on concentration range of each ion. EDTA concentration were: 3, 9, 15 & 30 µM for iron and zinc, 9, 15, 30 & 45 µM for magnesium, 45, 60, 75 & 90 µM for potassium, and 105, 120, 135 & 150 for calcium. Tandy *et al.* (2004) emphasizes the importance of adding excess

chelating agent (EDTA) in solutions containing various ions as they compete for chelation. Hence, the optimal EDTA concentration in this study should fully chelate the ion of interest, with free EDTA (not highly excessive amounts) still being available. The pH for each sample was adjusted to a constant 7.00 ± 0.05. The final samples were then transferred into 5mm NMR tubes and analyzed using ^{1}H-NMR. The effects of different EDTA concentration on the spectra were identified and optimal concentration for chelation was determined.

3.7.1.3.2 Experiment 2

The succeeding experiment 2 utilized the results of experiment 1 – the optimal EDTA concentration. The aim of experiment 2 was to determine the effects of the change in pH on the chemical shift in the ^{1}H-NMR spectra. To determine the effect of pH on chemical shift for each ion, 15 samples were prepared by transferring 510µL level 14 solutions into Eppendorf tubes and adding 60µL IS (2M TSP in D_2O) and 30µL of the optimal EDTA concentration determined in experiment 1. The pH was then adjusted to five different values 6.50, 6.80, 7.00, 7.20 and 7.50 (all ± 0.05) in triplicates. The specific pH range of 6.50-7.50 was used as this is within the typical physiological pH range in humans (Waugh & Grant, 2014). Lastly the samples were transferred to 5mm NMR tubes and analyzed.

3.7.1.3.3 Experiment 3

The aim of experiment 3 was to use the optimal conditions obtained in the preceding experiments and assess the method across the concentration ranges determined in Table 2. From the fourteen serial stock dilutions of Mg, Ca, K, Fe and Zn, 510 µL of each level in triplicate were mixed with 60µL of the IS and 30µL of optimal EDTA concentration, which was determined in Experiment 1. Similarly, pH was adjusted to the optimal value within the range of 6.50-7.50, that was determined in Experiment 2. The final samples were transferred to 5mm NMR tubes and analyzed.

3.7.1.4 ^{1}H-NMR analysis

To minimize technical variation, the NMR spectrometer was automatically calibrated prior to analysis of each sample. NMR calibration involved tuning the probe, locking onto the deuterated component, shimming to ensure a homogenous and aligned magnetic field, and calibration of the radio frequency pulse to precisely 90° to the nuclei. A 500 MHz Bruker Avance III HD NMR spectrometer equipped with a 5 mm triple resonance inverse (TXI) {^{1}H, ^{15}N, ^{13}C} probe head and x, y, z gradient coils were used to analyze all samples. For this method development, the TXI inner coil was optimized for ^{1}H observation as this was our nuclei of interest. Temperature within the probe was maintained at 300 K. Spectra were

acquired as 128 transients in 32K data points with a spectral width of 12,000 Hz (24.0 ppm). The H_2O resonance at 4.70 ppm was suppressed using the pulse sequence program NOESY-presat, which presaturates the H_2O resonance by single-frequency irradiation during a relaxation delay of 4 s, with a 90° excitation pulse of 10 µs. The acquisition time and receiver gain were set for 2.7 s and 64, respectively. The number of dummy scans = 4 and number of scans = 128, yielding a run time of 15 min and 45 s per sample. Fourier transformation and phase and baseline correction were done automatically. The quality of the spectra was checked by ensuring that resonance line width for TSP was <1 Hz. Bruker Topspin (V3.5) was used for NMR pre-processing, and Bruker AMIX (V3.9.14) was used for peak annotation and quantification.

3.8 Results

3.8.1.1 Experiment 1

For Experiment 1 we aimed to determine the concentration of EDTA considered sufficient to completely chelate the highest concentration of each biologically important ion in this study, with free EDTA (not highly excessive amounts) still being available because ions compete for chelation. For our method development we used a set volume of 510 µL of the highest concentration of each ion under study (Table 2), to which we added 60 µL 2mM TSP in D2O and 30 µL of varying concentrations of EDTA solution. A pH of 7.00 ± 0.05 was maintained across all samples. Thus, the only variable that changed for experiment 1 was the concentration of EDTA solution used. The range of EDTA concentration used depended upon the normal reference range of each ion (Table 2) and is shown in Table S1 in the Supplementary Information (SI). The assessment for experiment 1 was done qualitatively by examining the ^{1}H-NMR spectra (Fig. 5).

Visual examination of the top ^{1}H-NMR spectrum of Fig. 5 shows that Zn chelated with EDTA across all four concentrations of EDTA (3, 9, 15 & 30 mM). The lowest concentration of EDTA (3 mM) was able to completely chelate with the highest concentration of Zn in our study, and still have free EDTA visible. When visually examining the ^{1}H-NMR spectra of Mg chelated with EDTA (middle spectrum of Fig. 5; across the EDTA concentrations of 9, 15, 30 & 45 mM), it is evident that at 9 mM & 15 mM there was insufficient EDTA available. This can be seen be the chelated complexes showing insufficient chelation and zero free EDTA present – all the free EDTA was used to chelate the Zn in the sample, but free Zn was still present in the sample. At 30 mM EDTA complete chelation with Mg occurred but there was minimal free EDTA left. Similarly, to Mg, the ^{1}H-NMR spectra of Ca chelated with EDTA (bottom spectrum of Fig. 5; across the EDTA concentrations of 45, 60, 75 & 90 mM) show

that 45 mM EDTA resulted in incomplete chelation of Ca, with zero free EDTA remaining. At 60 mM EDTA, complete chelation occurred with Ca and ample free EDTA remaining. Hence, the optimal concentration of EDTA solution in our method development was 3, 30 & 45 mM EDTA for Zn, Mg and Ca, respectively.

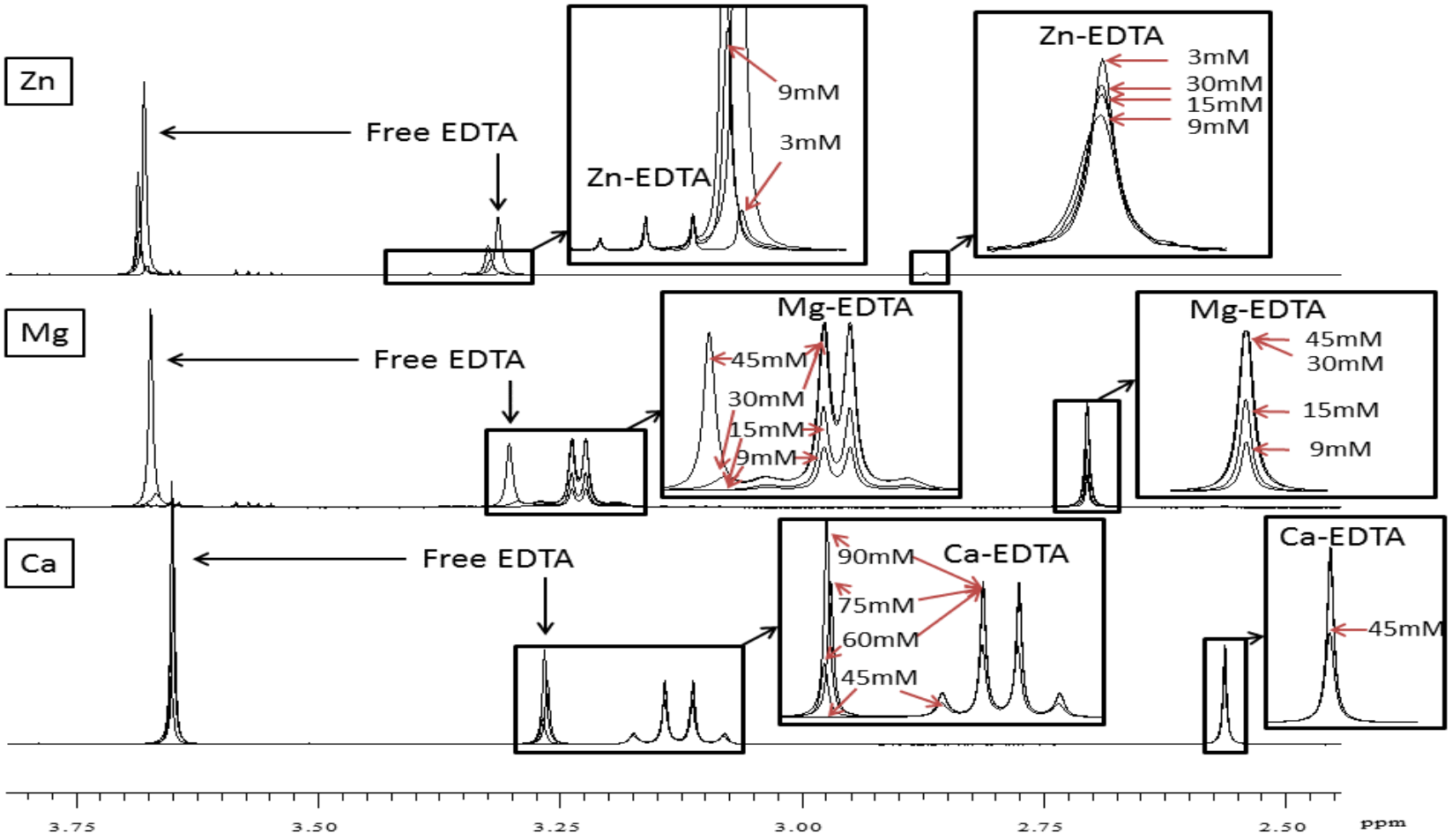

Figure 5: Qualitative assessment of ^{1}H-NMR spectra (relative to IS) to determine sufficient EDTA concentration for complete chelation of the highest concentration investigated for Zn (top), Mg (middle) and Ca (bottom). All measurements done at pH 7.00 ± 0.05.

A further result of experiment 1 provides information on the chemical shifts and peak splitting of EDTA-chelated Zn, Mg & Ca. This information is described in Table 3.

Table 3: Chemical shifts and peak splitting of EDTA-chelated Zn, Mg and Ca.

	8-proton EDTA chelated complex	4-proton EDTA chelated complex
Chemical moiety	$(-N-CH_2-COOH)_4$	$-N-CH_2-CH_2-N-$
Zn	3.36 q $(CH_2)_4$	2.87 s $(CH_2)_2$
Mg	3.23 q* $(CH_2)_4$	2.70 s $(CH_2)_2$
Ca	3.13 q $(CH_2)_4$	2.56 s $(CH_2)_2$

Peak splitting: q = quartet (*indicates tightly coupled); s = singlet.

Of note, the ^{1}H-NMR spectra of both Fe and K showed only the two single peaks representing free EDTA. This indicates that at pH 7.0, and with varying concentrations of EDTA, neither Fe nor K formed any chelated complexes with the free EDTA. For experiment 2, 30 mM and 150 mM EDTA solutions were used for Fe and K respectively to assess if any chelation would occur across the pH range of 6.5 to 7.5 ± 0.05. Similarly, to experiment 1, neither Fe nor K were observed to form any chelated complexes with free EDTA and were hence not measured in experiment 3. The inability of EDTA to complex with Fe and K is elaborated upon under the discussion.

3.8.1.2 Experiment 2

For Experiment 2 we aimed to determine the optimal pH for our method for each ion within the pH range of 6.50-7.50, which is within the human physiological pH range (Waugh & Grant, 2014). For our method development we used a set volume of 510 µL of the highest concentration of each ion under study (Table 2), to which we added 30 µL of the optimal EDTA solution – determined in experiment 1, and 60 µL 2mM TSP in D_2O. Thus, all volume concentrations remained the same for experiment 2. The only variable that was altered was the final pH of each sample. Five different points of pH were examined (6.50, 6.80, 7.00, 7.20 and 7.50; all ± 0.05), each in triplicate. Thus 15 samples were prepared for each ion. Table 2 (SI) shows the final pH measurements (individual and mean) recorded for Zn, Mg and Ca.

The results of experiment 2 are shown qualitatively by the ^{1}H-NMR spectra in Fig. 6, which illustrates that the chemical shift of all the free EDTA peaks are affected by the change in the pH. For Zn (Fig. 6 – left), the chemical shift for the quartet representing the 8-proton Zn-EDTA chelated complex was at 3.36 ppm (Table 3). For the pH values of 6.50, 6.80 and 7.00, the 4-proton free EDTA peak overlaps with the 8-proton Zn-EDTA quartet at 3.27, 3.27 and 3.35 ppm, respectively (highlighted by the red box). For the pH values of 7.20 and 7.50, no overlap occurs. Thus, for our study 7.50 was selected as the optimal pH for Zn.

For Mg (Fig. 6 – middle), the chemical shift for the quartet representing the 8-proton Mg-EDTA chelated complex was at 3.23 ppm (Table 3). Similarly, to Zn for the pH values of 7.00, 7.20 and 7.50, the 4-proton free EDTA peak infringes upon the 8-proton Mg-EDTA quartet at 3.25, 3.28 and 3.31 ppm, respectively (highlighted by the red box). For the pH values of 6.50 and 6.80, no overlap occurs. Thus, for our study 6.50 was selected as the optimal pH for Mg.

For Ca (Fig. 6 – right), the chemical shift for the quartet representing the 8-proton Ca-EDTA chelated complex was at 3.13 ppm (Table 3). None of the 4-proton free EDTA peaks across the examined pH range 6.50-7.50 infringed upon the 8-proton Ca-EDTA chelated complex. To select the optimal pH for Ca we examined the standard deviation (STD) at each pH measurement and found pH 7.20 to have the lowest STD. Hence, for our study 7.20 was selected as the optimal pH for Ca.

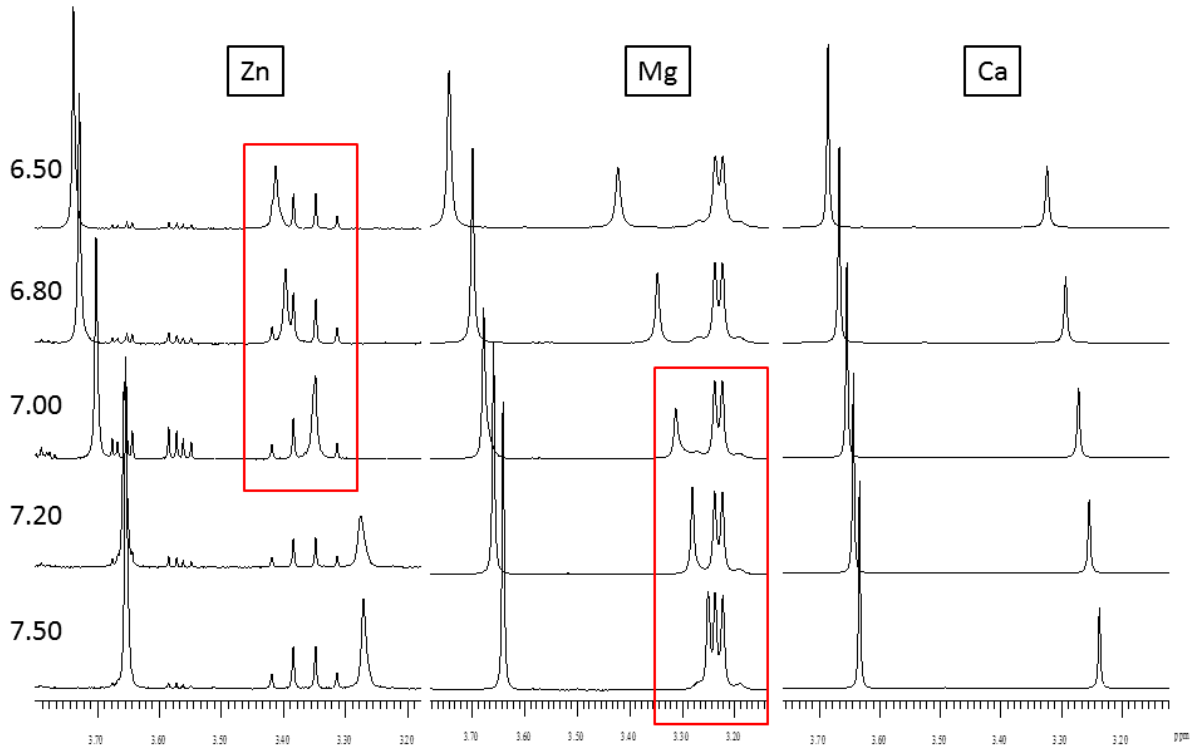

Figure 6: Qualitative assessment of representative 1H-NMR spectra across pH range 6.50, 6.80, 7.00, 7.20 and 7.50 for Zn (left), Mg (middle) and Ca (right). Red boxes indicate regions where free EDTA peak infringes upon chelated EDTA peak.

3.8.1.3 Experiment 3

For experiment 3, samples were prepared based upon the optimal EDTA and pH from experiments 1 and 2, respectively. Samples were prepared in triplicate across the dilution ranges of Zn, Mg and Ca, shown in Table 2. Hence, 42 samples were prepared for each ion and loaded randomly onto the NMR auto sampler to mitigate bias. For the assessment of our method four measures were examined, namely: accuracy, precision, linearity, and repeatability.

Table 4: Quantitative output of experiment 3 for the 4-proton and 8-proton EDTA chelated complexes across 14 concentration levels of Ca, Mg and Zn, including the true values.

LvL		4Ca-EDTA	8Ca-EDTA	True Ca	4Mg-EDTA	8Mg-EDTA	True Mg	4Zn-EDTA	8Zn-EDTA	True Zn
1	Mean	254,3	281,5	255	123,0	138,3	142,5	3,6	4,2	3,4
	Std	3,9	2,4		1,9	1,4		0,8	0,6	
	CV	1,5	0,9		1,6	1,0		23,5	14,5	
2	Mean	319,0	352,0	335	179,7	193,5	207,5	6,5	7,5	4,95
	Std	4,3	7,4		1,2	0,5		0,4	0,6	
	CV	1,4	2,1		0,7	0,3		6,5	7,9	
3	Mean	499,2	540,3	510	249,1	269,5	285	8,6	10,6	6,8
	Std	2,6	2,3		2,2	2,1		0,3	2,4	
	CV	0,5	0,4		0,9	0,8		3,3	22,5	
4	Mean	647,7	697,1	670	352,2	371,5	415	10,6	10,9	9,9
	Std	1,6	2,7		1,3	0,7		1,2	1,4	
	CV	0,3	0,4		0,4	0,2		11,2	12,6	
5	Mean	733,2	786,3	765	375,5	397,4	427	10,6	10,9	10,2
	Std	10,0	9,8		5,6	4,1		0,3	0,5	
	CV	1,4	1,2		1,5	1,0		2,7	4,5	
6	Mean	943,7	1007,8	1005	503,4	526,6	570	13,8	13,7	13,6
	Std	5,1	5,6		6,1	6,6		0,8	1,1	
	CV	0,5	0,6		1,2	1,3		5,9	8,3	
7	Mean	951,5	1017,4	1020	546,9	572,3	622,5	16,4	16,2	14,85
	Std	3,6	3,2		8,0	8,3		0,6	0,8	
	CV	0,4	0,3		1,5	1,4		3,4	5,0	
8	Mean	1236,4	1316,5	1275	626,5	652,1	712,5	17,0	17,0	17
	Std	5,8	4,1		11,6	12,9		1,4	1,2	
	CV	0,5	0,3		1,9	2,0		8,3	6,9	
9	Mean	1273,9	1356,0	1340	735,1	764,9	830	19,2	23,1	19,8
	Std	19,5	20,9		7,8	7,6		2,1	5,3	
	CV	1,5	1,5		1,1	1,0		11,1	22,9	
10	Mean	1426,8	1530,7	1530	765,0	797,1	855	20,0	20,1	20,4
	Std	2,9	5,0		7,4	4,8		0,8	0,6	
	CV	0,2	0,3		1,0	0,6		3,9	3,0	
11	Mean	1577,1	1676,0	1675	900,2	933,7	997,5	24,3	24,8	23,8
	Std	21,2	22,6		31,2	31,9		2,1	2,1	
	CV	1,3	1,4		3,5	3,4		8,6	8,8	
12	Mean	1691,3	1795,6	1785	913,0	945,8	1037	25,8	26,4	24,75
	Std	8,1	6,2		6,6	6,7		0,5	0,4	
	CV	0,5	0,4		0,7	0,7		2,0	1,5	
13	Mean	1857,4	1969,6	2010	1087,0	1124,1	1245	29,1	28,9	29,7
	Std	8,2	8,3		16,8	17,3		0,6	0,1	
	CV	0,4	0,4		1,5	1,5		2,2	0,5	
14	Mean	2240,3	2379,6	2345	1297,6	1340,2	1452,5	35,0	35,0	34,65
	Std	76,7	83,3		23,4	25,1		2,1	1,7	
	CV	3,4	3,5		1,8	1,9		6,0	4,9	

Concentrations given in micromolar (µM). Coefficients of variation (CVs) given in percentage (%).

3.8.1.3.1 Accuracy

For our study we used the % recovery to measure accuracy (Table 5). For Ca and Mg, the 8-proton EDTA complex (represented by the quartets at 3.13 and 3.23 ppm, respectively – Table 3) gave the more accurate results when compared to the 4-proton EDTA complex (represented by the singlets at 2.70 and 2.56 ppm, respectively – Table 3). For the medium to high concentrations of Mg and Ca the chelated quartet gave a median %error of 7.67% and 1.33%, for Mg and Ca respectively. However, the lower concentration ranges of Zn (~10 µM and lower, near the noise level), were difficult to quantify accurately. The 4-proton EDTA complex (represented by the singlet at 2.87 ppm – Table 3) gave the more accurate results for Zn, with a median %error of 2.81%. Overall, good accuracy was obtained by our method.

Table 5: Accuracy measured via % recovery for both the 4-proton and 8-proton EDTA complex of Ca, Mg and Zn.

LvL	% Recovery					
	4Ca-EDTA	8Ca-EDTA	4Mg-EDTA	8Mg-EDTA	4Zn-EDTA	8Zn-EDTA
1	99,72	110,39	86,28	97,07	104,35	123,03
2	95,24	105,07	86,59	93,24	130,38	150,78
3	97,87	105,95	87,39	94,56	126,83	156,06
4	96,67	104,04	84,86	89,52	106,72	110,19
5	95,85	102,79	87,93	93,07	103,72	106,66
6	93,90	100,28	88,32	92,38	101,56	100,43
7	93,28	99,75	87,86	91,93	110,27	108,81
8	96,97	103,25	87,93	91,53	99,94	100,08
9	95,07	101,19	88,57	92,16	96,83	116,49
10	93,25	100,04	89,47	93,23	97,67	98,71
11	94,16	100,06	90,24	93,60	101,89	104,20
12	94,75	100,59	88,04	91,21	104,25	106,54
13	92,41	97,99	87,31	90,29	97,94	97,24
14	95,53	101,48	89,34	92,27	100,91	101,00
Mean	95,33	102,35	87,87	92,58	105,95	112,87
Median	95,15	101,33	87,93	92,33	102,81	106,60

3.8.1.3.2 Precision and linearity

Both the precision and linearity of our results are illustrated in Fig. 7. For both Ca and Mg, a small amount of variation was evident at level 14 (highest concentration). For Zn, the 8-proton EDTA complex showed some varying degrees of variation, while the 4-proton EDTA complex showed minimal variation. Taking into consideration the qualitative (STD error bars in Fig. 7) and quantitative (STD in Table 4), it can be concluded that the variation was small enough to be considered negligible, across Ca, Mg and Zn. Hence, our method can be considered to have good precision. Furthermore, both Ca and Mg show good linearity in Fig 6 for both the 4-proton and 8-proton EDTA complexes, with a R^2 of 98% and 97%, respectively. For Zn, the linearity was considered good for the 4-proton EDTA complex with a R^2 of 97%, with the 8-proton EDTA complex exhibiting a lower R^2 of 96%. Overall, good linearity was achieved for our method.

3.8.1.3.3 Repeatability

For the final assessment of our method, the repeatability was assessed based upon the calculated CV (Table 6). For Ca, the CV ranged from 0.20 to 3.50%, with a median CV value of 0.53 and 0.49% for the 4-proton and 8-proton EDTA complexes, respectively. For Mg, the CV ranged from 0.20 to 3.47%, with a median CV value of 1.33 and 1.04% for the 4-proton and 8-proton EDTA complexes, respectively. For Zn, the CV ranged from 0.50 to 23.49%, with a median CV value of 5.91 and 7.40% for the 4-proton and 8-proton EDTA complex, respectively. Hence, both Ca and Mg showed excellent repeatability, each having an outlier CV at level 14 and 11, respectively. For Zn, because the concentration range was very low (close to the noise level), the repeatability was poorer. This highlights that the reliability of qNMR is poorer at low concentrations (~10 µM or below).

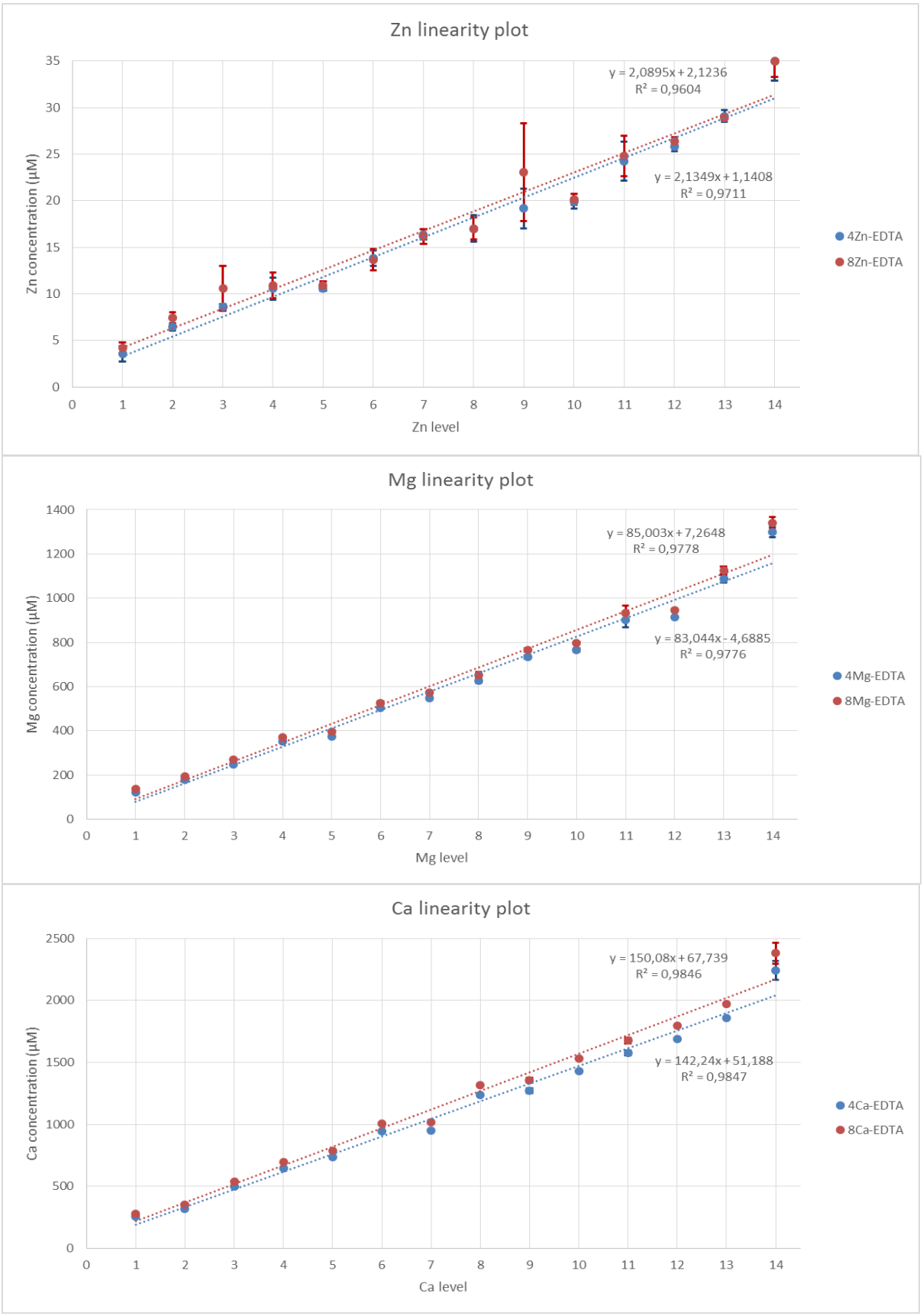

Figure 7: Linearity plots (with STD error bars) for Zn (top), Mg (middle) and Ca (bottom).

Table 6: Calculated CVs (%) across Ca, Mg and Zn chelated complexes.

LvL	4Ca-EDTA	8Ca-EDTA	4Mg-EDTA	8Mg-EDTA	4Zn-EDTA	8Zn-EDTA
1	1,52	0,85	1,57	1,04	23,49	14,50
2	1,36	2,11	0,67	0,28	6,50	7,89
3	0,52	0,43	0,88	0,78	3,28	22,54
4	0,25	0,39	0,38	0,20	11,23	12,56
5	1,37	1,24	1,48	1,04	2,73	4,45
6	0,54	0,55	1,20	1,26	5,86	8,25
7	0,38	0,32	1,47	1,44	3,37	4,95
8	0,47	0,31	1,86	1,98	8,34	6,90
9	1,53	1,54	1,06	0,99	11,05	22,86
10	0,20	0,33	0,96	0,60	3,92	2,97
11	1,34	1,35	3,47	3,42	8,62	8,75
12	0,48	0,35	0,72	0,71	2,01	1,53
13	0,44	0,42	1,54	1,54	2,17	0,50
14	3,42	3,50	1,80	1,87	5,95	4,92
Mean	0,99	0,98	1,36	1,22	7,04	8,83
Median	0,53	0,49	1,33	1,04	5,91	7,40
Max	3,42	3,50	3,47	3,42	23,49	22,86
Min	0,20	0,31	0,38	0,20	2,01	0,50

3.9 Discussion

The objectives of our study were to 1) determine the optimal concentration of chelating EDTA needed per ion based upon literature reference ranges, 2) identify the optimal pH per ion, within the physiological range of 6.50-7.50, and 3) apply these optimal conditions to evaluate our method for a linear concentration range of each ion. Of the five biologically important ions investigated, three ions (Ca, Mg and Zn) successfully chelated with free EDTA to produce complexes that produced unique ^{1}H-NMR spectral patterns. Based upon experiment 1, the optimal concentration of EDTA needed for Ca, Mg and Zn was 45, 30 and 3 mM, respectively. Based upon experiment 2, the optimal pH for analysis of Ca, Mg and Zn was 7.20, 6.50 and 7.50, respectively. With these method parameters experimentally determined, we set out to test our method in three different physiological concentration ranges (Table 2): “high” (Ca: 255–2345 µM), “medium” (Mg: 142,5–1452,5 µM), and “low” (Zn: 3,4–34,7 µM). Our method was evaluated based upon accuracy, precision, linearity, and repeatability.

- Accuracy – good. The “high” concentration range of Ca showed the highest accuracy (median %error of 1.33% for the 8-proton EDTA complex). Mg across all 14 levels examined showed lowered % recovery and an overall median %error of 7.67%. The “low” concentration range of Zn proved to show accurate results (median % error of 2.81%) for concentrations >10 µM, but Zn concentrations ~10 µM and lower were less accurate – a known limitation of quantitative metabolomics using NMR (Wishart, 2008). Within NMR metabolomics studies, the “detection threshold”, based on the signal to noise ratio in each spectrum (i.e., when the spectrum is noisy), is directly related to the number of scans during spectral acquisition. For our experiment we used 128 scans, most used for serum samples, which has a detection threshold of ~10 µM (Ravanbakhsh *et al*., 2015). Hence, concentrations ~10 µM and lower in ^{1}H-NMR metabolomics serum studies are typically quantitatively inaccurate.
- Precision – good. The standard deviation (STD; shown qualitatively in Fig. 7 and quantitatively in Table 4) was good across Ca, Mg and Zn, with a median STD of approximately 6, 7 and 1, respectively.
- Linearity – good. Ca and Mg had a consistent R^2 of 98% and 97%, respectively, across both the 4-proton and 8-proton EDTA chelated complexes. Zn had a R^2 of 96% for the 8-proton EDTA complex and 97% for the 4-proton EDTA complex.
- Repeatability – good. Ca and Mg had excellent median CVs of approximately 0.5 and 1.1%, respectively. Zn, however, proved less repeatable due its lower concentration values.

Hence, we achieved our aim by developing a qNMR method for metabolomics for the reliable quantification of Ca, Mg and Zn. The evaluation of the method showed good results, except for Zn

being less repeatable and less accurate at concentrations ~10 µM and lower. Our study also supports the work done by Somashekar *et al.* (2006), who observed that pH is inversely proportional to the error in quantitation in the case of Ca-EDTA – the higher the pH the lower the error of quantitation. According to Somashekar *et al*. (2006), at a pH less than 6.6 there is broadening of ^{1}H-NMR spectral peaks due to the elevated rate of destabilization of the complex as a result of partial protonation of the acetate groups. This was observed here for both Mg and Ca.

For our method, irrespective of EDTA concentration, both Fe and K did not chelate with EDTA within the physiological pH range of 6.50–7.50. For K we tried different substrates, such as potassium acetate and potassium formate, as well as potassium sulphate and potassium dichromate. All K substrates failed to chelate with EDTA. The specific reason as to why EDTA is known to bind to other metals and but not K^+ in the current setting, is unknown. For future method development, an alternative (biological) approach may be worth investigating. For example, nonactin, an antibiotic that is a medium sized organic molecule that transports metals across membranes, could potentially be used as a chelating agent in the quantitation of potassium (Zhan & Zheng, 2016). Stable complexes with cations such as K^+, NH_4^+ and Na^+ are formed with nonactin, giving nonactin the ability to transport these ions across membranes (Kusche *et al*., 2009). Conveniently, nonactin in $CDCl_3$ spectra have been identified using ^{1}H-NMR (Zhan & Zheng, 2016).

Like K, varying concentrations of EDTA within the physiological pH range of 6.50–7.50 did not lead to chelation of Fe. This was an unexpected result as EDTA is known to chelate both ferric and ferrous forms of iron. Further research identified that the synthesis of iron (III) EDTA is chemically more complex than originally anticipated (Loots *et al*., 2007). Further, a study on the recycling of lead contaminated EDTA wastewater Kim & Ong (1999) shed some more light on reasons as to why EDTA could not chelate with Fe in this study. According to Kim & Ong (1999) the relative stability of metal-EDTA chelation must be considered and in the presence of other metals it is determined by stability constants, pH of the solution, concentration of metals and EDTA. From Fig. 8 the optimal pH is inversely proportional to the log (stability constant) of the metal ion, and that Fe-EDTA is more stable at a pH lower than 3. At a higher pH, Fe-EDTA tends to precipitate (Kim & Ong, 1999). The role of EDTA-metal complex stability constants was further investigated by Flora & Pachauri (2010), where a metal with higher k constant competes for the chelating agent with a metal of lower stability value and ultimately removes the latter – shown in Table 7. However, other variables like the number of heterocyclic rings formed and relative concentration also play a role, which is why Ca^{2+} — readily available in body fluids — binds preferentially with EDTA in spite of the higher stability constant of Pb or Ni. Moreover, the predictability of the outcome in a biological fluid/system is limited regardless of all the known properties of an ideal chelator (Flora & Pachauri, 2010). Hence, more research of chelating agents within biological fluids/systems is warranted.

Table 7: EDTA-metal complex stability constants

Metal	Na	Li	Ba	Sr	Mg	Ca	Mn	Fe	Co	Zn	Cd	Pb	Ni
K (log)	1.7	2.8	7.8	8.6	8.7	10.6	13.4	14.4	16.1	16.1	16.4	18.3	18.4

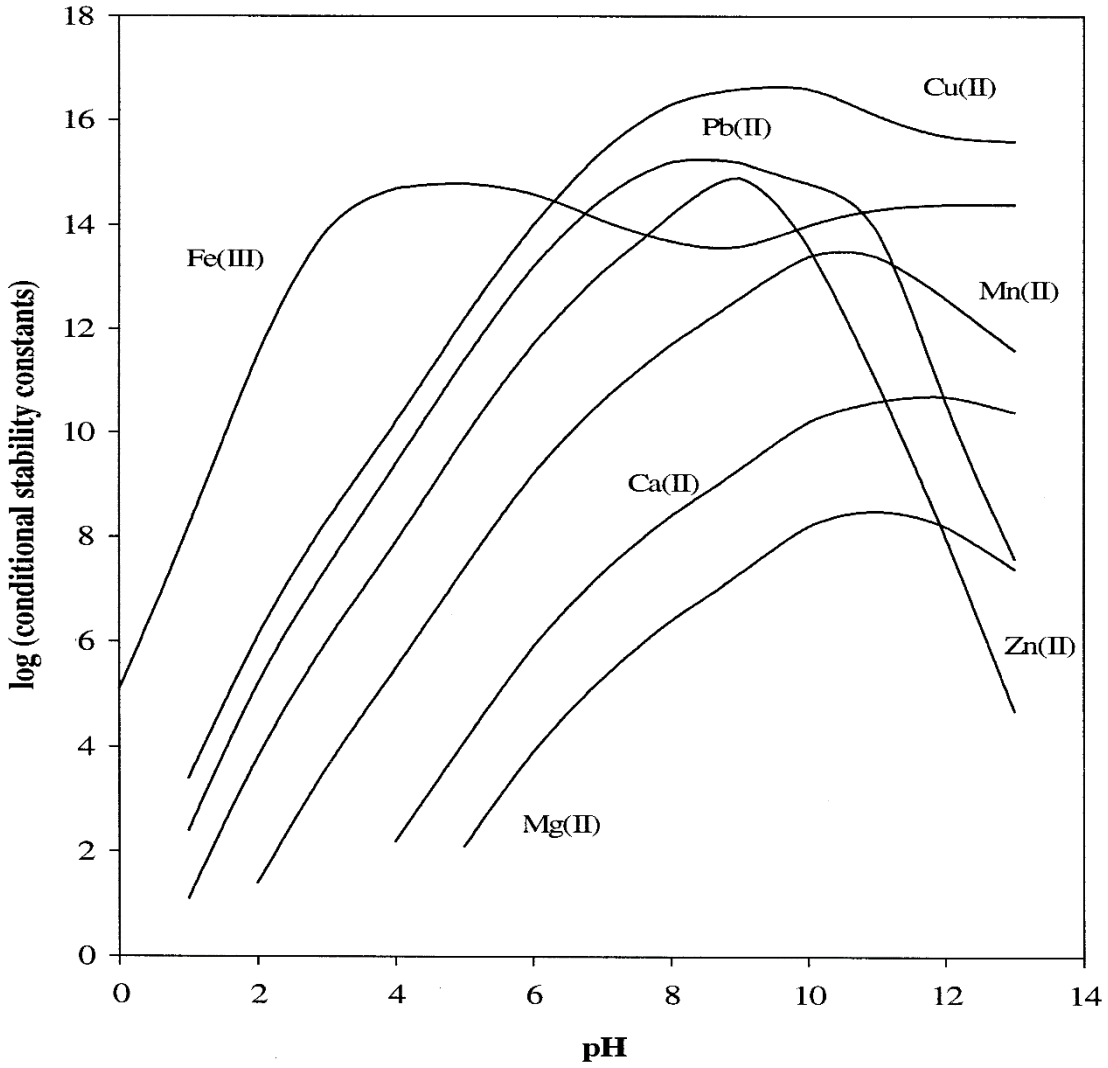

Figure 8: Comparison of conditional stability constants for various metal–EDTA complexes as a function of pH (Kim & Ong, 1999).

Since there was no chelation at the desired physiological pH range of 6.50–7.50, another chelating agent that forms a stable metal-chelating agent is needed for the absolute quantification of Fe. Therefore, deferoxamine mesylate (DFO), a well-known FDA-approved iron chelator, could be the

perfect substitute for EDTA. Under physiological conditions iron is extremely insoluble. Bacteria can secrete and use DFO in order to assimilate iron in highly scarce conditions. DFO exhibits a high affinity for Fe (III), which occurs in low concentrations under aerobic conditions. DFO has been the gold standard iron chelating agent in clinical practice for the past four decades (Lazaridou *et al*., 2020), used in treating iron overload-associated diseases like thalassemia and tumors (Umemura *et al*., 2017). The use of DFO has prolonged and improved the quality of life for numerous iron overload patients [Piccioni *et al*., 2020, Taher & Saliba, 2017]. *In vitro* and *in vivo* studies have shown that DFO can chelate with Fe (III) in a 1:1 reaction to form highly stable compounds preventing further chemical reactions (Yu *et al*., 2017). In the presence of other metal ions or chelating agents DFO binds to iron first. Conveniently, free DFO is expected to produce two clear triplet peaks in a ^{1}H-NMR spectrum – at 2.00 ppm and another at 2.80 ppm. Due to its high affinity for iron (III), DFO is the befitting chelating agent for further investigation in a metabolomics setting, for the development of a ^{1}H-NMR quantitative method of Fe (III) in serum under physiological conditions.

3.10 Conclusion We have presented a quantitative ^{1}H-NMR analysis of biologically important ions using EDTA as a chelating agent within physiological pH and concentration ranges for the field of metabolomics. The idea of quantifying metal ions using EDTA as a chelating agent and ^{1}H-NMR spectroscopy is one that has been put into practice in chemistry and our study supports the work done by Hafer et al. (2020) and Somashekar et al. (2006). Our ^{1}H-NMR method was able to accurately and reliably quantify Ca, Mg and Zn. A limitation was that for concentrations ~10 µM and lower our method became less accurate and repeatable. Fe and K failed to chelate with EDTA under our experimental conditions. We acknowledge that the scope of our study presented here was limited to pure single ion solutions; however, our study lays the foundation for the genesis of further quantitative ^{1}H-NMR method development of simultaneous analysis of Ca, Mg and Zn in biological samples, specifically within the field of metabolomics. Further development includes modelling ion mixtures to verify the application limits, as well as application to biological samples. Presumably, within a biological matrix (e.g., serum, CSF) where multiple ions are present, increased concentration of EDTA would be required and adjustments (pH and reagent concentrations) would need to be incorporated to account for possible interferences (e.g., overlapping ^{1}H-NMR peaks). Furthermore, once this ^{1}H-NMR method has been standardized for biological matrices, comparisons would need to be made to the ‘gold-standard’ methods utilized by chemistry (i.e., ion chromatography, flame atomic absorption spectrometry and inductively coupled plasma mass spectrometry). As for Fe, we have identified that there is a need to investigate further using potential catalysts and a more specific chelating agent, such as DFO. Lastly, Fe is known to bind to transferrin in biological samples, so an additional pre-treatment step (addition of

nitrilotriacetate or citrate) of the biological samples would be needed to release any bound Fe – a step to consider for other biological ions as well.

3.11 Declarations

Declaration of interest

Declarations of interest: none.

Funding

This research did not receive any specific grant from funding agencies in the public, commercial, or not-for-profit sectors.

CRediT authorship contribution statement

Emmanuel Mathuthu: Investigation, Formal analysis, Methodology, Writing - original draft, Writing - review & editing.

Angelique Janse van Rensburg: Investigation, Formal analysis, Methodology, Writing - review & editing.

Dean Du Plessis: Investigation, Formal analysis, Methodology, Writing - review & editing.

Shayne Mason: Conceptualization, Formal analysis, Methodology, Writing - original draft, Writing - review & editing, Supervision.

3.12 References

Abd El-Hafeez, M., Naser K.A., Mohamed, T.E., Mostafa, M., & Khairee, M.M. 2003. Complicated versus non-complicated cases of tuberculous meningitis as regard CSF cell count, polymorphs, lymphocytes, protein, glucose, sodium and cortisol. *Al- Azhar Assiut Medical Journal*, 1(3):168–180.

Aisen, P., Enns, C., & Wessling-Resnick, M. 2001. Chemistry and biology of eukaryotic iron metabolism. *The International Journal of Biochemistry & Cell Biology*, *33*(10):940–959.

Aldahl, M., Jensen, A.S.C., Davidsen, L., Eriksen, M.A., Møller Hansen, S., Nielsen, B.J., & Søgaard, P. 2017. Associations of serum potassium levels with mortality in chronic heart failure patients. *European Heart Journal*, 38(38):2890–2896.

Alimonti, A., Bocca, B., Pino, A., Ruggieri, F., Forte, G., & Sancesario, G. 2007. Elemental profile of cerebrospinal fluid in patients with Parkinson's disease. *Journal of Trace Elements in Medicine and Biology*, 21(4):234–241.

Arnaud, M.J. 2008. Update on the assessment of magnesium status. *British Journal of Nutrition*, 99(3):24–36.

Auld, D.S. 2009. The ins and outs of biological zinc sites. *Biometals*. 22:141–148.

Avino, P., Capannesi, G., Manigrasso, M., Sabbioni, E., & Rosada, A. 2011. Element assessment in whole blood, serum and urine of three Italian healthy sub-populations by INAA. *Microchemical Journal*, 99(1):548–555.

Baltaci, A.K., Yuce, K., & Mogulkoc, R. 2018. Zinc metabolism and metallothioneins. *Biological Trace Element Research*, 183(1):22–31.

Barbagallo, M., Belvedere, M., & Dominguez, L.J. 2009. Magnesium homeostasis and aging. *Magnesium Research*, *22*(4):235–246.

Beckonert, O., Keun, H.C., Ebbels, T.M., Bundy, J., Holmes, E., & Nicholson, J.K. 2007. Metabolic profiling, metabolomic and metabonomic procedures for NMR spectroscopy of urine, plasma, serum and tissue extracts. *Nature Protocols*, 2(11):2692–2703.

Bittner, S., & Meuth, S.G. 2013. Targeting ion channels for the treatment of autoimmune neuroinflammation. *Therapeutic Advances in Neurological Disorders*, 6(5):322–336.

Bittner, S., & Meuth, S.G. 2013. Targeting ion channels for the treatment of autoimmune neuroinflammation. *Therapeutic Advances in Neurological Disorders*, *6*(5):322–336.

Bocca, B., Forte, G., Petrucci, F., Pino, A., Marchione, F., & Bomboi, G. 2005. Monitoring of chemical elements and oxidative damage in patients affected by Alzheimer's disease. *Annali Dell'Istituto Superiore di Sanita*, 41(2):197–203.

Bouillon, R. 2019. Calcium homeostasis in humans. In Encyclopedia of Endocrine Diseases (Second Edition). Huhtaniemi, I. & Martini, L., eds. Oxford: Academic Press:52–57.

Camaschella, C. 2015. Iron-deficiency anemia. *New England Journal of Medicine*, 372(19):1832–1843.

Cassandri, M., Smirnov, A., Novelli, F., Pitolli, C., Agostini, M., Malewicz, M., & Raschellà, G. 2017. Zinc-finger proteins in health and disease. *Cell Death Discovery*, 3(1):1–12.

Da Silva, J.F., & Williams, R.J.P. 2001. The biological chemistry of the elements: the inorganic chemistry of life. Oxford University Press.

Dave, D.D., & Jha, B.K. 2018. Analytically depicting the calcium diffusion for Alzheimer's affected cell. *International Journal of Biomathematics*, 11(7):1850088.

De Baaij, J.H., Hoenderop, J.G., & Bindels, R.J. 2015. Magnesium in man: implications for health and disease. *Physiological Reviews*, 95(1):1–46.

Dierichs, L., Kloubert, V., & Rink, L. 2018. Cellular zinc homeostasis modulates polarization of THP-1-derived macrophages. European *Journal of Nutrition*, 57(1):2161–2169.

Dierichs, L., Kloubert, V., & Rink, L. 2018. Cellular zinc homeostasis modulates polarization of THP-1-derived macrophages. *European Journal of Nutrition*, 57(1):2161–2169.

Elin, J.R. 2010. Assessment of magnesium status for diagnosis and therapy. *Magnesium Research*, 23 (4):194–198.

Emwas, A.H., Roy, R., McKay, R.T., Tenori, L., Saccenti, E., Gowda, G.A., & Wishart, D.S. 2019. NMR spectroscopy for metabolomics research. *Metabolites*, 9(7):123–162.

Farthing, M.J., 1989. Iron and immunity. *Acta Paediatrica*, 78:44–52.

Fawcett, W.J., Haxby, E.J., & Male, D.A. 1999. Magnesium: physiology and pharmacology. *British Journal of Anaesthesia,* 83(2):302–20.

Flora, S.J. & Pachauri, V. 2010. Chelation in metal intoxication. International Journal of *Environmental Research and Public Health*, 7(7):2745–2788.

Forte, G., Alimonti, A., Pino, A., Stanzione, P., Brescianini, S., Brusa, L., Sancesario, G., Violante, N. & Bocca, B. 2005a. Metals and oxidative stress in patients with Parkinson's disease. *Annali Dell'Istituto Superiore di Sanita*, 41(2):189–195.

Forte, G., Visconti, A., Santucci, S., Ghazaryan, A., Figà-Talamanca, L., & Cannoni, S. 2005b. Quantification of chemical elements in blood of patients affected by multiple sclerosis. *Annali Dell'Istituto Superiore di Sanita*, 41(2):213–216.

Ganz, T. 2019. Erythropoietic regulators of iron metabolism. *Free Radical Biology and Medicine*, 133:69–74.

Gibson, R.S., Hess, S.Y., Hotz, C., & Brown, K.H. 2008. Indicators of zinc status at the population level: a review of the evidence. *British Journal of Nutrition*, 99(3):14–23.

Giraudeau, P. 2017. Challenges and perspectives in quantitative NMR. *Magnetic Resonance in Chemistry*, 55(1):61–69.

Goldstein, D.A. 1990. Serum calcium. In Clinical Methods: The History, Physical, and Laboratory Examinations. 3rd edition. Butterworths.

Hafer, E., Holzgrabe, U., Kraus, K., Adams, K., Hook, J.M., & Diehl, B. 2020. Qualitative and quantitative 1H NMR spectroscopy for determination of divalent metal cation concentration in model salt solutions, food supplements, and pharmaceutical products by using EDTA as chelating agent. *Magnetic Resonance in Chemistry*, 58(7):653–665.

Han, S., & Ba, Y. 2004. Determination of the concentrations of metal cations in aqueous solutions using proton NMR spectral area integration of the EDTA complexes. *Journal of Solution Chemistry,* 33:301–312.

Harrison, P.M., & Arosio, P. 1996. The ferritins: molecular properties, iron storage function and cellular regulation. *Biochimica et Biophysica Acta (BBA)-Bioenergetics*, 1275(3):161–203.

Hegde, M.L., Shanmugavelu, P., Vengamma, B., Rao, T.S., Menon, R.B., Rao, R.V., & Rao, K.J. 2004. Serum trace element levels and the complexity of inter-element relations in patients with Parkinson's disease. *Journal of Trace Elements in Medicine and Biology*, 18(2):163–171.

Hegde, M.L., Shanmugavelub, P., Vengammac, B., Raod, T.S.S., Menon, R.B., Raob, R.V. & Jagannatha Rao, K.S. 2004. Serum trace element levels and the complexity of inter-element relations in patients with Parkinson’s disease. *Journal of Trace Elements in Medicine and Biology*,18:163–171.

Hess, S.Y., Peerson, J.M., King, J.C., & Brown, K.H. 2007. Use of serum zinc concentration as an indicator of population zinc status. *Food and Nutrition Bulletin*, *28*(3):403–429.

Ifeanyi, O.E. 2018. A review on iron homeostasis and anaemia in pulmonary tuberculosis. *International Journal of Healthcare and Medical Sciences*, 4(5):84–89.

Jahnen-Dechent, W., & Ketteler, M. 2012. Magnesium basics. *Clinical Kidney Journal*, 5(1):3–14.

Jimenez-Jimenez, F.J., Molina, J.A., Aguilar, M.V., Meseguer, I., Mateos-Vega, C.J., & Gonzalez-Munoz, M.J. 1998. Cerebrospinal fluid levels of transition metals in patients with Parkinson's disease. *Journal of Neural Transmission*, 105(4-5):497–505.

Jomova, K., & Valko, M. 2011. Importance of iron chelation in free radical-induced oxidative stress and human disease. *Current Pharmaceutical Design*, *17*:3460–3473.

Keowmaneechai, E., & McClements, D.J. 2002. Influence of EDTA and citrate on physicochemical properties of whey protein-stabilized oil-in-water emulsions containing CaCl2. *Journal of Agricultural and Food Chemistry*, 50(24):7145–7153.

Kim, C., & Ong, S.K. 1999. Recycling of lead-contaminated EDTA wastewater. Journal of Hazardous Materials, 69(3):273–286.

Kondaiah, P., Yaduvanshi, P.S., Sharp, P.A., & Pullakhandam, R. 2019. Iron and zinc homeostasis and interactions: does enteric zinc excretion cross-talk with intestinal iron absorption. *Nutrients*, 11(1):1885–1899.

Kusche, B.R., Smith, A.E., McGuirl, M.A., & Priestley, N.D. 2009. Alternating pattern of stereochemistry in the nonactin macrocycle is required for antibacterial activity and efficient ion binding. *Journal of the American Chemical Society*, 131(47):17155–17165.

LaFerla, F.M. 2002. Calcium dyshomeostasis and intracellular signaling in Alzheimer's disease. *Nature Reviews Neuroscience*, 3(11):862–872.

Laires, M.J., Monteiro, C.P., & Bicho, M. 2004. Role of cellular magnesium in health and human disease. *Frontiers in Bioscience*, 9:262–276.

Lanza, I.R., Zhang, S., Ward, L.E., Karakelides, H., Raftery, D. & Nair K.S. 2010. Quantitative metabolomics by 1H-NMR and LC-MS/MS confirms altered metabolic pathways in diabetes. *Metabolomics in Diabetes*, 5(5):10538.

Lazaridou, M., Christodoulou, E., Nerantzaki, M., Kostoglou, M., Lambropoulou, D.A., Katsarou, A., & Bikiaris, D.N. 2020. Formulation and in-vitro characterization of chitosan-nanoparticles loaded with the iron chelator deferoxamine mesylate (DFO). *Pharmaceutics*, 12(3):238–255.

Lentner, C. ed., 1992. Geigy Scientific Tables: Bacteria, Fungi, Protozoa, Helminths (6) Ciba-Geigy.

Lim, N.C., Freake, H.C., & Brückner, C. 2005. Illuminating zinc in biological systems. *Chemistry–A European Journal*, 11(1):38–49.

Loots, D.T., Lieshout, M.V., & Lachmann, G. 2007. Sodium iron (III) ethylenediaminetetraacetic acid synthesis to reduce iron deficiency globally. *European Journal of Clinical Nutrition*, 61(2):287–289.

Lowe, N.M., Fekete, K., & Decsi, T. 2009. Methods of assessment of zinc status in humans: a systematic review. *The American Journal of Clinical Nutrition*, 89(6):2040–2051.

Lvova, L., Gonçalves, C.G., Di Natale, C., Legin, A., Kirsanov, D., & Paolesse, R. 2018. Recent advances in magnesium assessment: from single selective sensors to multisensory approach. *Talanta*, *179*:430–441.

Maret, W. 2009. Molecular aspects of human cellular zinc homeostasis: redox control of zinc potentials and zinc signals. *Biometals*, 22(1):149–157.

McEwen, I. 2010. Broadening of 1H NMR signals in the spectra of heparin and OSCS by paramagnetic transition metal ions. The use of EDTA to sharpen the signals. *Journal of Pharmaceutical and Biomedical Analysis,* 51(3):733–735.

Mewara, A., Bhosale, H.S.T.V.S., & Ramadoss, P.D.R. 2018. Assessment of serum levels of copper and zinc in OSMF patients: a preliminary study. *Journal of Research and Advancement in Dentistry,* 8(1):38–41.

Milto, I.V., Suhodolo, I.V., Prokopieva, V.D., & Klimenteva, T.K. 2016. Molecular and cellular bases of iron metabolism in humans. *Biochemistry (Moscow)*, 81(6):549–564.

Mohammadi, Z., Shalavi, S., & Jafarzadeh, H. 2013. Ethylenediaminetetraacetic acid in endodontics. *European Journal of Dentistry*, 7(1):135–142.

Molina, J.A., Jimenez-Jimenez, F.J., Aguilar, M.V., Meseguer, I., Mateos-Vega, C.J., & Gonzalez-Munoz, M.J. 1998. Cerebrospinal fluid levels of transition metals in patients with Alzheimer's disease. *Journal of Neural Transmission*, 105(4-5):479–488.

Muñoz, M., Villar, I., & García-Erce, J.O. 2009. An update on iron physiology. World *Journal of Gastroenterology*, 15(37):4617–4626.

Murakami, M., & Hirano, T. 2008. Intracellular zinc homeostasis and zinc signalling. *Cancer Science*, 99(8):1515–1522.

Musso, C.G. 2009. Magnesium metabolism in health and disease. *International Urology and Nephrology,* 41:357–362.

Nasrallah, G.K., Salem, R., Da'as, S., Ahmad Al-Jamal, O.L., Scott, M., & Mustafa, I. 2019. Biocompatibility and toxicity of novel iron chelator Starch-Deferoxamine (SDFO) compared to zinc oxide nanoparticles to zebrafish embryo: an oxidative stress-based apoptosis, physicochemical and neurological study profile. *Neurotoxicology and Teratology,* 72:29–38.

Nicholson, J.K., Buckingham, M.J. & Sadler, P.J. 1983. High resolution ^{1}H NMR studies of vertebrate blood and plasma. *Biochemical Journal*, 211(3), 605–615.

Nicholson, J.K., Holmes, E., & Wilson, I.D. 2005. Gut microorganisms, mammalian metabolism and personalized health care. *Nature Reviews Microbiology*, 3:431–438.

Noronha, J.L. & Matuschak, G.M. 2002. Magnesium in critical illness: metabolism, assessment, and treatment*. Intensive Care Med*, 28:667–679.

Osredkar, J. & Sustar, N. 2011. Copper and zinc, biological role and significance of copper/zinc imbalance. *The Journal of Clinical Toxicology*, 3(2161):0495.

Ozcankaya, R., & Delibas, N. 2002. Malondialdehyde, superoxide dismutase, melatonin, iron, copper, and zinc blood concentrations in patients with Alzheimer disease: cross-sectional study. *Croatian Medical Journal*, 43(1):28–32.

Ozment, C.P., & Turi, J.L. 2009. Iron overload following red blood cell transfusion and its impact on disease severity. *Biochimica et Biophysica Acta (BBA)-General Subjects*, 1790(7):694–701.

Panda, S.K., & Chaudhuri, S. 2007. Chelating ligand-mediated synthesis of hollow ZnS microspheres and its optical properties. *Journal of Colloid and Interface Science*, 313(1):338–344.

Piccioni, M.G., Capone, C., Vena, F., Del Negro, V., Schiavi, M.C., D'Ambrosio, V., & Brunelli, R. 2020. Use of deferoxamine (DFO) in transfusion-dependent β-thalassemia during pregnancy: A retrospective study. *Taiwanese Journal of Obstetrics and Gynecology*, 59(1):120–122.

Pravina, P., Sayaji, D., & Avinash, M. 2013. Calcium and its role in human body. *International Journal of Research in Pharmaceutical and Biomedical Sciences*, 4(2):659–668.

Provan, D., & Gribben, J., eds. 2010. *Molecular hematology*. John Wiley & Sons.

Puntarulo, S. 2005. Iron, oxidative stress and human health. *Molecular Aspects of Medicine*, 26(4-5):299–312.

Ravanbakhsh, S., Liu, P., Bjordahl, T.C., Mandal, R., Grant, J.R., Wilson, M., & Greiner, R. 2015. Accurate, fully-automated NMR spectral profiling for metabolomics. *PloS One,* 10(5):e0124219.

Razzaque, M.S. 2018. Magnesium: are we consuming enough? *Nutrients*, *10*(12):1863–1870.

Rude, R.K. 1998. Magnesium deficiency: a cause of heterogenous disease in humans. *Journal of Bone and Mineral Research*, 13(4):749–759.

Sahiratmadja, E., Wieringa, F.T., Van Crevel, R., De Visser, A.W., Adnan, I., Alisjahbana, B., Slagboom, E., & Marx, J.J.M. 2007. Iron deficiency and NRAMP1 polymorphisms (INT4, D543N and 30UTR) do not contribute to severity of anaemia in tuberculosis in the Indonesian population. *British Journal of Nutrition*, 98:684–690.

Sampson, B., Kovar, I.Z., Rauscher, A., Fairweather-Tait, S., Beattie, J., & Mcardle, H.J. 1997. A case of hyperzincemia with functional zinc depletion: a new disorder? *Pediatric Research*, 42(2):219–225.

Sepehri, Z., Mirzaei, N., Sargazi, A., Sargazi, A., Mishkar, A.P., Kiani, Z., & Ghavami, S. 2017. Essential and toxic metals in serum of individuals with active pulmonary tuberculosis in an endemic region. *Journal of Clinical Tuberculosis and Other Mycobacterial Diseases,* 6:8–13*.*

Skalny, A.V., Simashkova, N.V., Skalnaya, A.A., Klyushnik, T.P., Zhegalova, I.V., Grabeklis, A.R., ... Tinkov, A.A. 2018. Trace element levels are associated with neuroinflammatory markers in children with autistic spectrum disorder. *Journal of Trace Elements in Medicine and Biology*, *50*: 622-628.

Smith, I. 2005. Convulsions and coma associated with estrogenically elevated CSF calcium levels post spinal surgery: a case report. *Critical Care Resuscitation*, 7:173–176.

Somashekar, B. S., Ijare, O. B., Nagana Gowda, G. A., Ramesh, V., Gupta, S., & Khetrapal, C.L. 2006. Simple pulse-acquire NMR methods for the quantitative analysis of calcium, magnesium and sodium in human serum*. Spectrochimica Acta Part A*, 65, 254–260.

Sousa, C., Moutinho, C., Vinha, A.F., & Matos, C. 2019. Trace minerals in human health: iron, zinc, copper, manganese and fluorine. *International Journal of Science and Research Methodology*, 13:57–80.

Swaminathan, R. 2003. Magnesium metabolism and its disorders. *Clinical Biochemistry Review*, 24:47–66.

Taher, A.T., & Saliba, A.N. 2017. Iron overload in thalassemia: different organs at different rates. *Hematology*, 2017(1):265–271.

Tandy, S., Bossart, K., Mueller, R., Ritschel, J., Hauser, L., Schulin, R., & Nowack, B.,2004. Extraction of heavy metals from soils using biodegradable chelating agents. *Environmental Science & Technology*, 38(3):937–944.

Umemura, M., Kim, J.H., Aoyama, H., Hoshino, Y., Fukumura, H., Nakakaji, R., & Tanaka, R. 2017. The iron chelating agent, deferoxamine detoxifies Fe (Salen)-induced cytotoxicity. *Journal of Pharmacological Sciences*, 134(4):203–210.

Vigil, F.A., Bozdemir, E., Bugay, V., Chun, S.H., Hobbs, M., Sanchez, I., & Carver, C. 2020. Prevention of brain damage after traumatic brain injury by pharmacological enhancement of KCNQ (Kv7,“M-type”) K+ currents in neurons. *Journal of Cerebral Blood Flow & Metabolism*, 40(6):1256–1273.

Vormann, J. 2016. Magnesium: nutrition and homoeostasis. *AIMS Public Health*, 3(2):329–340.

Vormann, J., 2003. Magnesium: nutrition and metabolism. *Molecular Aspects of Medicine*, 24(1):27–37.

Watari, H., Tose, A.J., & Bosma, M.M. 2012. Hyperpolarization of resting membrane potential causes retraction of spontaneous Ca^{2+} transients during mouse embryonic circuit development. *The Journal of Physiology*, 591(4):973–983.

Waugh, A., & Grant, A. 2014. Ross & Wilson Anatomy and physiology in health and illness E-book. Elsevier Health Sciences.

Weiss, G. 2002. Iron and immunity: a double-edged sword. *European Journal of Clinical Investigation*, 32:70–78.

Wieringa, F.T., Dijkhuizen, M.A., Fiorentino, M., Laillou, A., & Berger, J. 2015. Determination of zinc status in humans: which indicator should we use? *Nutrients*, *7*(5):3252–3263.

Wishart, D.S. 2008. Quantitative metabolomics using NMR. TrAC *Trends in Analytical Chemistry*, 27(3):228–237.

Wu, A.H.B. 2006. Tietz clinical guide to laboratory tests. 4th ed. St. Louis: Saunders/Elsevier.

Yiannikourides, A., & Latunde-Dada, G.O. 2019. A short review of iron metabolism and pathophysiology of iron disorders. *Medicines*, 6:85–100.

Yu, J., Yuan, Q., Sun, Y.R., Wu, X., Du, Z.Y., Li, Z.Q., & Hu, J. 2017. Effects of deferoxamine mesylate on hematoma and perihematoma edema after traumatic intracerebral hemorrhage. *Journal of Neurotrauma*, 34(19):2753–2759.

Zhan, Y., & Zheng, S. 2016. Efficient production of nonactin by Streptomyces griseus subsp. griseus. *Canadian Journal of Microbiology*, 62(8):711–714.

CHAPTER 4 EVALUATING DFO AS A CHELATING AGENT USING ^{1}H-NMR SPECTROSCOPY

Introduction

Metal chelators have a wide range of applications in both in scientific research and medicine (Cho, 2020). One example is lanthanide metal-chelator, used as signal shifting agent to increase ^{1}H-NMR resolution (Von Ammon & Fischer, 1972). Deferoxamine (DFO) is an iron chelator that has been used for more than four decades to treat hemosiderosis (Porter et al., 2005). Body cells require adequate amount of iron. Progressive iron accumulation overwhelms the body's capacity of adequate sequestration of excess iron, leading to iron overload (Brittenham & Badman, 2003). Iron is tremendously important in haemoglobin synthesis of erythrocytes, oxidation–reduction reactions, and cellular proliferation (Kohgo *et al.,* 2008). Nutritional deficiency can provoke increased susceptibility to infectious diseases. Iron deficiency can be due to malabsorption or iron deprivation (Punnonen *et al.,* 1994). Non-transferrin bound iron (NTBI) was associated with iron overload conditions (Gosriwatana *et al.,* 1999). Many potential ligands have been used to capture iron in serum (Gosriwatana *et al.,* 1999). The capacity of DFO to chelate and excrete iron in overload patients has been well documented in literature (Breuer *et al.,* 2001).

The first NMR-based metabolic studies date back to the 1970's, and NMR has since played a central role in our understanding of metabolism and metabolic processes of both healthy and diseased tissue (Wishart, 2008). Up to date, NMR still has several advantages over its competitors: it is a non-destructive, non-biased and easily quantifiable method which requires little or no sample preparation. It is particularly amenable to compounds that are difficult to analyse by its counterparts GC-and LC-MS (Wishart, 2008). Currently, there is no ^{1}H-NMR serum iron quantification method. The manuscript that follows describes the development of a method to use DFO as a chelating agent of iron to quantify iron in serum using ^{1}H-NMR.

Paper 2: Chelation ^{1}H-NMR method development for quantifying iron in serum using deferoxamine

Emmanuel Mathuthu[a] & Shayne Mason[a,*]

[a] Human Metabolomics, Faculty of Natural and Agricultural Sciences, North-West University, Potchefstroom, South Africa.

[*] Corresponding author: Shayne Mason (https://orcid.org/0000-0002-2945-5768)
North-West University
Private Bag X6001
Potchefstroom
South Africa
2531

Email: nmr.nwu@gmail.com

Email addresses:
Emmanuel Mathuthu: emmanuelmathuthu@gmail.com

Keywords:

Proton nuclear magnetic resonance (^{1}H-NMR) spectroscopy; iron; chelation; deferoxamine; ferroxamine; method development

Submitted for peer-review to the journal *Biochemistry and Cell Biology* on 26 March 2021.

Proof of submission:

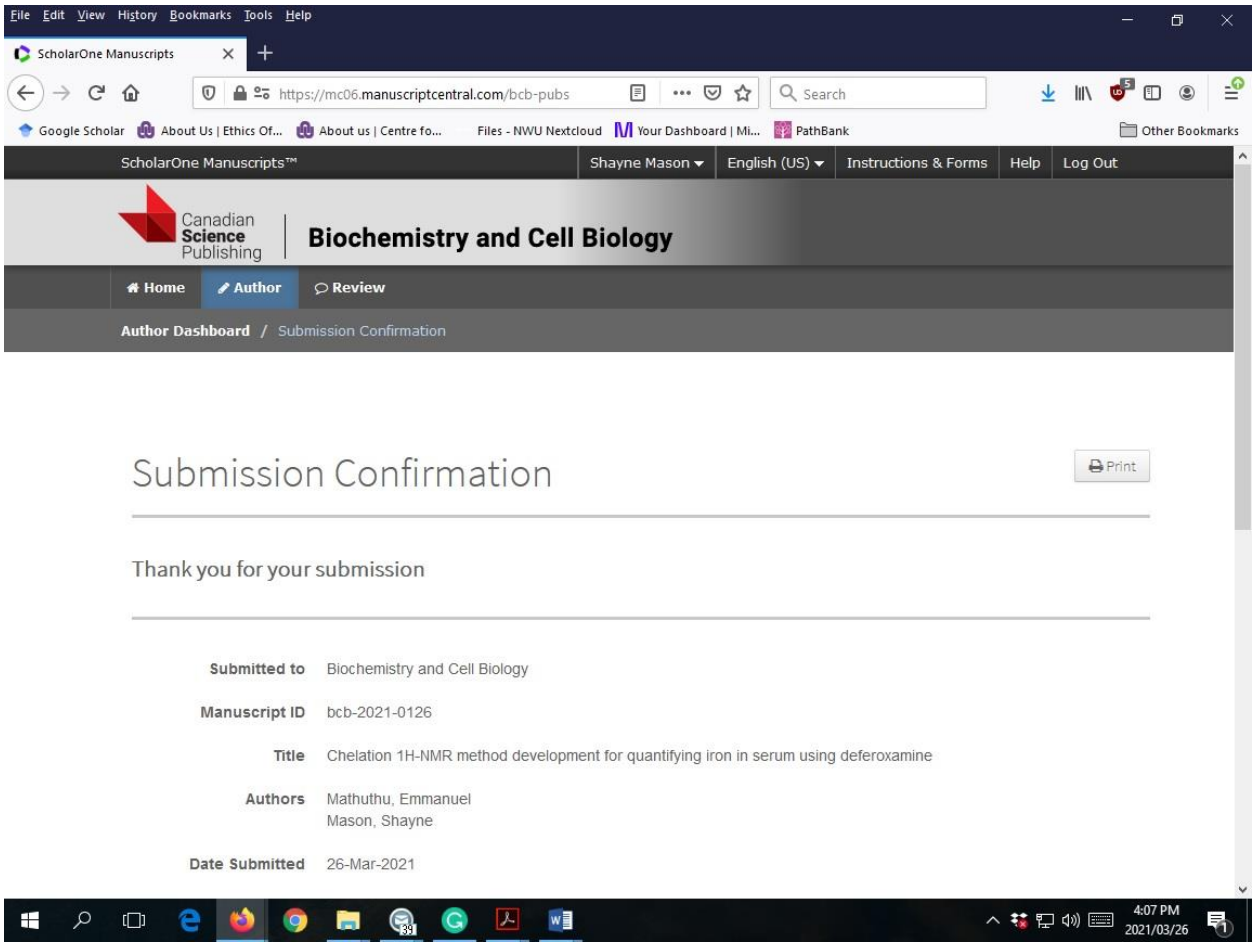

Figure 9: Proof of submission

Abstract

Accurate body iron assessment is crucial for the diagnosis of several diseases associated with abnormal iron levels. Current methods rely on serum-based indicators and are faced with challenges of their own. Deferoxamine (DFO), a chelating agent with a high affinity for ferric iron (Fe^{3+}), is used in clinical practice to treat for iron overload and can be exploited to quantify serum iron using proton nuclear magnetic resonance (^{1}H-NMR) spectroscopy. Here, we developed a new ^{1}H-NMR method based upon past kinetics studies to quantify serum iron utilizing DFO as a chelating agent. While the ^{1}H-NMR spectrum of free DFO has been well documented, the complex Fe-DFO (ferrioxamine; FOB) has not. In our method development we identified a ^{1}H-NMR peak as the best candidate to measure FOB as this peak increased proportionally with Fe^{3+} concentration, concurrently the ^{1}H-NMR peaks representing DFO decreased. However, upon application to serum samples spiked with Fe^{3+}, it became evident that the prepared samples were not stable when measured over 72 hours, indicating further development of the method is needed. This study avails towards a new, non-destructive, non-invasive and, possibly, more efficient method for a rapid assessment of serum iron status using ^{1}H-NMR spectroscopy.

Introduction

In the human body, iron is the most abundant transition metal, crucial for the utilisation of oxygen, and a vital component of oxidases and oxygenases (Puntarulo, 2005). Iron is present both inside and outside of cells within extracellular fluids, such as interstitial fluid, blood and lymph (Milto *et al*., 2016).

One of the most important properties of iron is that it can take part reversibly in oxidation/reduction reactions (Milto *et al*., 2016). Iron functions as the catalytic component (cofactor or prosthetic group) of enzymes that mediate crucial cellular redox reactions such as energy production (Farthing, 1989). Iron also stabilises the tertiary or quaternary structure of enzymes and promotes formation of an enzyme-substrate complex (Milto *et al*., 2016). Subtle harnessing of iron's ability to change valence can provide the electron transport chain with a range of redox potential (Harrison & Arosio, 1996). Living cells are in constant need of iron due to its major role as a cofactor in mitochondrial enzymes (Weiss, 2002). In the blood circulatory system, iron is the central molecule for the binding and transport of oxygen by erythrocytes. Quantitatively, the proteins with the most amount of iron are haemoglobin and myoglobin (Anderson & Vulpe, 2009). Iron modulates many immune effect mechanisms such as nitric oxide formation, host immune cell proliferation and cytokine activities (Weiss, 2002). Furthermore, iron plays an important role in immunosurveillance because of its growth-promoting role in immune cells (Weiss *et al*., 1995). Thus, iron is needed in a myriad of biological processes, making iron quantification a fundamental assay for various types of diagnoses.

Despite the abundance of iron in the human body, usable iron is typically in the deficit; the reason being that iron is insoluble at circumneutral pH (Sánchez *et al*., 2017, Harrison & Arosio, 1996). Iron burden assessment is crucially important as the tissue damage extent is partly related to iron content (Beutler *et al*., 2002). According to Burns *et al.* (1990), most used tests for screening iron deficiencies have significant limitations. Since the late 1970's it has been well established that the most effective way to diagnose iron deficiency is by bone marrow biopsy (Burns *et al.,* 1990). In fact, the gold standard methods for accurate quantification of iron are quite invasive, such as liver biopsy and bone marrow biopsy (Alústiza *et al*., 2004, Pietrangelo, 2005). Up until now, scientists are still developing non-invasive methods to efficiently quantify iron to diagnose conditions such as iron deficiency. One of the more sensitive analytical methods for iron quantification is inductively coupled plasma mass spectrometry (ICP-MS). However, ICP-MS has numerous disadvantages, including spectral interferences, destruction of the sample and high detection limits for some applications (Olesik, 1991), and requires complex sample preparation (Sooriyaarachchi & Gailer, 2010). One of the major disadvantages of ICP-MS being the need to use high volumes of serum (de Oliveira *et al*. 2020). Higher serum volumes are not feasible for diagnostic purposes because

multiple assays are often performed on the same serum sample. Obviously, only an adequate volume of blood can be collected due to ethical and medical reasons.

Proton nuclear magnetic resonance (^{1}H-NMR) spectroscopy is a nondestructive analytical tool that do not require elaborate sample preparation or fractionation. Relative to ICP-MS, ^{1}H-NMR is well suited to analyze limited volume serum samples (Mason *et al.* 2018). H-NMR has both quantitative and qualitative capabilities and the ability to determine structures at a molecular level.

However, ^{1}H-NMR is a stranger to iron quantification in serum samples. Only specific metabolites containing hydrogen(s) linked to carbon atoms can be analysed with ^{1}H-NMR. Iron on its own is invisible on a ^{1}H-NMR spectrum, but when in complex with a molecule visible on a ^{1}H-NMR spectrum, such as an iron chelator, then iron can be identified and potentially quantified using ^{1}H-NMR. Iron chelators on their own produce a unique ^{1}H-NMR spectral pattern. When in chelation with iron there is a three dimensional (3D) conformational change in the chemical structure. This 3D conformation change also changes the resulting ^{1}H-NMR spectral pattern.

Deferoxamine (DFO), a bacterial siderophore that has been a clinical drug for more than four decades is considered the best iron chelating agent (Sooriyaarachchi & Gailer, 2010). DFO was the first high molecular weight (MW) iron chelator that was efficient in maintaining iron stores (Ozment & Turi, 2009). Iron is rendered unreactive by DFO in all reactive oxygen species producing reactions; thus, DFO can reduce oxidative damage (Hallaway *et al*., 1989). DFO is hydrophilic, non-toxic, and can bind both ferrous (Fe^{2+}) and ferric (Fe^{3+}) iron but is highly specific to the later (Jomova & Valko, 2011). Hayes *et al*. (1994), investigated the stability of DFO solution and they concluded that DFO in sterile water remains stable for at least 17-21 days. DFO becomes physically unstable when stored over this time period as it begins to form precipitates. The high affinity of DFO for iron is shown by the high stability constant, which gives it the capability to extract iron from iron-bearing minerals and aqueous Fe^{3+} complexes (Dayani *et al*., 2004; Domagal-Goldman *et al*., 2008). Formation of Fe-DFO complex by naturally synthesized siderophores is efficient because of the remarkably large association constants for Fe (III)–siderophore complexes. According to Albrecht-Gary and Crumbliss (1998) and Hernlem *et al*. (1996), the association constants for Fe (III)–siderophore complexes range between 1023 and 1052. The association constant for DFO with different tri and divalelent metals are as follows: Fe (III) = 1042.33, Ga (III) = 1038.96, Al (III) = 1036.11, Ni (II) = 1027.66, Cu (II) = 1023.98, and Zn (II) = 1020.40 (Hernlem *et al*., 1996). In the presence of these metals DFO will bind iron since their association constants are smaller (Domagal-Goldman *et al*., 2008).

It is important to note that in a bio-matrix, such as blood, that iron binds to ligands (proteins). DFO can remove iron from endogenous ligands (ferritin and transferrin) in blood, albeit slowly, increasing with chelator concentration, temperature and time of incubation (Hamilton *et al*., 2017).

Ferritin iron can be released by many reducing agents under aerobic conditions, including ascorbate which is found in cells (Roginsky *et al*., 1997). In serum, some of the iron is transferrin (Tf)-bound; however, DFO does not mobilize significant amounts of Fe from transferrin, unless exogenous mediators such as nitrilotriacetate (NTA) or citrate are added. Just like in ferritin studies (Breuer *et al*., 2000), the removal of Tf-bound iron by DFO is dependent on incubation time. A substantial proportion of iron overloaded patients also have non–transferrin-bound iron (NTBI) in the serum. NTBI is more labile than Tf-bound Fe and therefore it constitutes a potential source of catalytically active Fe and it is a target for chelation by DFO. *In vitro* studies in serum of patients with iron overload conditions have shown that DFO does not effectively chelate NTBI (Jacobs *et al*., 2005; Breuer *et al*., 2000). These studies have also shown that citrate and citrate-acetate-Fe complexes are components of NTBI but are slowly chelated by DFO, even in excess (in the mM range). Also, the prior mobilization of NTBI with agents such as EDTA, citrate, NTA, or oxalate was necessary for its detection in various NTBI assays. Hamilton *et al.* (2017) showed that Fe (III) ion binds to DFO more strongly than to the apparent Fe (III)–NTA complex. Thus, the exact mechanisms of iron chelation with DFO in humans, the effects of ligands, how much total iron (bound or free) is chelated (quantifiable) and the kinetics are still areas of research. Hence, developing a ^{1}H-NMR method for rapid quantification of iron in serum samples, using DFO as an iron chelating agent, is needed.

Since DFO is an organic molecule with C-H bonds it can form a unique ^{1}H-NMR spectrum. Free DFO is expected to form two unique triplet peaks in the ^{1}H-NMR spectrum at 2.00 ppm and 2.80 ppm (Tian *et al*., 2016). DFO chelates Fe^{3+} (Fig. 10) in a 1:1 reaction stoichiometrically (Dayani *et al*., 2004). DFO is characterized by a chain which includes three hydroxamate groups, with an amine as a terminal free group (Galinetto *et al*., 2016).

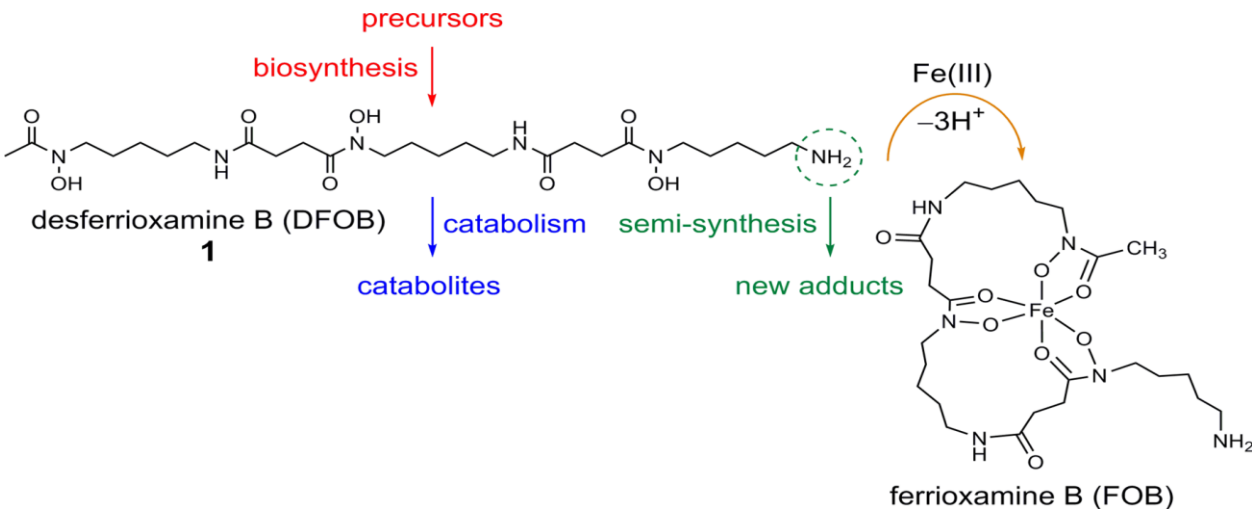

Figure 10: Change in 3D conformation of DFO during chelation with ferric iron (reprinted with permission from Codd *et al*., 2018).

The complex Fe-DFO (ferrioxamine; FOB) has different pharmacokinetic properties (Bentur *et al*., 1994). In Tesoro et al. (2005) FOB was stable for a few days During complexation, two closed loops and an open chain containing a protonated amine are formed resulting in six hydroxamate oxygen atoms coordinating with the Fe (III) centre to form a distorted octahedron around the metallic centre (Galinetto *et al*., 2016), as shown in Fig. 10. FOB is expected to produce its own unique ^{1}H-NMR spectrum due to the 3D conformational structure. In this study, a method was developed that chelates Fe^{3+} with DFO to form FOB in both pure compound solutions and serum spiked with Fe^{3+}. Our assay was then assessed to determine if ^{1}H-NMR spectroscopy – an analytical method that requires minimal sample preparation and can analyze samples non-destructively with high repeatability, can identify and quantify FOB in order to rapidly assess the iron status in serum.

Materials and methods

Chemicals

Trimethylsilyl-2,2,3,3-tetradeuteropropionic acid (TSP; Merck; CAS#: 24493-21-8) as a chemical shift reference. Deuterium oxide (D_2O; Merck; CAS#: 7789-20-0). Deferoxamine mesylate as the chelation agent (DFO; CAS#: 138-14-7). Cadmium chloride ($CdCl_3$; Sigma-Aldrich; CAS#: 10108-64-2). Double-distilled water (ddH_20; Sigma-Aldrich; CAS#: 7732-18-5). Ferric chloride ($FeCl_3$; Sigma-Aldrich; CAS#: 7705-08-0). Solutions of sodium hydroxide (NaOH; Sigma-Aldrich; CAS#: 1310-73-2) and hydrogen chloride (HCl (10M); Sigma-Aldrich; CAS#: 7647-01-0) used to adjust pH values. Nitrilotriacetic acid disodium salt monohydrate (NTA; Sigma-Aldrich; CAS#: 18662-53-8) used as a catalyst. Citric acid trisodium salt (Sigma-Aldrich; CAS#: 68-04-2). Sodium bicarbonate ($NaHCO_3$; Sigma-Aldrich; CAS#: 144-55-8). Sodium chloride (NaCl; Sigma-Aldrich; CAS#: 7647-14-5).

Precautions to avoid iron contamination

With DFO being a siderophore with the strongest affinity for Fe^{3+} it is of utmost importance that it does not encounter unwanted iron in the analytical instrument or in solution (D'Haese *et al*., 1989). All test tubes, and other glassware, used were pre-rinsed with 2mM HCl solution to ensure the removal of any trace amounts of iron.

Stock solutions

Adjustments of pH were performed using 5M HCl and 2M NaOH solutions, prepared by 50% dilution of 10M HCl with ddH_20 and dissolving 80g NaOH in 1L ddH_20. A 0.5M Fe (III) ion solution was prepared by dissolving 0.811g $FeCl_3$ in 10ml of 2mM HCl to prevent precipitation of the Fe (III) ions (Biruš *et al*., 1984). Conventional organic buffers, like MES and HEPES, were not used to prepare the DFO solution because they cause interference with the absorbance measurements used for FOB determination (Pham *et al*., 2006), and show up as peaks on ^{1}H-NMR spectra. Hence, a 10mM solution of DFO was prepared by dissolving 0.065679g of DFO in 10mL of 2mM $NaHCO_3$, with 0.01M NaCl, and the pH adjusted to 8.1. A mass of 0.000917g of $CdCl_3$ was dissolved in 2mM HCl to make a 0.5mM $CdCl_3$ solution. 10mM NTA and 0.1M citrate solutions were made by dissolving 0.019114g and 0.019212g, respectively, in 2mM $NaHCO_3$. An NMR internal standard (IS) solution of 20mM TSP was prepared by dissolving 0.34454g TSP in 100 mL D_2O, and aliquoted into 10mL tubes and frozen, until needed, to maintain stability of TSP.

Method development

The design of the development of our method is illustrated as a schematic in Fig. 11. Briefly, UV spectrophotometry was used to determine $FeCl_3$, DFO, FOB and catalyst presence and ^{1}H-NMR spectroscopy was used to identify and quantify DFO and FOB. Method assessment was done by measuring linearity (R^2), repeatability (coefficient of variation (CV)), accuracy (% recovery) and precision (error bars).

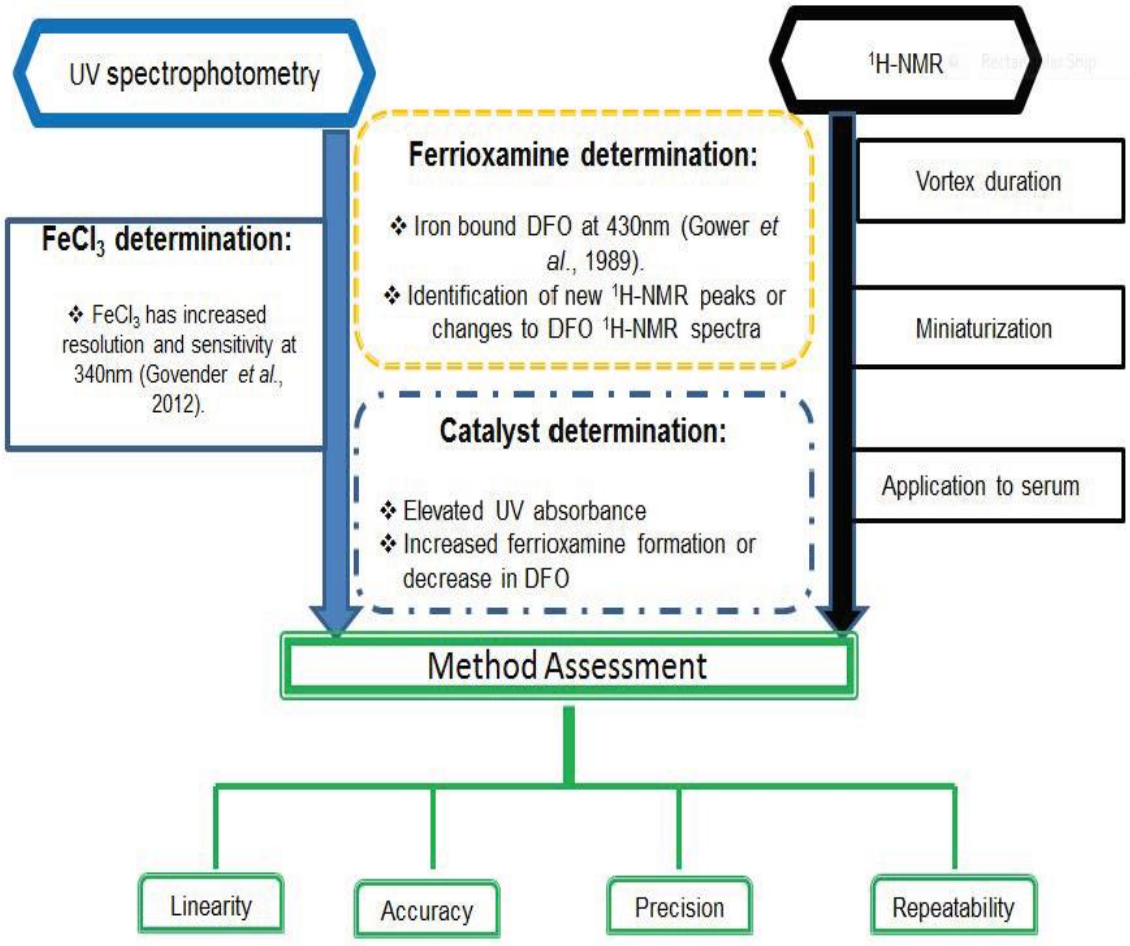

Figure 11: Schematic of method development.

In a similar approach to our method development using EDTA as a chelating agent (Mathuthu *et al*., 2021), a volume of 510µL sample with 60µL IS (2M TSP in D_2O) and 30µL chelation agent (10mM DFO solution) were added to an Eppendorf tube to give a final volume of 600µL, and then vortexed briefly. It is important to note that the ratio of volume of overall sample to D_2O be kept at a ratio of 90:10 before being transferred to the 5mm NMR glass tubes, for the purposes of locking during the ^{1}H-NMR analysis, and for absolute quantification.

Determining $FeCl_3$ levels

As with our previous method development (Mathuthu *et al*., 2021), 14 serial dilutions of $FeCl_3$ were created as 25%, 50%, 75%, 100%, 125%, 150% & 175% of both the upper (31,3µM) and the lower (9,0 µM) range values of the normal physiological reference range of iron found in serum (Lentner, 1992; Wu, 2006).

Deferoxamine determination

A 10mM solution of DFO, diluted to 500µM in the final volume, used for our method development, was pre-determined qualitatively (clear peaks of good resolution) on a ^{1}H-NMR spectrum to be of enough abundance. Free form 10mM DFO was also analysed using a UV spectrophotometer to confirm the presence of a DFO peak at an absorbance of 226nm (Gower *et al*., 1989).

Ferrioxamine determination

A 10mM DFO solution was mixed with a 0.5mM $FeCl_3$ solution (1:1 volume) and vortexed. The resulting solution was incubated for 30 minutes at room temperature. 1mL of the solution was transferred to 1ml cuvettes and analyzed using UV spectrophotometry at 430nm (Gower *et al*., 1989). For the ^{1}H-NMR analysis, 510µm 0.5mM $FeCl_3$ was added to an Eppendorf tube containing 30µL 10mM DFO and 60µL IS and incubated for 30 minutes at room temperature. Samples were transferred to 5mm NMR tubes and analyzed by comparing the spectra to that of free-form DFO.

Determining possible catalyst(s)

The aim of this experiment was to identify the best ligand to catalyse the chelation of Fe^{3+} with DFO. Three potential ligands based upon literature (Faller & Nick, 1994; Kontoghiorghes & Kontoghiorghe, 2020), were assessed: NTA, $CdCl_3$ and citrate. Four solutions were prepared for this experiment. 1) 0.5mM $FeCl_3$ was added in a 1:1 volumetric ratio with 10mM DFO to determine the presence of FOB without a ligand present. 2) A solution containing 10mM NTA and 10mM DFO (pH adjusted to 8.1) was prepared and mixed with 0.5M $FeCl_3$ in a 1:1 volumetric ratio. 3) A solution containing 0.5mM $CdCl_3$ and 0.5mM DFO was prepared and mixed with 0.5M $FeCl_3$ in a 1:1 volumetric ratio. 4) Similar to NTA, a solution containing 10mM citrate and 10mM DFO (pH

adjusted to 8.1) was prepared and mixed in a 1:1 volumetric ratio. All samples were incubated for 30 minutes at room temperature before being analysed at 430nm on a UV spectrophotometer

The effects of the ligands (NTA, $CdCl_3$ and citrate) on the chelation of Fe^{3+} with DFO were further investigated using ^{1}H-NMR. A high (0.5M), medium (0.25M) and low (0.1M) concentration of $FeCl_3$ solution was prepared. Samples were prepared as per our protocol: 510µL $FeCl_3$ sample with 60µL IS and 30µL ligand solution, as described above, vortexed, and transferred to a 5mm NMR glass tube. Each sample preparation was repeated in triplicate.

Vortex duration

The aim of this experiment was to assess if vortex duration affected repeatability of the method. Nine samples were prepared utilizing the results of the previous experiments. In nine Eppendorf tubes, 510µL solution consisting of 0.5mM $FeCl_3$, 60µL IS and 30µL of 10mM DFO solution containing the best ligand determined from the previous experiment was added. Samples were divided into groups of three and vortexed for 0, 30 and 60 seconds respectively. Samples were then transferred to 5mm NMR glass tubes for analysis.

Repeatability

To determine the repeatability of our method, 10 experimental samples as replicates were prepared by adding to an Eppendorf tube: 510µL of 250µM $FeCl_3$ solution with 60µL IS (2M TSP in D_2O) and 30µL 10mM DFO solution containing 10mM NTA. A second set of 10 samples were similarly prepared, but as blanks – 510µL ddH_2O instead of 510µL 250µM $FeCl_3$, the rest of the conditions were the same. ^{1}H-NMR spectra were obtained for all 20 samples and the CVs were assessed.

Linearity and precision

From the 14 concentration levels of $FeCl_3$ that were prepared, samples were prepared in triplicate for NMR analysis based upon optimal method conditions determined from the outcomes of the previous experiments. To determine linearity, the observed and true concentration values were plotted, and linearity of the method was determined by R^2. Precision was assessed by adding error bars at each level based upon the information from the triplicates at each level.

Miniaturization: from 600µL to 60µL

The aim of this experiment was to determine whether our developed method could be miniaturized, from 600µL to 60µL (Mason *et al.*, 2018) and assess if using an *eVol* NMR digital syringe would improve the repeatability of the method. The digital syringe was set to aspirate 6µL of 20mM IS, 46µL $FeCl_3$ solution, 4µL of 250mM NTA and 4µL of 10mM DFO, and then purge, aspirate 60µL and purge within Hilgenberg 2mm NMR glass tubes, for the purpose of mixing. This was followed

by the cleaning of the syringe by aspirating and purging 100µL ddH_2O, three times. The 2mm NMR glass tubes were loaded onto the auto-sampler using the Bruker MATCH gripper to hold the 2mm tube in a 10mm spinner.

Application to human serum

Upon approval of ethics by the North-West University health research ethics committee (approval #: NWU-00413-20-A1), blood samples were collected in BD Vacutainer® SST™ tubes from healthy volunteers of 18 – 60 years of age and allowed to coagulate for 1 hour at room temperature. Subsequently, samples were centrifuged at 1300 *g* for 10 minutes, the serum collected and pooled into a single volume, and stored at -80 degrees Celsius until required. Prior to analysis the pooled serum was removed from the freezer and thawed at room temperature.

For the first application experiment, five aliquots of serum were spiked with $FeCl_3$ based upon the 14 levels of $FeCl_3$ used previously – see Table 1. Five repeat samples at each level (total samples = 25) were prepared using the described miniaturized method in 2mm NMR glass tubes. For the second application experiment, five spiked aliquots of serum were created as before. 140µL of 255µM NTA was added to 2mL of each spiked serum sample and incubated at room temperature for 30 min (Gosriwatana *et al.,* 1999) – the aim here was to release iron bound to proteins such as ferritin. After incubation the samples were centrifuged at 3000 *g* for an hour (Gosriwatana *et al.,* 1999). The supernatant was then transferred to pre-rinsed 10 kDa Amicon Ultra-2 mL centrifugal filters (Van Zyl *et al*., 2020) and centrifuged at 3000 *g* for 30 min. For preparation of these filtered serum samples for NMR analysis, the miniaturized method was adjusted as follows: aspirate 6µL of 20mM IS, 50µL of sample, and 4µL of 10mM DFO with the *eVol* NMR digital syringe, and then continue as described in Section 2.14.

Table 8: Spiked serum iron concentrations based upon 14 serial dilutions of $FeCl_3$ used in method development.

Level	Calculation	Spiked [Fe] in µM
1	L1= 1st quartile	8,1
2	L2 = (L1 + L3)/2	11,4
3	L3 = median	14,6
4	L4 = (L2 + L5)/2	22,0
5	L5 = 3rd quartile	29,3

^{1}H-NMR parameters

All samples were measured at 500 MHz on a Bruker Avance III HD NMR spectrometer equipped with a 5mm triple resonance inverse (TXI) {^{1}H, ^{15}N, ^{13}C} probe head and x,y, z gradient coils. The TXI inner coil must be optimized for ^{1}H observation, the focus of this study. Sample temperature must be maintained at a constant 300K. ^{1}H spectra acquired as 64 transients for pure compound analysis and 128 transients for serum analysis, in 32K data points with a spectral width of 12,000 Hz (24.0 ppm) for the standard 600µL method and 6000 Hz (12.0 ppm) for the miniaturized 60µL method (Mason *et al,.* 2018). The H_2O resonance at 4.70 ppm must be suppressed using the pulse sequence program NOESY-presat, which presaturates the H_2O resonance by single-frequency irradiation during a relaxation delay of 4s, with a 90° excitation pulse of 10µs. The acquisition time and receiver gain were set for 2.7s and 64, respectively. Fourier transformation and phase and baseline correction were done automatically using Bruker Topspin (V3.5). Bruker AMIX (V3.9.14) was used for spectral analysis, annotations and quantification.

Statistical analysis

Basic descriptive statistics – medians, means, standard deviations and CVs, as well as plotting of data onto a scatter plot to determine linearity, was done using Excel (2013). For the serum NMR data, a binned (set widths of 0.05ppm, between 0.5-4.15ppm) NMR spectral data set was created and normalized relative to the TSP. MetaboAnalyst 5.0 (www.metaboanalyst.ca) was used on the binned NMR spectral data set to perform an ANOVA (ANalysis Of VAriance) on the raw binned data to identify significant bins based upon the cut-off values of fold change > 2.0 and p-value <0.05. PLS-DA (Partial Least Squares-Discriminant Analysis) was also performed on the binned data after log transformation and auto-scaling to illustrate patterns in the data and identify the variables important in projection (VIPs).

Results

Method development

UV spectrophotometry

Firstly, the 14 serial dilutions of $FeCl_3$ were checked using UV spectrophotometry and actual concentrations of each level were determined using their absorbance at 340nm (Table 9). These results indicate that the serial dilution expected values are approximately correct.

Table 9: Actual $FeCl_3$ values (µM) at 14 concentration levels, as determined by UV spectrophotometry at 340nm.

Lower level		Upper level	
	[Fe]		[Fe]
1	2.29	8	15.65
2	4.48	9	15.71
3	6.75	10	23.5
4	7.81	11	31.3
5	8.97	12	39.12
6	11.24	13	47
7	13.53	14	54.81

Secondly, the presence of DFO was confirmed using UV spectrophotometry. A wave scan was done with a wavelength range from 200nm to 400nm. Points between 200-240nm were plotted for 10mM DFO, but an over-abundance was clear (Fig. 12A). The sample was subsequently diluted by a factor of 10 to make a 1mM DFO solution. The results in Fig. 12B show that 1mM DFO produces a peak at 226nm. These results are in accordance with the product information sheet of deferoxamine mesylate, as provided by the supplier (Sigma-Aldrich), as well as with the HPLC results reported by Gower *et al*. (1989).

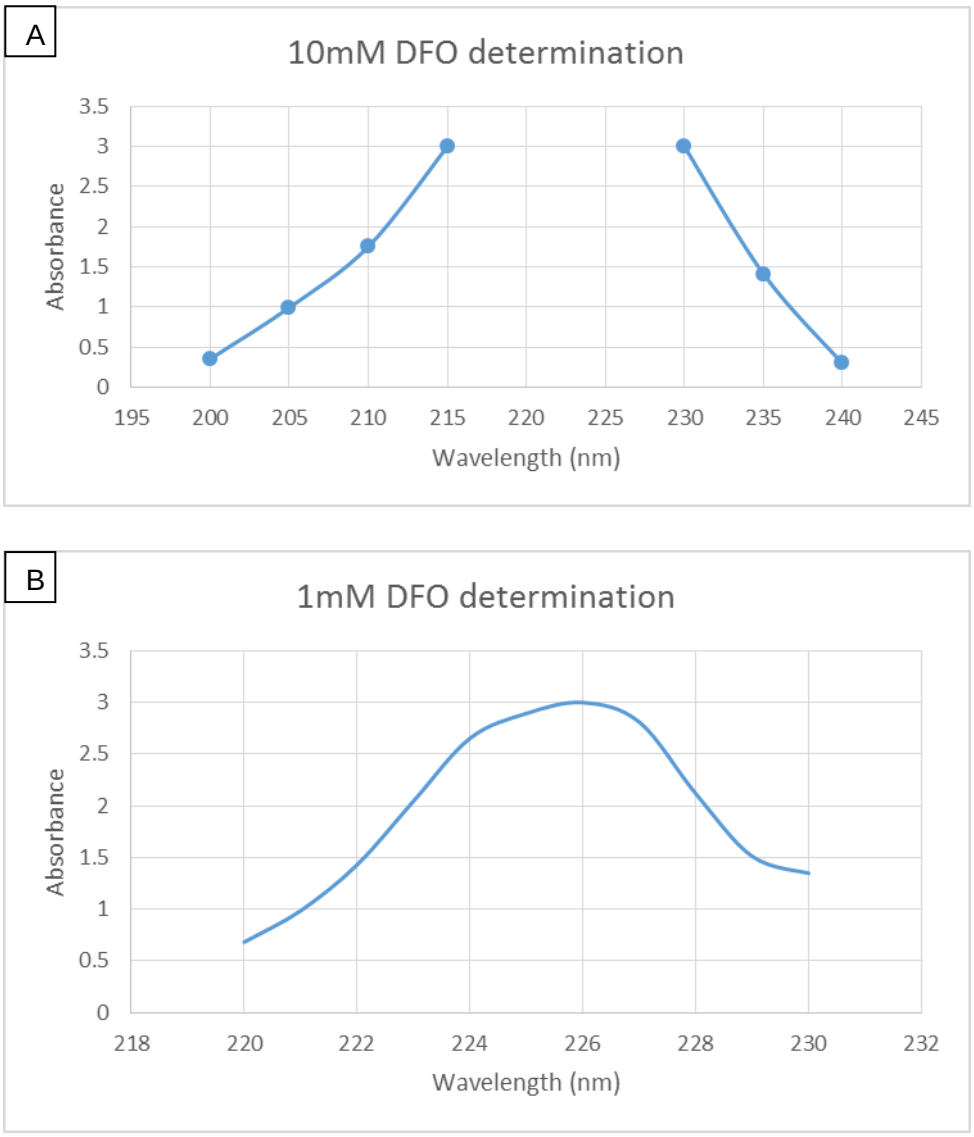

Figure 12: UV spectrophotometric determination of DFO between 200-240nm for A: 10mM DFO, and B: 1mM DFO

.

Lastly, FOB determination was done by preparing five samples in Eppendorf tubes for UV spectrophotometric analysis with varying catalyst(s) candidates and keeping all other variables constant. Fig. 13 shows that without any ligand (pure) that there is a slow rate/less of FOB formation. Citrate has little effect on the rate of FOB formation. Adding $CdCl_3$ increases the rate of FOB formation with absorbance increasing by more than a sixth. Addition of NTA increases the absorbance slightly more than $CdCl_3$, and the combination of both NTA and $CdCl_3$ yields approximately the same absorbance as NTA only. Thus, these results (Fig. 13) confirm that a ligand is needed for optimal chelation of DFO with $FeCl_3$ to produce FOB. In our study, NTA was determined as being the best ligand (catalyst) for optimal FOB formation.

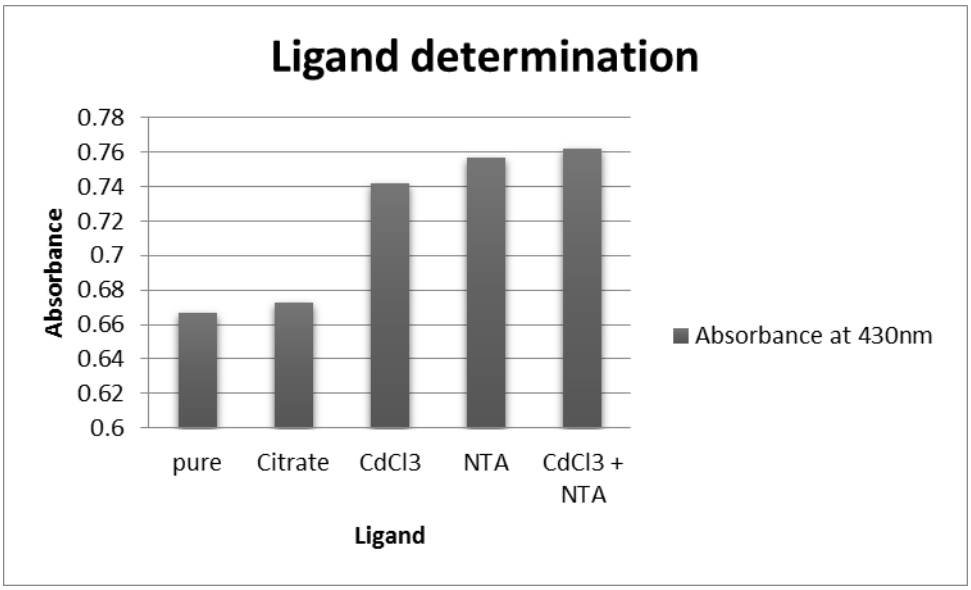

Figure 13: UV spectrophotometric determination at absorbance of 430nm of FOB alone (pure) and effects of ligands. NTA = nitrilotriacetic acid; CdCl3 = cadmium chloride

Hence, the results from UV spectrophotometry showed that 1) the 14 levels of $FeCl_3$ concentrations were accurate, 2) DFO was certainly present in solution, and 3) NTA is the preferred ligand to produce the optimal amount of FOB. Our study then continued onto ^{1}H-NMR spectroscopy to confirm these results.

^{1}H-NMR spectroscopy

Firstly, in order to identify and quantify FOB using ^{1}H-NMR spectroscopy, differences in the DFO and FOB ^{1}H-NMR spectra (Fig. 14) were closely inspected, qualitatively. A list of the chemical shifts of the peaks for DFO are as follows: 1.34m, 1.54m, 1.66m, 2.06s, 2.48t, 2.74t, 3.00t, 3.18q, 3.63m (s=singlet, t=triplet, m=multiplet).

The first major difference was the chemical shift of NTA – a broad singlet at 3.50 ppm in DFO, which shifts to 3.58 ppm in FOB, due to a change in pH caused by the presence of the $FeCl_3$ solution. It is important to note here that NTA was kept in the sample preparation method here as NTA would be needed in the application to serum samples. Another visual difference between the spectra are that most DFO peaks decreased in intensity in the FOB spectrum – indicating that DFO was being used/transformed into something else. The singlet at 2.80ppm in the FOB spectrum slightly increased in intensity, suggesting that this is the best spectral region for measuring FOB. However, these are not the results we expected, as more discernible differences between DFO

and FOB ^{1}H-NMR spectral patterns were expected. This expectation is based upon our previous study using EDTA (Mathuthu *et al*., 2021); namely, when a linear chemical compound changes into a new 3D conformational structure (after chelation with an ion) it produces a uniquely new ^{1}H-NMR spectral pattern. This was not the case in our ^{1}H-NMR results of FOB.

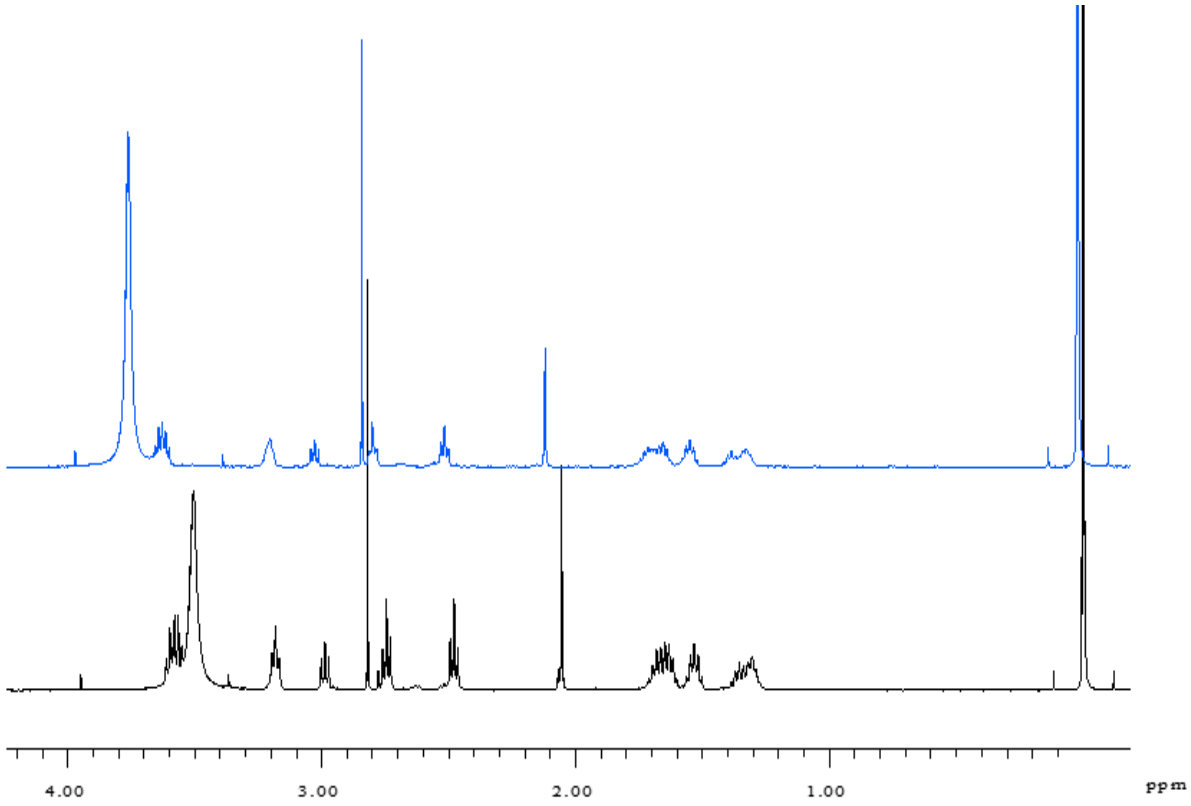

Figure 14: ^{1}H-NMR spectra of DFO (bottom; black) and FOB (top; blue), relative to IS.

Secondly, when looking at the ^{1}H-NMR results of $CdCl_3$ and NTA as potential ligands (catalysts) for FOB formation (Fig. 15) we looked at the concentrations of DFO, because we could not find a discernibly distinct peak to represent FOB in the ^{1}H-NMR spectra. It was evident that adding $CdCl_3$ did not significantly change the concentrations of DFO in the presence of varying concentrations of Fe^{3+}, indicating that increased amounts of DFO were not used for chelation as the $FeCl_3$ concentrations increased. These results for $CdCl_3$ differed from the UV spectrophotometry results obtained (Fig. 13). On the other hand, the NTA results, excluding the outlier at the low $FeCl_3$ concentration, showed a general trend of the DFO concentrations decreasing as the $FeCl_3$ concentrations increased. The results of the NTA were like those of the blank (no ligand added). However, since the UV spectrophotometry data showed improved FOB formation with NTA, and based upon literature, we kept NTA as the ligand of choice in our method.

Thirdly, for the ^{1}H-NMR experiments, we aimed at determining the optimal vortex duration for the method. All experimental variables were kept constant except vortex duration. From Fig. 16, the first set of triplicate samples were not vortexed and had an average CV of 7.5%. Votexing for 30 seconds yielded an average CV of 10%, whilst 60 seconds of vortexing produced the optimal results of a CV less than 2%.

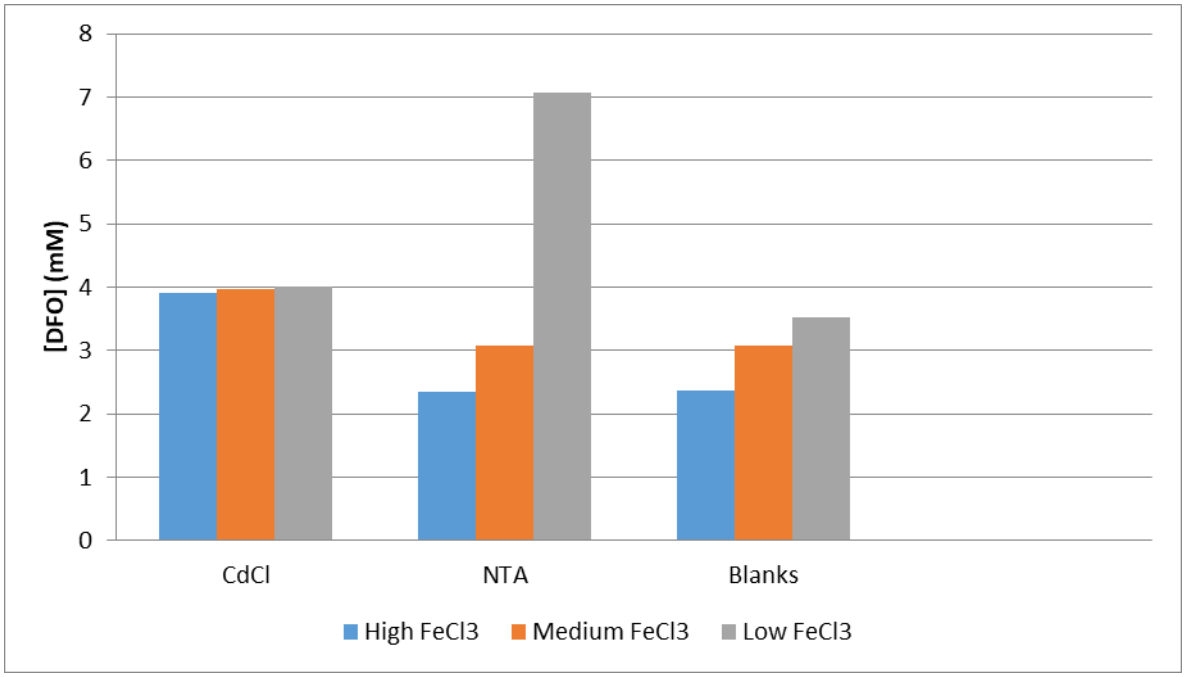

Figure 15: The effect of the ligands CdCl3 and NTA on the concentrations of DFO and high (500µM), medium (250µM) and low (125µM) levels of $FeCl_3$.

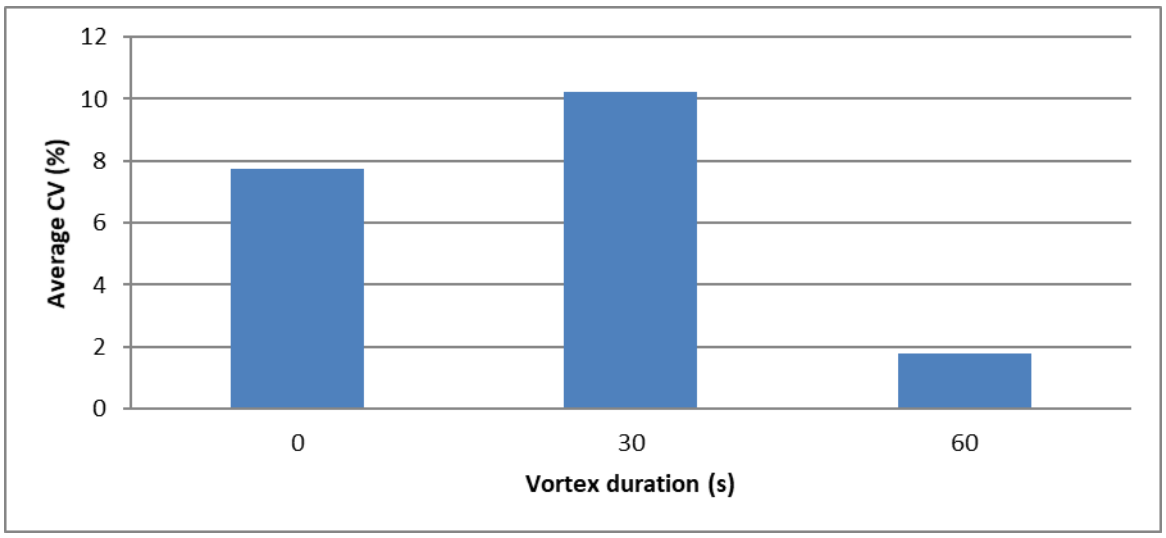

Figure 16: The effect of vortex duration on method repeatability.

Fourthly, we assessed the repeatability of our method by analysing 10 experimental samples as replicates, using 250µM $FeCl_3$ solution. The average CV values across all the measured peaks were approximately between 3% and 4% (Fig. 17). Following this experiment, we aimed to determine whether our developed method could be miniaturized, from 600µL to 60µL using the *eVol*® NMR digital syringe, by assessing the ^{1}H-NMR spectra visually and examining the CV values across the 10 replicates. Visually, apart from a slight chemical shift in the NTA peak, the ^{1}H-NMR spectra appeared very similar. Quantitatively, the miniaturization of the method improved the CV values slightly (between 2% and 3%), except for the peak at 2.61 ppm which increased in CV (Fig. 17). Hence, the method can not only be miniaturized but doing so also slightly improved upon the overall repeatability. These results are ideal for metabolomics studies of serum samples as, typically, limited volume of serum samples are available.

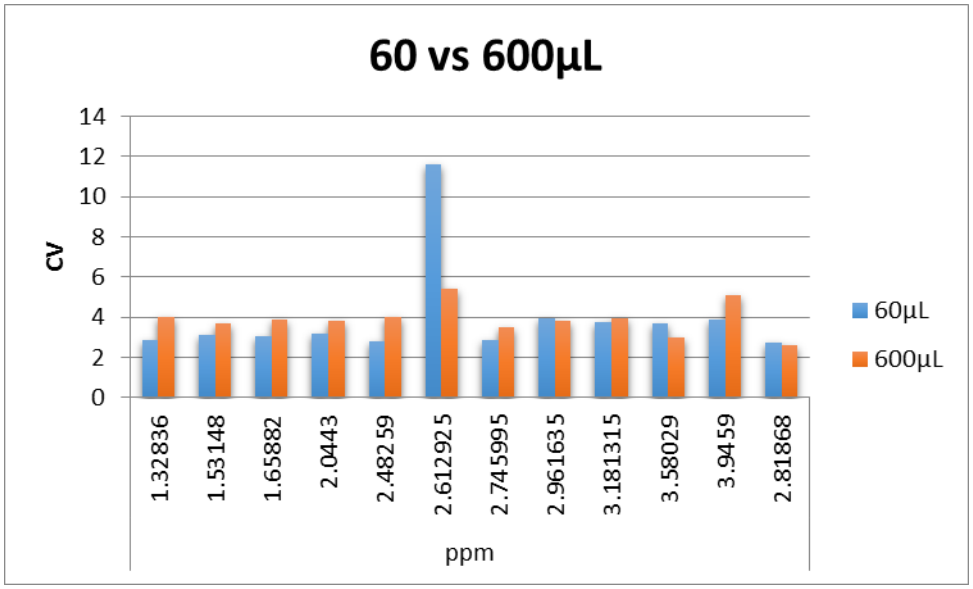

Figure 17: Assessment of repeatability (CV) of method at 600µL and comparison to miniaturization of method at 60µL, which shows slightly, improved repeatability.

Lastly, we assessed the linearity and precision of the method on ^{1}H-NMR spectroscopy by using all the optimal experimental parameters described above and applying it across 14 levels of $FeCl_3$ concentrations, with each level analysed in triplicate (total of 42 samples). Based upon the UV spectrophotometry results (Fig. 12), $FeCl_3$ chelates with DFO, in presence of NTA, to form FOB. Fig. 14 showed that DFO decreases in the presence of $FeCl_3$ by qualitatively examining the ^{1}H-NMR spectra. Hence, FOB is expected to form in the presence of DFO and $FeCl_3$. When overlaying all ^{1}H-NMR spectra across the 14 levels of $FeCl_3$ and upon close inspection of all the spectra, not much change was observed. However, zooming into the spectra at 2.775 ppm reveals the presence of a singlet that was identified as changing with increasing concentrations of $FeCl_3$

(Fig. 18). A quantitative assessment of this peak at 2.775 ppm was done. Since we were uncertain about the number of protons represented by this peak, we could not calculate the absolute concentration, but instead presented the quantitative data as a percentage value relative to TSP. Based upon these quantitative results (Table 10 & Fig. 19), linearity is observed with a R^2=0.95. However, the error plots at each level indicate that quantification at 2.775 ppm is not sufficiently precise, and the CV values indicate poor repeatability. Lastly, since we could not compare to the true expected absolute concentration values, accuracy could not be assessed. Nonetheless, we proceeded to test our method further by means of application to human serum samples spiked with $FeCl_3$.

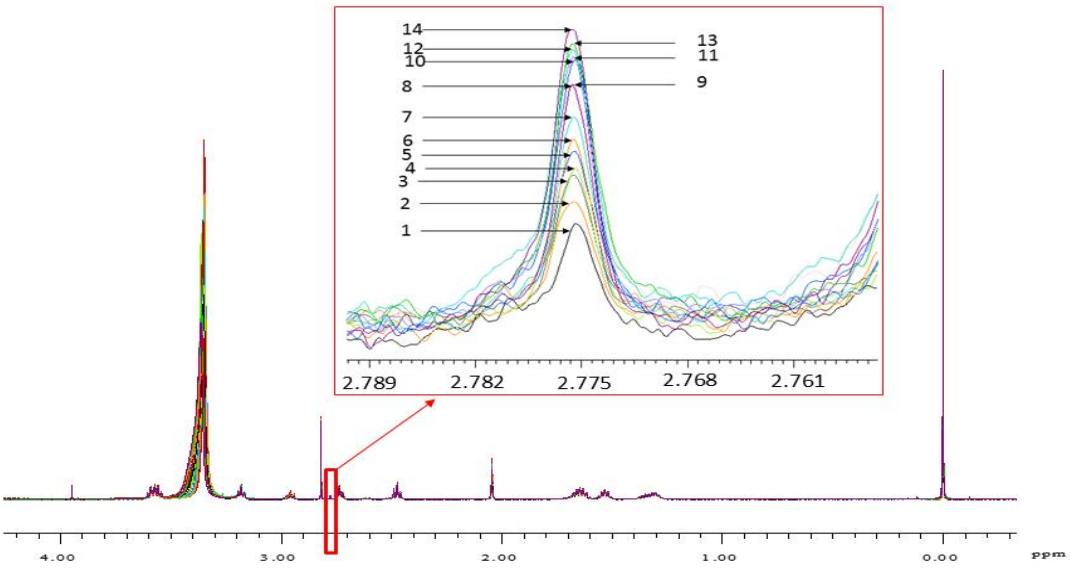

Figure 18: Overlay of ^{1}H-NMR spectra at 14 levels of $FeCl_3$ concentrations, relative to TSP, with the box zoomed in at the spectral region of 2.775 ppm to illustrate that a singlet was observed to increase with $FeCl_3$ concentration.

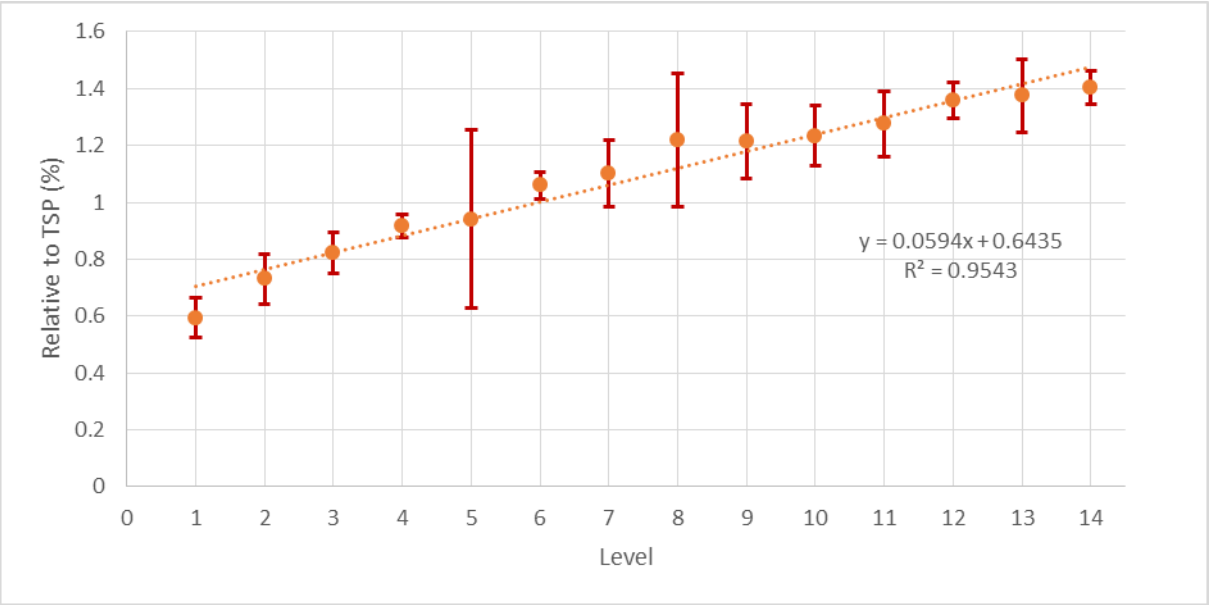

Figure 19: Quantitative results of the singlet at 2.775ppm for all 42 samples, analysed in triplicate across 14 concentration levels of $FeCl_3$. The measured values are relative to the TSP(%). A trend line was added to show that a linearity of R^2=0.95 was obtained.

Table 10: Quantitative results of method assessment across 14 levels of $FeCl_3$ concentrations, measured in triplicate. Values were calculated as percentages relative to TSP.

Level	Mean	Std.Dev	CV (%)
1	0,59	0,07	11,80
2	0,73	0,09	12,23
3	0,82	0,07	8,86
4	0,92	0,04	4,41
5	0,94	0,31	33,40
6	1,06	0,05	4,56
7	1,10	0,12	10,61
8	1,22	0,23	19,21
9	1,21	0,13	10,92
10	1,23	0,11	8,56
11	1,28	0,11	8,90
12	1,36	0,06	4,58
13	1,37	0,13	9,41
14	1,40	0,06	4,26

Application of method to human serum

Unfiltered serum

For the first application of our method to human serum samples, we tested it on unfiltered serum samples (i.e. proteins and lipids still present). Five unfiltered serum samples were spiked as described in Table 8 and analyzed in replicates of five (total of 25 samples). These data were binned, as described in Section 2.16, and an ANOVA (Fig. 20) was used to examine the variances. Fifteen bins (^{1}H-NMR spectral regions representing chemical compounds) were identified as having significant variance across the 5 levels of $FeCl_3$ concentrations. A general downward trend is observed across the 5 levels for all 15 significant bins. These results suggest an inverse relationship, that the chemical compounds represented by these bins decrease in intensity – are being consumed/converted into something else, as the concentration of the $FeCl_3$ increases. The ^{1}H-NMR peak found at 2.775 ppm in the pure compound analysis was not clearly discernible in the unfiltered serum samples and therefore could not be quantified.

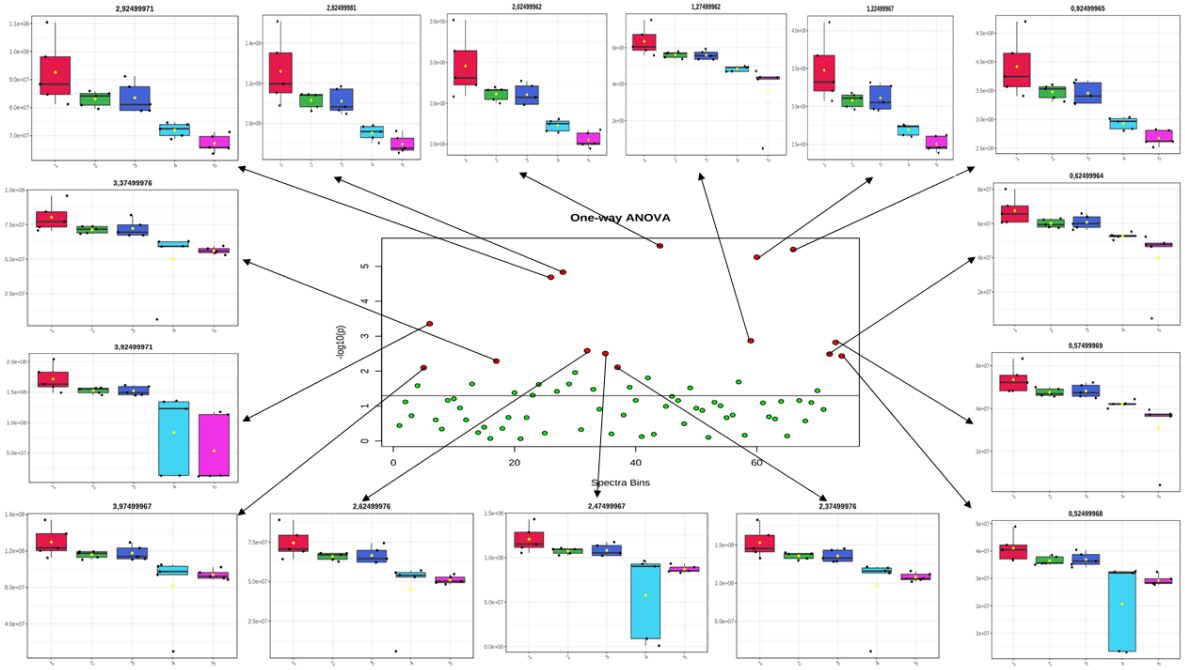

Figure 20: ANOVA of binned, unfiltered serum samples spiked across 5 levels of $FeCl_3$ concentrations. Red dots in the ANOVA indicate regions in the 1H-NMR spectra that showed statistically significant variance. The box plots of these 15 spectral regions are also given. A general downward trend is observable across all 15 significant bins (i.e. chemical compounds in the serum samples are decreasing as the $FeCl_3$ concentrations increase).

Filtered serum

For the second application of our method to human serum samples, we first incubated the serum in NTA to release iron bound to protein and then filtered the serum samples in order to remove all macromolecules (>10 000 Da) so that we could closely examine the low molecular weight compounds (metabolites) closer to the baseline of the ^{1}H-NMR spectra. The ANOVA analysis of the raw binned data produced similar output with an overall downward trend, but with 20 significant bins instead of the 15 significant bins for the unfiltered serum samples. As an additional experiment, to test the stability of the serum samples, we analyzed the same prepared samples after 24 hours and 72 hours. Visual inspection of the PLS-DA (Fig. 21) shows a drift in the ellipses of the data over time. A conclusion that can be drawn from the PLS-DA is that the samples sitting in the auto-sampler of the NMR over a period of 24 hours and 72 hours, are not stable. This drift in the data is not major (only 4.3% variance over the total 72 hours), but still visible. Looking at the VIP scores from the loadings of the PLS-DA plot, four bins (1.025, 1.425, 2.425 and 2.475) have a VIP score greater than 2.0 (Fig. 22).

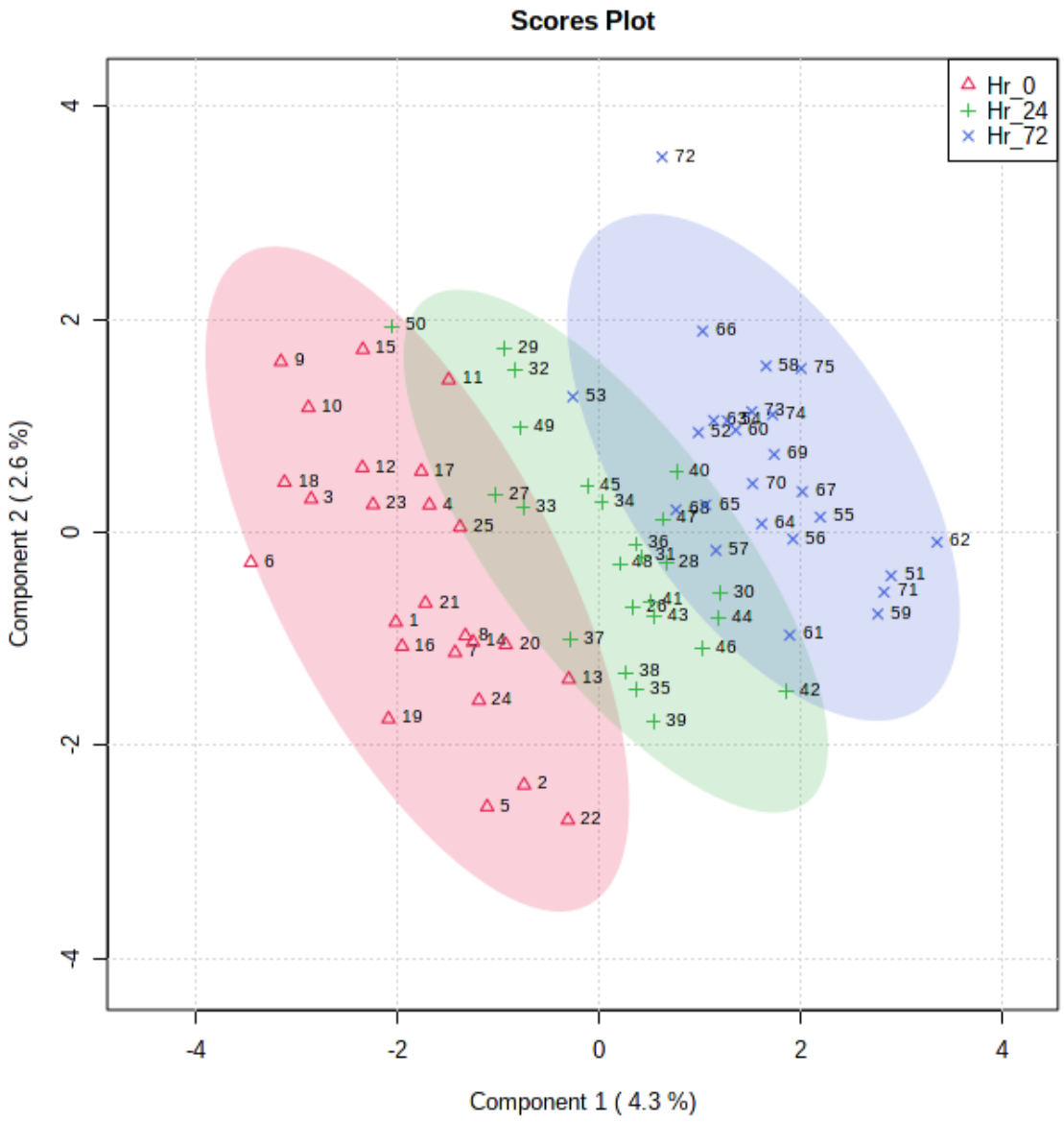

Figure 21: PLS-DA scores plot showing a drift in the data sets over time, indicating that the prepared serum samples are not stable at room temperature. Hr_0 (red Δ) is the initial experiment, Hr_24 (green +) is the experiment repeated after sitting for 24 hours in the auto-sampler, and Hr_72 (blue X) is the experiment repeated after sitting for 72 hours in the auto-sampler.

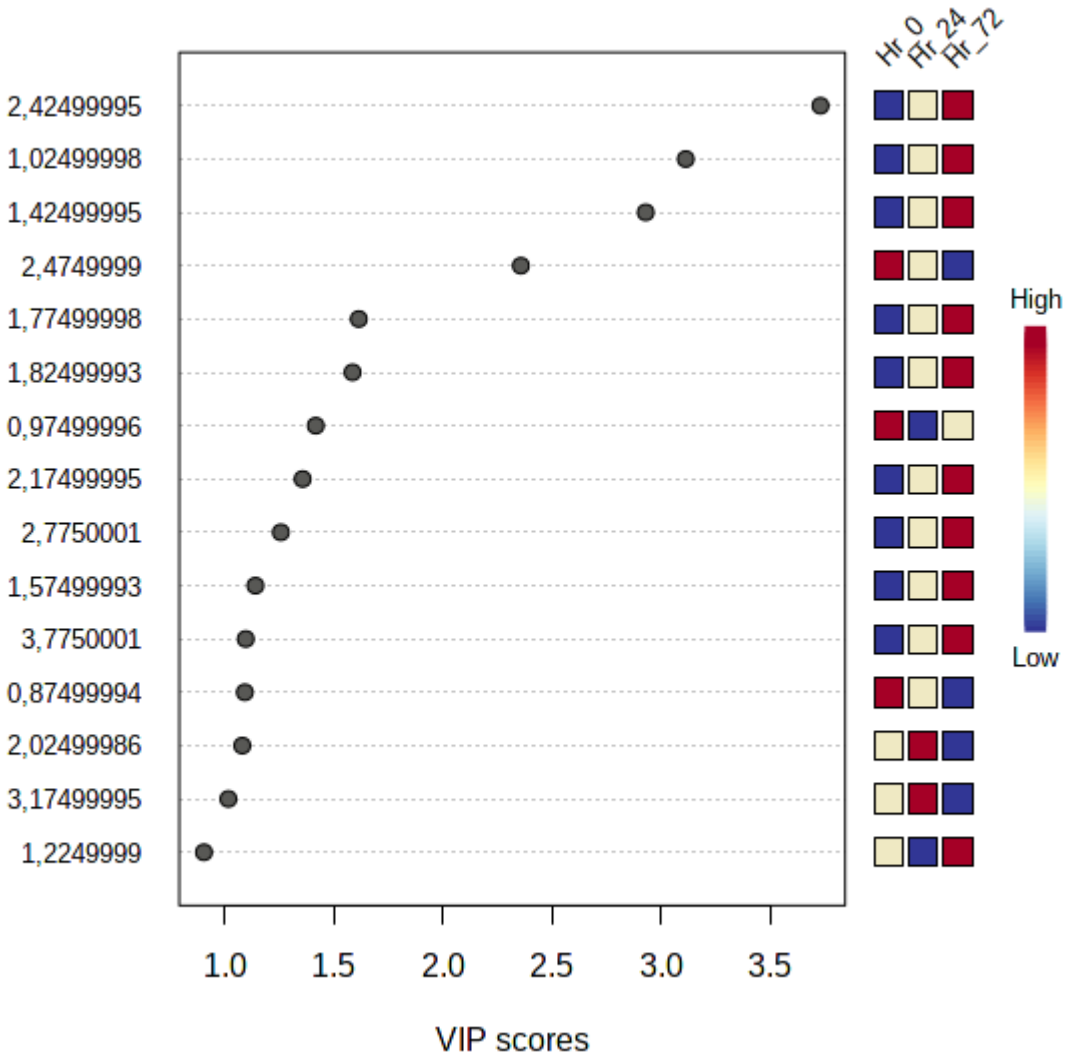

Figure 22: VIP scores of the PLS-DA plot showing four bins with VIP scores greater than 2.0.

Going back to the original ^{1}H-NMR spectra, we were able to explain the differences that were occurring due to these 4 VIP bins: 1) 1.025; 2) 1.425; 3) 2.425; 4) 2.475. From Fig. S1, it can be seen that initially the bin 1.025 is empty (Hr_0), but as time progresses (Hr_24 and Hr_72) part of the doublet of valine shifts to the left from bin 0.975 into bin 1.025. This shifting in the peak is most likely due to a change in pH occurring in the sample. This is also supported by the fact that 0.975 is 7th in the list of VIPs – spectral density of bin 0.975 is decreasing over time because the peaks are shifting into bin 1.025. For the bin 1.425 (Fig. S2), a similar result to bin 1.025 is occurring – part of the doublet of alanine is shifting left from bin 1.375 into bin 1.425 over time. An additional feature

evident at bin 1.425 is that the doublet of alanine is splitting into a double doublet over time. Of interest for our study are the neighboring VIP bins 2.425 and 2.475 (-+. S3). Bin 2.475 is represented by the triplet of DFO, as first identified in the results of 3.1.2 of pure DFO. Bin 2.475 (DFO) is decreasing in intensity over time, which is in-line with the data from our previous experiments and shifting slightly to the left. However, bin 2.425 shows that in the initial experiment (Hr_0) there is no peak present but after 24 hours in the auto-sampler a small peak begins to appear at 2.48 ppm, which increases in intensity after 72 hours in the auto-sampler.

Thus, two regions in the ^{1}H-NMR spectra (singlet at 2.775 ppm and singlet at 2.48 ppm) show an increase in intensity of a chemical compound. Initially, the singlet at 2.775 ppm showed a linear increase over the increasing concentrations of FeCl3 during the initial experiment; however, this trend continued over time suggesting a time effect. The singlet at 2.48 ppm only appears after 24 hours and continues to increase in intensity after 72 hours after the initial experiment, also suggesting a time effect. Hence, the stability of the prepared samples is questionable.

Linearity of DFO

As a final experiment, the linearity of DFO in the filtered serum samples was investigated in all the DFO peaks – Table 11. A triplet representing DFO at 2.06 ppm had the highest average R^2 value (R^2=0.90). Fig. 23 illustrates the linearity of DFO at 2.06 ppm, with the downward trend lines for the initial experiment (Hr_0) and after 24 hours in the auto-sampler (Hr_24) having the same R^2 value of 0.90. This linearity decreases after 72 hours in the auto-sampler (Hr_72) to give R^2=0.82. This general pattern is seen across other DFO peaks – Table 11, except for 1.65 ppm where the linearity is initially low and increases with time.

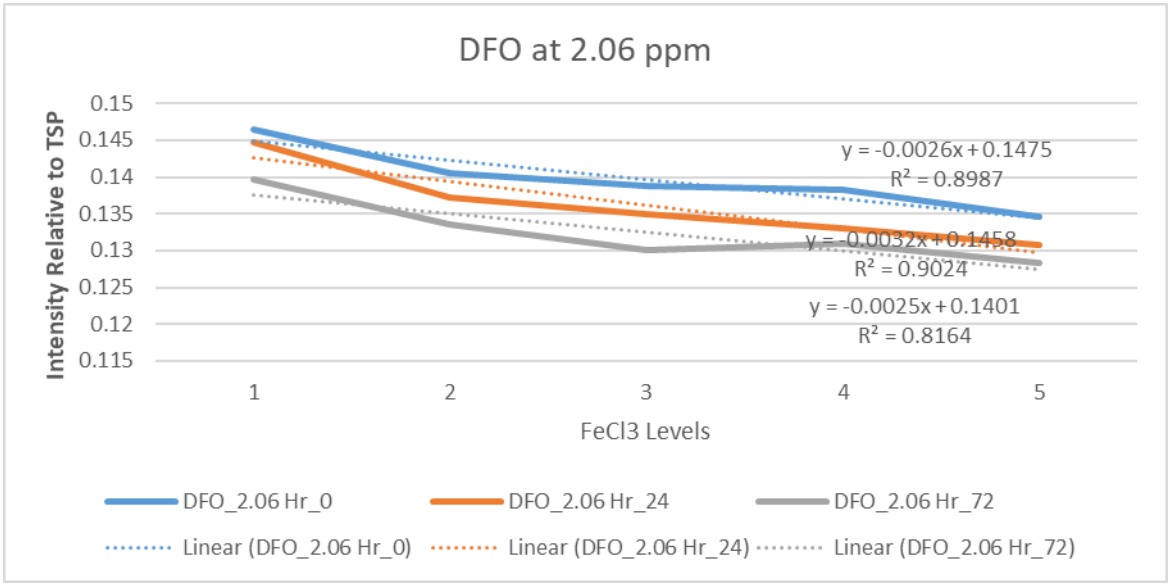

Figure 23: Plot showing linearity of DFO at 2.06 ppm measured (averages of triplicates) as spectral intensity relative to TSP across 5 concentration levels of FeCl3, for the initial

experiment (Hr_0) and after sitting for 24 hours (Hr_24) and 72 hours (Hr_72) in the auto-sampler.

Table 11: Average R2 values for DFO peaks for the initial experiment (Hr_0), and after 24 hours (Hr_24) and 72 hours (Hr_72) in the auto-sampler.

ppm	1.53	1.65	2.06	2.48	2.75	3.18
			Average R^2 of DFO			
Hr_0	0.86	0.65	0.90	0.90	0.82	0.78
Hr_24	0.89	0.87	0.90	0.86	0.86	0.34
Hr_72	0.73	0.90	0.81	0.52	0.35	0.008

Discussion

The method developed in this study was based upon information from kinetics and equilibrium data in complexation studies of Fe^{3+} by DFO in the literature. The main objectives for this study were as follows: 1) Determine what, if any, catalysts are required for chelation of iron using DFO in pure compound solutions. 2) Optimize the conditions of the method. 3) Assess the method by determining linearity, precision and repeatability across triplicates and a linear physiological range of iron. 4). Apply developed quantitative ^{1}H-NMR method to human serum samples spiked with $FeCl_3$.

Firstly, both DFO and FOB were identified using both UV spectrophotometry and ^{1}H-NMR. FOB formation proved to be a slow process, as in literature. Therefore, there was a need to find a catalyst to expedite the process without affecting the general reaction. This study is in accord with studies done by Evans *et al*. (2008) as we concluded that NTA is the best ligand to catalyse FOB formation. Unlike the study done by Evans *et al*. (2008), 250µM NTA was considered more than enough, as higher concentrations of NTA (800mM) would result in broadening of ^{1}H-NMR peaks and hence less resolution of the spectra.

Other components based upon literature – HCl, NaCl, $NaHCO_3$ and NaOH play pivotal roles in the method. There have always been constructive debates in the science community about iron hydrolysis. Scientists are finding it difficult to reach a consensus on the solubility of Fe^{3+} or the exact composition of ferric hydroxides (Pham *et al*., 2005). Biruš *et al*. (1983) evaded the hydrolysis issue by diluting Fe^{3+} in HCl/NaCl, keeping the solution acidic to prevent hydrolysis. Since compounds containing C-H bonds appear on the ^{1}H-NMR spectra and ^{1}H-NMR is pH sensitive, it is crucial to add a buffer that does not appear on the ^{1}H-NMR spectra. According to Pham *et al*. (2005), conventional buffers interfere with ferrioxamine absorbance. 2mM $NaHCO_3$ and 0.01M NaCl are thus used instead of conventional buffers (MES and HEPES) for optimal ferrioxamine determination.

Evidently the main ^{1}H-NMR spectral differences between pure DFO and expected FOB was the gradual decrease in pure DFO peaks and the emergence of two new ^{1}H-NMR peaks at 2.775 ppm and 2.48 ppm. UV spectrophotometry confirmed the presence of DFO and FOB. During the development of the method, the ^{1}H-NMR peak at 2.775 ppm is directly proportional to $FeCl_3$ concentration, making it the focus of this study. To get a higher resolution of the ^{1}H-NMR peak the method was optimized by adjusting the pH of NTA and DFO to 11.5 and 8.1 respectively. Different incubation temperatures were tested but no change was observed (results not reported). Longer vortexing improved the repeatability of the experiments hence the lower CV. To improve the repeatability of the method a digital syringe was used instead of conventional manual pipettes and

at the same time the method was miniaturised from 600µL to 60µL. The developed method had a good linearity at the 2.775 ppm peak with R^2 = 0.95. However, precision was poor, and accuracy could not be assessed.

Application of the developed method to unfiltered spiked serum revealed that the FOB peak at 2.775 ppm could be quantified, which is not unexpected since transferrin is only 20-40% saturated (Kolb *et al*., 2009). All the $FeCl_3$ that was added to the serum samples is expected to have saturated the empty apo-transferrin. From the ANOVA of the unfiltered serum (Fig. 20), all the bins showing variance indicated a general decrease in intensity. These results posed a question: if existing chemical compounds are decreasing, then where are they going? Are all the disappearing compounds being converted into compounds that are undetectable to ^{1}H-NMR? Or are new peaks going to increase after a certain period? The subsequent experiment of adding NTA to the serum samples first, followed by incubation and then filtration with 10 000 Dalton centrifugal units, aimed to remove all proteins from the serum sample so that no proteins would be present to bind the $FeCl_3$ added to the sample, before it could chelate with DFO. An illustration of this final developed method using the filtration of the serum samples is given as a schematic in Fig. 24.

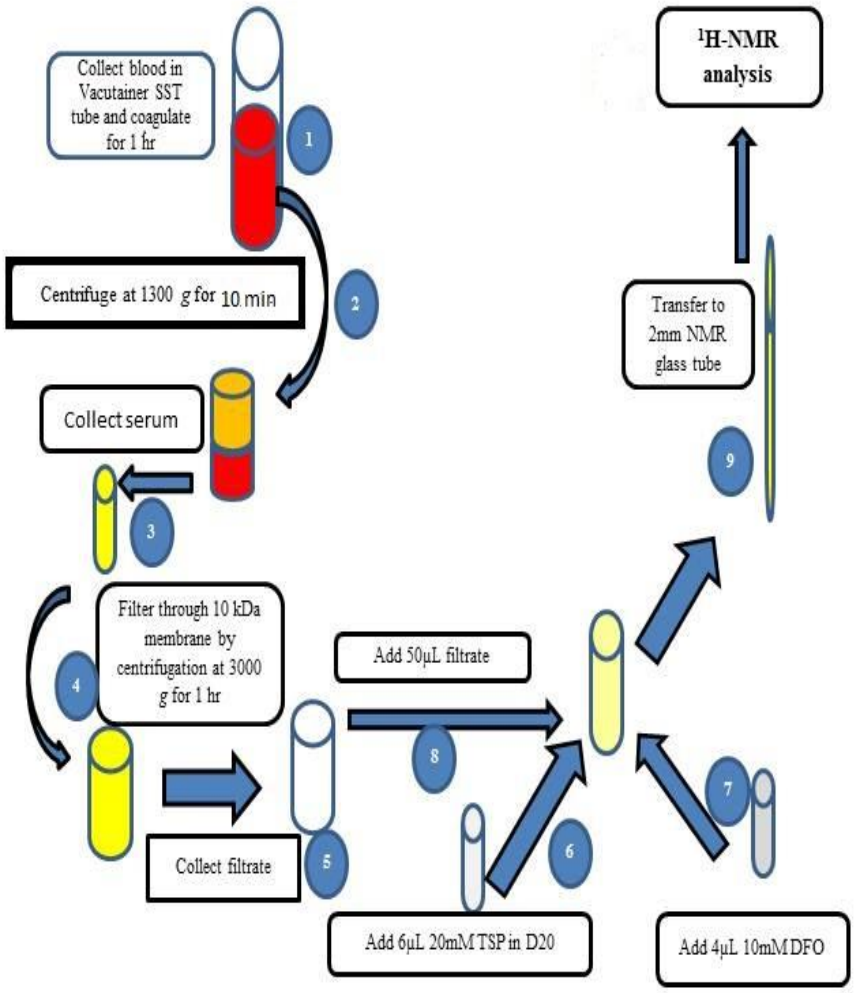

Figure 24: Newly proposed method. 5ml of blood is collected in Vacutainer SST tubes and allowed to coagulate at room temperature for an hour. The blood is centrifuged at 1300 *g* for 10 minutes to collect serum. 255Mm NTA is added to the serum samples to bind any NTBI if present in serum. Proteins including apo-transferrin may interfere with the iron measurements hence serum is filtered through a 10kDa membrane at 3000 *g* for 10 minutes. 50µL of the filtrate is collected using an e*Vol* analytical syringe and 6µL of the 20mM internal standard is added to the sample before 4µL of 10mM DFO. The sample is transferred into 2mm NMR tubes then analysed using ^{1}H-NMR.

The serum samples prepared by our method, however, were not stable over time, as measured over 72 hours. According to Anton *et al*. (2015), serum samples have a clear signature of degradation after being left at room temperature for some time. ^{1}H-NMR is pH sensitive and can

lead to chemical shifting of ^{1}H-NMR peaks. The PLS-DA (Fig. 21) clearly illustrates a drift in time. Inspection of the 4 VIP bins from the PLS-DA analysis of the filtered serum over time showed that 2 of the VIP bins were due to chemical shifts attributed to a change in pH of the samples. The continued decrease in DFO after 72 hours and the gradual emergence in new peaks at 24 hours indicates that there are still chemical processes occurring in the samples. Further studies on serum iron quantification using DFO on ^{1}H-NMR must be done. We suggest using higher field strength catalyst(s) that can transfer more iron from iron binding ligands must be further investigated, as well as stabilizing the final prepared serum sample to quench chemical reactions. Due to the complex current ways to quantify iron, it is equally important to initially define blood samples in terms of haemoglobin concentration, serum ferritin and TIBC before validating this method.

Conclusion

In conclusion, it is possible to use ^{1}H-NMR to identify and quantify serum iron using DFO as a chelating agent. In this study we confirmed a linear decrease in DFO in pure compound samples spiked with levels of Fe^{3+} and the gradual increase in intensity of a new ^{1}H-NMR peak at 2.775 ppm, potentially representing FOB. From quantitative results of peak 2.755 ppm across 14 concentration levels of $FeCl_3$ measured in triplicate, a good linearity of R^2 = 0.95 was obtained. Hence, DFO managed to chelate iron but the method shows limited precision, and accuracy could not be determined. In the application of the method to spiked serum samples, DFO peaks were also found to decrease over time and an additional new ^{1}H-NMR peak at 2.48 ppm began to emerge after 24 hours. However, the constant decrease of most the ^{1}H-NMR peaks over time raised questions concerning the stability over time of the prepared serum samples. This study should be the genesis of more development of ^{1}H-NMR methods for the quantification of serum iron concentration. We believe that ^{1}H-NMR is a viable analytical tool that can one day provide a rapid quantitative picture of iron in human blood.

Declarations

Declaration of interest

Declarations of interest: none.

Funding

This research did not receive any specific grant from funding agencies in the public, commercial, or not-for-profit sectors.

CRediT authorship contribution statement

Emmanuel Mathuthu: Investigation, Formal analysis, Methodology, Writing - original draft, Writing - review & editing.
Shayne Mason: Conceptualization, Formal analysis, Methodology, Writing - original draft, Writing - review & editing, Supervision.

6. References

Albrecht-Gary, A.M. & Crumbliss, A.L. 1998. Coordination chemistry of siderophores: thermodynamics and kinetics of iron chelation and release. *Metal Ions in Biological Systems*, 35:239.

Alústiza, J.M., Artetxe, J., Castiella, A., Agirre, C., Emparanza, J.I., Otazua, P., ... Recondo, J.A. 2004. MR quantification of hepatic iron concentration. *Radiology*, *230*(2): 479-484.

Anderson, G.J. & Vulpe, C.D. 2009. Mammalian iron transport. *Cellular and Molecular Life Sciences*, 66(20):3241.

Anton, G., Wilson, R., Yu, Z.H., Prehn, C., Zukunft, S., Adamski, J., ... Hveem, K., 2015. Pre-analytical sample quality: metabolite ratios as an intrinsic marker for prolonged room temperature exposure of serum samples. *PloS One*, *10*(3):e0121495.

Bentur, Y., McGuigan, M. & Koren, G. 1991. Deferoxamine (desferrioxamine). *Drug Safety*, 6(1):37-46.

Beutler, E., Felitti, V., Ho, N.J. & Gelbart, T. 2002. Relationship of body iron stores to levels of serum ferritin, serum iron, unsaturated iron binding capacity and transferrin saturation in patients with iron storage disease. *Acta Haematologica*, 107(3):145-149.

Biruš, M., Bradić, Z., Kujundžić, N. and Pribanić, M. 1983. Iron (III) complexation by desferrioxamine B in acidic aqueous solutions. The formation of binuclear complex diferrioxamine B. *Inorganica Chimica Acta*, *78*:87-92.

Biruš, M., Bradic, Z., Kujundzic, N. and Pribanic, M. 1984. Iron (III) complexation by desferrioxamine B in acidic aqueous solutions. Kinetics and mechanism of the formation and hydrolysis of the binuclear complex diferrioxamine B. *Inorganic Chemistry*, *23*(14):2170-2175.

Breuer, W., Hershko, C. & Cabantchik, Z.I. 2000. The importance of non-transferrin bound iron in disorders of iron metabolism. *Transfusion Science*, 23: 18-192.

Breuer, W., Ermers, M.J., Pootrakul, P., Abramov, A., Hershko, C. and Cabantchik, Z.I. 2001. Desferrioxamine-chelatable iron, a component of serum non–transferrin-bound iron, used for assessing chelation therapy: Presented in preliminary form at the 10th International Conference on Oral Chelators symposium on iron chelators held in Limassol, Cyprus, March 2000 (Transfusion Science, in press). *Blood, the Journal of the American Society of Hematology*, *97*(3):792-798.

Brittenham, G.M. & Badman, D.G. 2003. Noninvasive measurement of iron: report of an NIDDK workshop. *Blood, The Journal of the American Society of Hematology*, *101*(1):15-19.

Burns, E.R., Goldberg, S.N., Lawrence, C. & Wenz, B. 1990. Clinical utility of serum tests for iron deficiency in hospitalized patients. *American Journal of Clinical Pathology*, 93(2): 239–245.

Cho, H., 2020. Development of Metal Chelators and Metal Chelating Polymers for Mass Cytometry and Positron Emission Tomography (*Doctoral dissertation*).

Codd, R., Richardson-Sanchez, T., Telfer, T.J. and Gotsbacher, M.P. 2018. Advances in the chemical biology of desferrioxamine B. *ACS Chemical Biology*, *13*(1):11-25.

Dayani, P.N., Bishop, M.C., Black, K. & Zelter, P.M. 2004. Desferoxamine (DFO)–mediated iron chelation: rationale for a novel approach to therapy for brain cancer. *Journal of Neuro-Oncology*, 67(3):367-377.

de Oliveira, M., Gianeti, T.M.R., da Rocha, F.C.G., Lisboa-Filho, P.N. and Piacenti Silva, M. 2020. A preliminary study of the concentration of metallic elements in the blood of patients with multiple sclerosis as measured by ICP-MS. *Scientific Reports*, *10*(1):1-8.

D'Haese, P., Lamberts, L.V. and De Broe, M.E. 1989. Indirect measurement of desferrioxamine and its chelated compounds aluminoxamine and ferrioxamine by Zeeman atomic absorption spectrometry. *Clinical Chemistry*, *35*(5):884-887.

Domagal-Goldman, S.D., Paul, K.W., Sparks, D.L. & Kubicki, J.D. 2008. Quantum chemical study of the Fe (III)-desferrioxamine B siderophore complex—Electronic structure, vibrational frequencies, and equilibrium Fe-isotope fractionation. *Geochimica et Cosmochimica Acta*, 73:1–12.

Evans, R.W., Rafique, R., Zarea, A., Rapisarda, C., Cammack, R., Evans, P.J., Porter, J.B. and Hider, R.C. 2008. Nature of non-transferrin-bound iron: studies on iron citrate complexes and thalassemic sera. *JBIC Journal of Biological Inorganic Chemistry*, *13*(1):57-74.

Faller, B. & Nick, H. 1994. Kinetics and mechanism of iron (III) removal from citrate by desferrioxamine B and 3-hydroxy-1, 2-dimethyl-4-pyridone. *Journal of the American Chemical Society*, *116*(9):3860-3865.

Farthing, M.J. 1989. Iron and immunity. *Acta Paediatrica*, 78:44–52.

Galinetto, P., Taglietti, A., Pasotti, L., Pallavicini, P., Dacarro, G., Giulotto, E. & Grandi, M.S. 2016. SERS activity of silver nanoplastics functionalised with a deferoxamine B derived ligand for Fe (III) binding and sensing. *Journal of Applied Spectroscopy*, 82(6):1052-1059.

Gosriwatana, I., Loreal, O., Lu, S., Brissot, P., Porter, J. and Hider, R.C., 1999. Quantification of non-transferrin-bound iron in the presence of unsaturated transferrin. *Analytical Biochemistry*, *273*(2): 212-220.

Govender, E., Harrison, S.T.L. and Bryan, C.G. 2012. Modification of the ferric chloride assay for the spectrophotometric determination of ferric and total iron in acidic solutions containing high concentrations of copper. *Minerals Engineering*, *35*: 46-48.

Gower, J.D., Healing, G. and Green, C.J. 1989. Determination of desferrioxamine-available iron in biological tissues by high-pressure liquid chromatography. *Analytical Biochemistry*, *180*(1):126-130.

Hallaway, P.E., Eaton, J.W., Panter, S.S. and Hedlund, B.E. 1989. Modulation of deferoxamine toxicity and clearance by covalent attachment to biocompatible polymers. *Proceedings of the National Academy of Sciences*, *86*(24):10108-10112.

Hamilton, J.L., ul-haq, M.I., Creagh, A.L., Haynes, C.A. and Kizhakkedathu, J.N. 2017. Iron binding and iron removal efficiency of desferrioxamine based polymeric iron chelators: influence of molecular size and chelator density. *Macromolecular Bioscience*, *17*(3):1600244.

Harrison, P.M., & Arosio, P. 1996. The ferritins: molecular properties, iron storage function and cellular regulation. *Biochimica et Biophysica Acta (BBA)-Bioenergetics*, 1275(3):161–203.

Hayes, D.M., Reilly, R.M. & Lee, M.M. 1994. The pharmaceutical stability of deferoxamine mesylate. *The Canadian Journal of Hospital Pharmacy*, 47(1).

Hernlem, B.J., Vane, L.M. and Sayles, G.D. 1996. Stability constants for complexes of the siderophore desferrioxamine B with selected heavy metal cations*. Inorganica Chimica Acta*, 244(2):179-184.

Jacobs, E.M., Hendriks, J.C., van Tits, B.L., Evans, P.J., Breuer, W., Liu, D.Y., ... Scheiber-Mojdehkar, B. 2005. Results of an international round robin for the quantification of serum non-transferrin-bound iron: need for defining standardization and a clinically relevant isoform. *Analytical Biochemistry*, *341*(2):241-250.

Jomova, K., & Valko, M., 2011. Importance of iron chelation in free radical-induced oxidative stress and human disease. *Current Pharmaceutical Design*, 17:3460–3473.

Kohgo, Y., Ikuta, K., Ohtake, T., Torimoto, Y. & Kato, J. 2008. Body iron metabolism and pathophysiology of iron overload. *The Japanese Society of Hematology*. 88:7–15.

Kolb, A.M., Smit, N.P.M., Lentz-Ljuboje, R., Osanto, S & Van Pelt, J. 2009. Non-transferrin bound iron measurement is influenced by chelator concentration. *Analytical Biochemistry*, 385:13-19.

Kontoghiorghes, G.J. and Kontoghiorghe, C.N. 2020. Iron and chelation inbiochemistry and medicine: new approaches to controlling iron metabolism and treating related diseases. *Cells*,*9*(6):1456.

Lentner, C. ed. 1992. *Geigy Scientific Tables: Bacteria, Fungi, Protozoa, Helminths* (Vol. 6). Ciba-Geigy.

Mason, S., Terburgh, K. and Louw, R. 2018. Miniaturized ^{1}H-NMR method for analyzing limited-quantity samples applied to a mouse model of Leigh disease. *Metabolomics*, *14*(6):1-12.

Mathuthu, E., Janse van Rensburg, A., Du Plessis, D. & Mason, S. 2021. EDTA as a chelating agent in quantitative ^{1}H-NMR of biologically important ions. *Biochemistry and Cell Biology*, *online, ahead of print* (doi.org/10.1139/bcb-2020-0543).

Milto, I.V., Suhodolo, I.V., Prokopieva, V.D., & Klimenteva, T.K. 2016. Molecular and cellular bases of iron metabolism in humans. *Biochemistry (Moscow)*, 81(6):549–564.
Olesik, J.W. 1991. Elemental analysis using ICP-OES and ICP/MS. *Analytical Chemistry*, *63*(1):12A-21A.

Ozment, C.P., & Turi, J.L. 2009. Iron overload following red blood cell transfusion and its impact on disease severity. *Biochimica et Biophysica Acta (BBA)-General.*

Pham, A.N., Rose, A.L., Feitz, A.J. and Waite, T.D. 2006. Kinetics of Fe (III) precipitation in aqueous solutions at pH 6.0–9.5 and 25 C. *Geochimica et Cosmochimica Acta*, *70*(3):640-650.

Pietrangelo, A. 2005. Non-invasive assessment of hepatic iron overload: are we finally there? *Journal of Hepatology*, *42*(1):153-154.

Punnonen, K., Irjala, K. & Rajamäki, A. 1994. Iron-deficiency anemia is associated with high concentrations of transferrin receptor in serum. *Clinical Chemistry*, *40*(5):774-776.

Puntarulo, S. 2005. Iron, oxidative stress and human health. *Molecular Aspects of Medicine*, 26(4-5):299–312.

Roginsky, V.A., Barsukova, T.K., Bruchelt, G. & Stegmann, H.B. 1997. Iron bound to ferritin catalyzes ascorbate oxidation: effects of chelating agents. *Biochimica et Biophysica Acta*, 1335:33–39.

Sánchez, M., Sabio, L., Gálvez, N., Capdevila, M. and Dominguez-Vera, J.M. 2017. Iron chemistry at the service of life. *IUBMB Life*, *69*(6):382-388.

Sooriyaarachchi, M. & Gailer, J. 2010. Removal of Fe^{3+} and Zn^{2+} from plasma metalloproteins by iron chelating therapeutics depicted with SEC-ICP-AES. *Dalton Transactions*, 39(32):7466-7473.

Tesoro, A., Novakovic, J., Thiessen, J.J. & Spino, M. 2005. Validated HPLC assay for iron determination in biological matrices based on ferrioxamine formation. *Journal of Chromatography B*, 823:77–183.

Tian, M., Chen, X., Li, H., Ma, L., Gu, Z., Qi, X., ... You, C. 2016. Long-term and oxidative-responsive alginate–deferoxamine conjugates with a low toxicity for iron overload. RSC Advances, 6(39):32471-32479.

Van Zyl, C.D.W., Solomons, R., Van Reenen, M. and Mason, S. 2020. Metabolic characterization of tuberculous meningitis in a South African paediatric population using ^{1}H NMR metabolomics. *Journal of Infection*, *81*(5):743-752.

Von Ammon, R. and Fischer, R.D. 1972. Shift reagents in NMR spectroscopy. *Angewandte Chemie International Edition in English*, *11*(8):675-692.

Weiss, G. 2002. Iron and immunity: a double-edged sword. *European Journal of Clinical Investigation*, 32:70–78.

Weiss, G., Wachter, H. and Fuchs, D. 1995. Linkage of cell-mediated immunity to iron metabolism. *Immunology Today*, *16*(10):495-500.

Wishart, D. S. 2008. Quantitative metabolomics using NMR. TrAC Trends in Analytical Chemistry, 27, 228-237.

Wu, A.H.B. 2006. *Tietz clinical guide to laboratory tests*. 4th ed. St. Louis: Saunders/Elsevier.

CHAPTER 5 DISCUSSION

Introduction

One major challenge facing analysts is quantifying biologically important elements. The challenge is a product of their scarcity in biological fluids, as well as the risk of contamination during sample collection, storage and analysis (Bocca *et al.*, 2004). To confront this challenge, many technologies have been used to quantify biologically important elements but ^{1}H-NMR in the field of metabolomics is relatively new. According to Pauli *et al*. (2012) quantitative ^{1}H-NMR has produced a wealth of knowledge in various industrial settings such as pharmaceutical, chemical, and food sectors. In Chapter 2.5, properties of ^{1}H-NMR were discussed, and they indicate its capability to tackle such projects. Ions are invisible on a ^{1}H-NMR spectrum, but chelating agents such as EDTA and DFO, which bind to ions of interest, can be used to overcome this challenge. Developing a new quantitative ^{1}H-NMR method for analysis of biologically important elements, particularly iron, may improve diagnosis and responses to therapies for infectious diseases.

Proof-of-concept of chelation NMR as a quantitative ^{1}H-NMR method for biologically important ions using EDTA as a chelating agent.

Hafer *et al*. (2020) and Mathuthu *et al*. (2021), simultaneously worked on almost identical projects in 2019. The distinction between the two studies was that Hafer et al. (2020) was focused upon the analysis of divalent cations intended for food and pharmaceutical products, whereas Mathuthu et al. (2021) focused upon biologically important ions (Mg, Ca, K, Zn and Fe), specifically for application in the field of ^{1}H-NMR metabolomics. For our study (Mathuthu *et al*. 2021), biologically important ions were separately chelated with excess EDTA in a 90% sample to 10% IS ratio at physiological pH range and ^{1}H-NMR spectra compared to that of pure EDTA solution. Spectral differences between pure EDTA and chelated metals were identified and quantified. Mg and Ca were successfully quantified with high repeatability, accuracy, precision and linearity; however, the sensitivity limits of ^{1}H-NMR resulted in the results of Zn in concentrations less than 10µM being less reliable than. More importantly for this MSc study, iron could not chelate with EDTA under the experimental conditions, neither could K. However, upon further research, a study (Kim & Ong, 1999) shed some more light on the concept that the relative stability of metal-EDTA chelation must be taken into account, and that Fe-EDTA is more stable at a pH lower than 3. Hence, objective 1 of this MSc study was achieved by showing proof-of-concept of chelation NMR, namely that ^{1}H-NMR can be used to quantify Ca, Mg and Zn using EDTA as a chelating agent.

Iron quantification using EDTA as a chelating agent in ^{1}H-NMR

In Mathuthu et al. (2021), excess EDTA was added to $FeCl_3$ at a physiological pH range of 6.50–7.50; however, there were no ^{1}H-NMR spectral differences, aside from free EDTA being present. Failure to chelate iron with EDTA meant that iron could not be quantified. Previous studies done by Kim & Ong, (1999) showed that Fe-EDTA complex is stable at lower pH values. Loots et al. (2007) showed similar results, with pH values >6 resulting in the failure of EDTA to chelate with iron. Based on these studies, the quantification of iron using EDTA as a chelating agent should be done at pH values <6 (acidic). The conclusion of the use of EDTA as a chelating agent for iron (objective 2) was that an alternative chelating agent was needed; specifically, deferoxamine was the best candidate for chelating iron, based upon literature.

Developing a quantitative DFO chelation NMR for iron using as a pure compound.

Fe chelation using DFO is a gradual process. NTA, citrate and $CdCl_3$ in literature were determined to be possible catalyst for the chelation of iron with DFO. Experimental variables were tested using both UV spectrophotometric and ^{1}H-NMR analysis. NTA was the best ligand to catalyse as it had the highest rate of reaction in pure compound solutions. ^{1}H-NMR is pH and temperature sensitive. Chelation of iron using DFO was optimal at room temperature, DFO (pH adjusted to 8.1) and samples were incubated for 30minutes after addition of NTA. Analysing at room temperature is consistent with Birus et al. (1995) because of the higher resolution than at higher temperatures. pH and incubation temperature were adopted from studies done by Breuer et al. (2001) and Gosriwatana et al. (1999). At higher $FeCl_3$ concentrations (250µM) a new peak at 2.775ppm and it showed accurate, repeatable and precise results. After analysing 14 levels, the method was repeatable. However, precision and repeatability became poor. Accuracy, repeatability and precision are extremely good at higher $FeCl_3$ concentrations.

Applying developed quantitative NMR method to spiked serum samples

The optimal experimental parameters obtained from testing the DFO method using pure compounds (objective 4) were applied to serum samples spiked with known $FeCl_3$ concentrations. ^{1}H-NMR analysis on unfiltered spiked serum samples with our developed method did not reveal the presence of the singlet at 2.775 ppm in the ^{1}H-NMR spectrum. It is hypothesized that the presence of apo-transferrin bound all free iron in the unfiltered serum samples. This is in accord with Jacobs (2005) that transferrin is 20-35% saturated as all the added $FeCl_3$ saturated apo-

transferrin. Based upon these findings, it was concluded that the application of the method to serum could be optimized – that NTA be added to unfiltered serum, incubated and filtered using 10 000 Dalton centrifugal filter units. The aim here was to release as much iron bound to transferrin as possible by incubating the serum in NTA, and then removing all proteins by filtration in order to prevent iron binding to proteins, thereby yielding the best bio-matrix to assess iron quantification.

Filtered serum sample ^{1}H-NMR analysis

In filtered serum samples changes were identified, monitored and analysed. ^{1}H-NMR samples showed signs of degradation with time at room temperature. Consequently, pH changed leading to chemical shift on the ^{1}H-NMR peaks. These findings are consistent with Anton et al. (2005) that serum samples degrade after being left at room temperature for a long time. Sustained decrease of DFO concentration showed that chemical reactions were still occurring within the samples. The drift in time illustrated by the PLS-DA data cements that the reactions were still on going. The developed method had a good linearity but poor accuracy and repeatability. Consequently, further studies on serum iron quantification using DFO on ^{1}H-NMR must be done.

Conclusions

Serum iron has gained a strong foothold in the biomedical world as its clinical significance has been vividly seen in a wide spectrum of infectious diseases. DFO can not only be used to cure iron overload conditions but also to quantify serum iron. ^{1}H-NMR is capable of identifying and quantifying serum iron using spectral differences between pure DFO and expected FOB (i.e. the gradual decrease in pure DFO peaks and the emergence of two new ^{1}H-NMR peaks at 2.775 ppm and 2.48 ppm). Fortunately, the method had good linearity and it is hypothesized that it was able to detect the presence of apo-transferrin, hence no iron overload was evident in the pooled serum sample. Unfortunately, the method had poor accuracy and repeatability which is likely due to instability of the samples. Analysis of the same serum samples at room temperature over 72 hours showed that chemical reactions were continuing. ^{1}H-NMR could be the solution to a universal, non-invasive method to assess iron status that cannot be affected by inflammation (Burns *et al.*, 1990). Further investigations should be aimed at finding higher field strength catalyst(s) that can transfer more iron from iron binding proteins, as well as stabilizing the final prepared serum sample to quench chemical reactions. Alternatively, reducing the amount of time the samples are at room temperature by simply adding excess Co^{3+} for apo-transferrin saturation (Gosriwatana *et al*., 1999).

References

Birus, M., Gabricevic, M., Kronja, O. and Klaic, B. 1995. 13C and ^{1}H NMR Line Broadening in Desferrioxamine B Spectra. Kinetics and Mechanism of Siderophore Chemistry. *Inorganic Chemistry*, *34*(11):3110-3113.

Bocca, B., Alimonti, A., Petrucci, F., Violante, N., Sancesario, G., Forte, G. and Senofonte, O. 2004. Quantification of trace elements by sector field inductively coupled plasma mass spectrometry in urine, serum, blood and cerebrospinal fluid of patients with Parkinson's disease. *Spectrochimica Acta Part B: Atomic Spectroscopy*, *59*(4):559-566.

Breuer, W., Ermers, M.J., Pootrakul, P., Abramov, A., Hershko, C. and Cabantchik, Z.I. 2001. Desferrioxamine-chelatable iron, a component of serum non–transferrin-bound iron, used for assessing chelation therapy: Presented in preliminary form at the 10th International Conference on Oral Chelators symposium on iron chelators held in Limassol, Cyprus, March 2000 (Transfusion Science, in press). *Blood, The Journal of the American Society of Hematology*, *97*(3):792-798.

Cramer, S.M., Nathanael, B. & Horvath, C. 1984. High-performance liquid chromatography of deferoxamine and ferrioxamine: Interference by iron present in chromatographic system. *Journal of Chromatography, 295:*405-411.

D'Haese, P.C., Ludwig V. Lamberts, L.V. & De Broe, M.E.1989. Indirect Measurement of Desferrioxamine and Its Chelated Compounds Aluminoxamine and Fernoxamine by Zeeman Atomic Absorption Spectrometry. *Clinical chemistry***,** 35(5):884-887.

Gosriwatana, I., Loreal, O., Lu, S., Brissot, P., Porter, J. & Hider, R.C. 1999. Quantification of Non-Transferrin-Bound Iron in the presence of unsaturated transferrin. *Analytical Biochemistry,* 273:212-220.

Hafer, E., Holzgrabe, U., Kraus, K., Adams, K., Hook, J.M., & Diehl, B. 2020. Qualitative and quantitative ^{1}H NMR spectroscopy for determination of divalent metal cation concentration in model salt solutions, food supplements, and pharmaceutical products by using EDTA as chelating agent. *Magnetic Resonance in Chemistry*, 58(7):653–665.

Pauli, G.F., Godecke, T., Jaki, B.U. and Lankin, D.C. 2012. Quantitative ^{1}H NMR. Development and potential of an analytical method: an update. *Journal of Natural Products*, *75*(4):834-851.

Sun, H., Cox, M.C., Li, H., Mason, A.B., Woodworth, R.C. & Sadler, P.J. 1998. [^{1}H,^{13}C] NMR determination of the order of lobe loading of human transferrin with iron: comparison with other metal ions. *FEBS Letters,* 422:315-320.

Wishart, D. S. 2008. Quantitative metabolomics using NMR. TrAC Trends in Analytical Chemistry, 27:228-237.

ANNEXURES (TOC_HEADING)

Supplementary Information

Chelation ^{1}H-NMR method development for quantifying iron in serum using deferoxamine

Emmanuel Mathuthu[a] & Shayne Mason[a,*]

[a] Human Metabolomics, Faculty of Natural and Agricultural Sciences, North-West University, Potchefstroom, South Africa.

[*] Corresponding author: Shayne Mason (https://orcid.org/0000-0002-2945-5768)

North-West University
Private Bag X6001
Potchefstroom
South Africa
2531

Email: nmr.nwu@gmail.com

Email addresses:

Emmanuel Mathuthu: emmanuelmathuthu@gmail.com

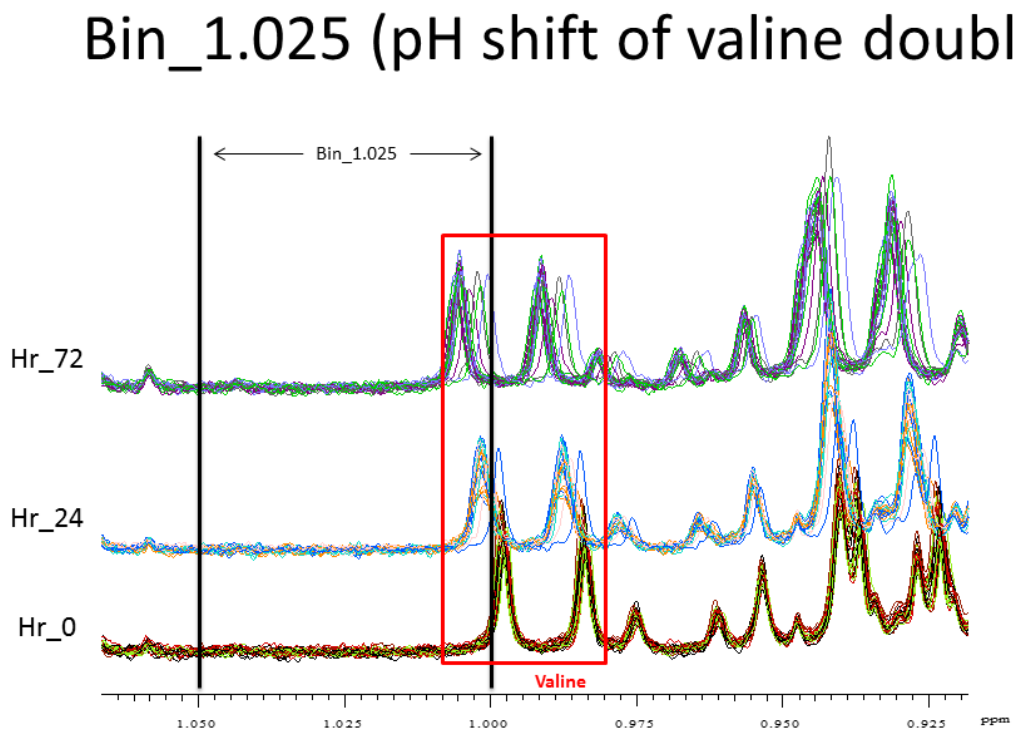

Figure S 1: pH shift of valine doublet at Bin_1.025.

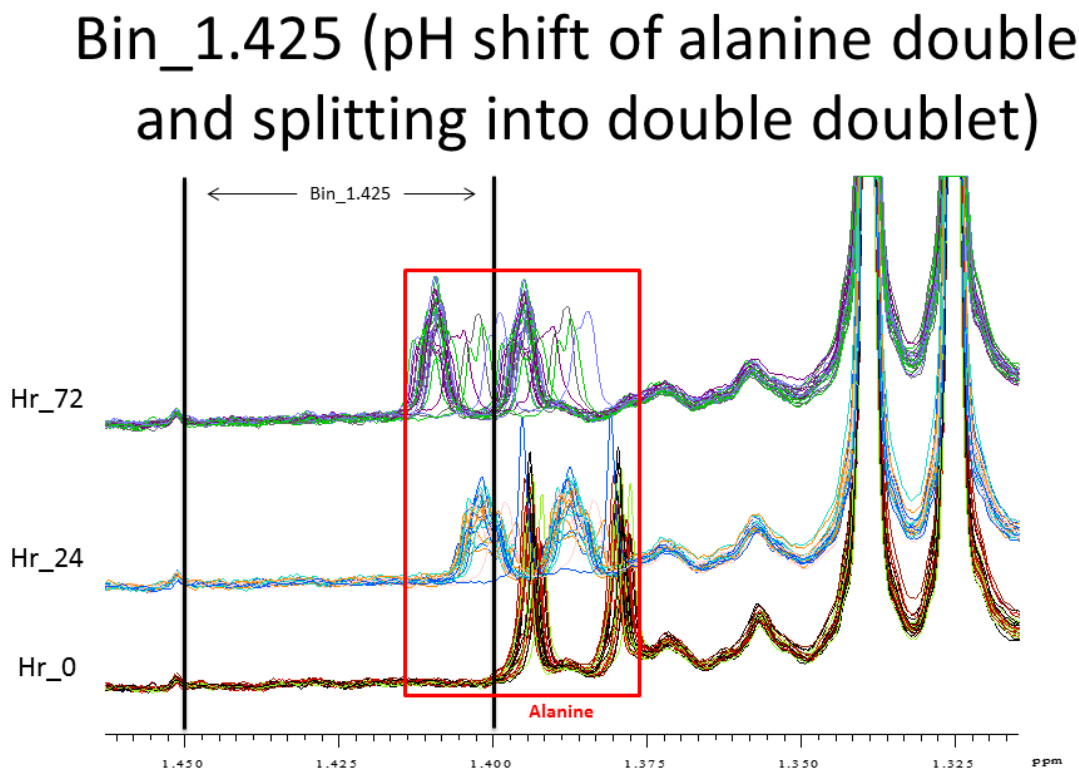

Figure S 2: pH shift of alanine doublet at Bin_1.425.

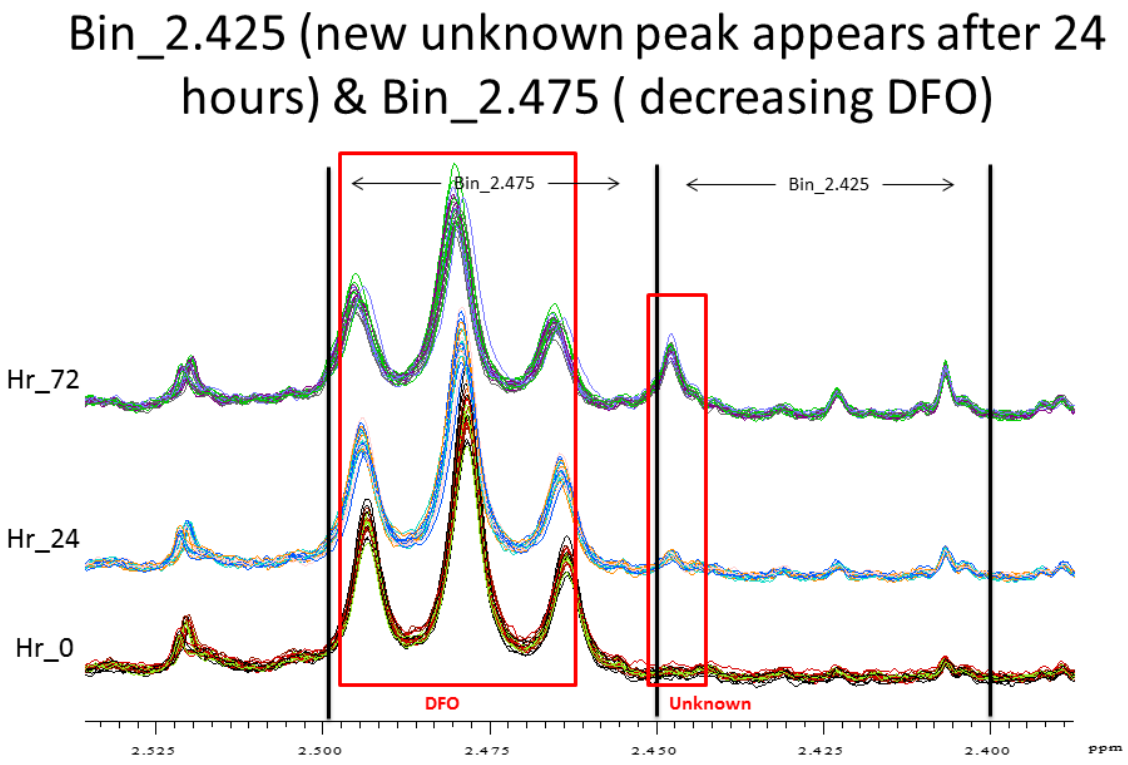

Figure S 3: Unknown peak appears after 24hrs time in Bin_2.425, and DFO decreases over time in Bin_2.475.

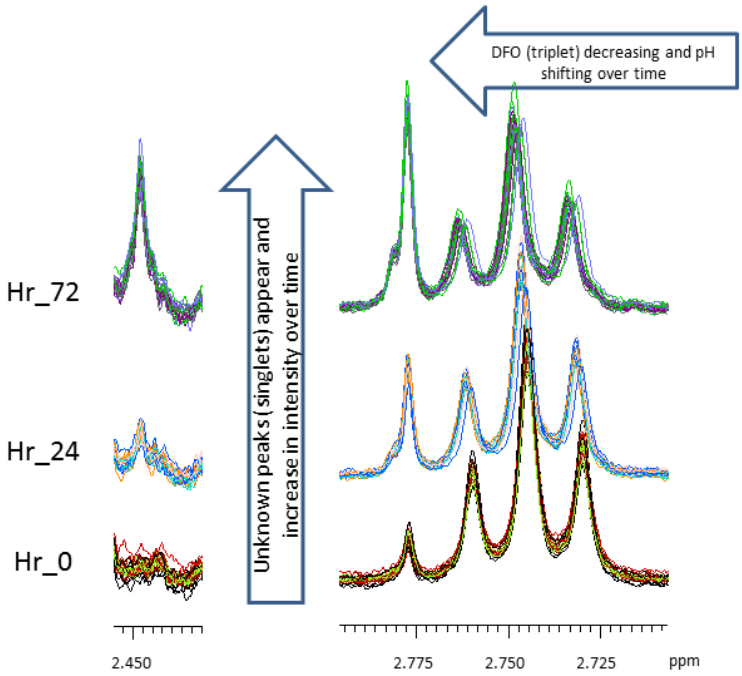

Figure S 4: New peaks at 2.775 ppm and 2.48 ppm, increasing with time (0 – 72)Hrs after chelating iron with DFO.

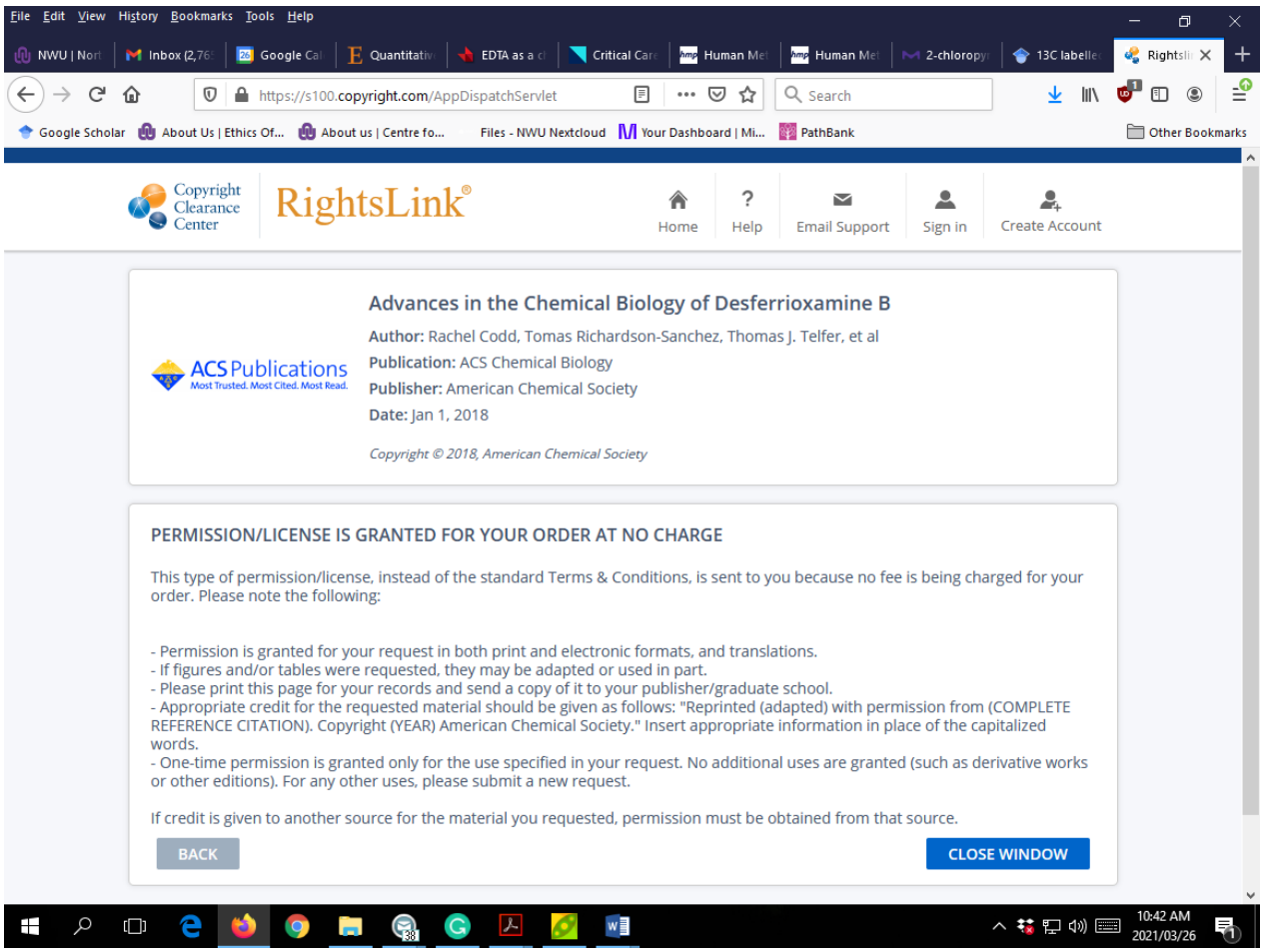

Figure S 5: Copyright agreement for permission to reprint Figure 1 in manuscript.

Private Bag X6001, Potchefstroom
South Africa 2520

Tel: +2718 299-1111/2222
Web: http://www.nwu.ac.za

Faculty of Health Sciences Ethics Office for Research, Training and Support

Tel: 018 299 2092
Email: minrie.greeff@nwu.ac.za

Mr Emmanuel Mathuthu

8 March 2019

Dear Mr Mathuthu

PROOF OF ATTENDANCE

This letter certifies that you have attended the half-day ethics training entitled:

The SANS document: As regulation for research with animals

Presenter: Prof CB Brink (Chairperson: NWU-AnimCareREC) on the **24 January 2019.**

This letter of attendance, is recognised by the NWU-AnimCareREC and the Health Science Ethics Office for Research, Training and Support and is valid for three (3) years and expires on 31 January 2022.

Yours sincerely

Digitally signed by Prof Minrie Greeff
Date: 2019.03.20 16:31:22 +02'00'

Prof Minrie Greeff
Head of Health Sciences Ethics
Office for Research, Training and Support

Prof Jeanetta du Plessis
Deputy Dean: Research and Innovation
Faculty of Health Sciences

Current details: (20636890) G:\My Drive\9. Research and Postgraduate Education\9.1.5.7 Training\9.1.5.7.6_Letter of Attendance_ SANS.docm
7 March 2019

File reference: 9.1.5.7.6

Figure S 6: Ethics proof of attendance 1 a prerequisite for Post graduate science research study

NWU®
NORTH-WEST UNIVERSITY
NOORDWES-UNIVERSITEIT
YUNIBESITI YA BOKONE-BOPHIRIMA

Private Bag X6001, Potchefstroom
South Africa 2520
Tel: +2718 299-1111/2222
Web: http://www.nwu.ac.za

Faculty of Health Sciences Ethics Office for Research, Training and Support

Tel: 018 299 2092
Email:minrie.greeff@nwu.ac.za

8 March 2019

Mr Emmanuel Mathuthu

Dear Mr Mathuthu

PROOF OF ATTENDANCE AND ASSESSMENT

This letter certifies that you have attended the 2-day ethics training entitled:

The Basics of Health Research Ethics

(Accreditation number: PSB002/110/01/2019 from University of Free-State CPD accreditation department accredited by the HPCSA)

Presenter: Prof M Greeff (Head of the Health Sciences Ethics Office for Research, Training and Support) on the **22nd – 23rd January 2019.**

This letter of attendance, serves as proof of ethics training and assessment and is valid for three (3) years and expires on 31 January 2022. (Where applicable, Ethics CEUs awarded: 14 CEUs)

Yours sincerely

Digitally signed by Prof Minrie Greeff
Date: 2019.03.19 08:39:21 +02'00'

Prof Minrie Greeff
Head of Health Sciences Ethics
Office for Research, Training and Support

Prof Jeanetta du Plessis
Deputy Dean: Research and Innovation
Faculty of Health Sciences

Current details: (20536690) G:\My Drive\8. Research and Postgraduate Education\R.1.S.7 Training\ 9.1.S.7.6_Letter of Attendance_Template_SOHRE.docm
8 March 2019

File reference: 9.1.S.7.6

Figure S 7: Ethics proof of attendance 2 a prerequisite for Post graduate science research study